Neuromusculoskeletal human multibody models for the gait of healthy and spinal-cord-injured subjects

Florian Michaud

Doctoral thesis

2020

Neuromusculoskeletal human multibody models for the gait of healthy and spinal-cord-injured subjects

Florian Michaud

Advisors: Urbano Lugris Armesto
Javier Cuadrado Aranda

Doctoral thesis

Programa de Enxeñería Industrial

Ferrol, 2020

Dr. Urbano Lugrís Armesto, Doctor by the University of A Coruña, and Dr. Javier Cuadrado Aranda, Doctor by the University of Navarra, certify that this doctoral dissertation, entitled Neuromusculoskeletal human multibody models for the gait of healthy and spinal-cord-injured subjects, has been developed by Florian Michaud under their supervision in order to obtain the International Doctor mention by the University of A Coruña.

Dr. Urbano Lugrís Armesto, Doctor por la Universidad de A Coruña, y Dr. Javier Cuadrado Aranda, Doctor por la Universidad Navarra, certifican que la presente memoria, titulada Neuromusculoskeletal human multibody models for the gait of healthy and spinal-cord-injured subjects, ha sido desarrollada por Florian Michaud bajo su supervisión para optar al grado de Doctor con mención Internacional por la Universidad de A Coruña.

Ferrol, 2020.

Florian Michaud, PhD. student *Doctorando*	Dr. Urbano Lugrís Armesto Advisor *Director*	Dr. Javier Cuadrado Aranda Advisor *Director*

Acknowledgments

A doctoral thesis represents an important part of life. From its beginning to the end, things evolve and the help of other people is required to succeed during this personal work.

So, I would like to acknowledge first my advisors of this thesis, Javier Cuadrado and Urbano Lugrís for transmitting to me a part of their knowledge and for the good direction of this work. I also want to thank the good working environment and help provided to me by all my colleagues at the Laboratorio de Ingeniería Mecánica of the University of A Coruña: Emilio, David, Amelia, Daniel, Alberto, Lolo, Urbano, Francisco González, Francisco Mouzo and Antonio. Without forgetting the last arrived: Borja, Sarath, Álvaro, Mario and Alejandro. I would like to highlight the great help provided by Alberto to solve programing issues, Emilio with the written part of this work and Amelia for her general support during all the thesis.

I could enjoy the help from people from other universities, in particular during my stay at the University of Rice in Houston, where the supervisor of my stay, Benjamin J. Fregly and Mohammad S. Shourijeh participated in part of this thesis. I also acknowledge Andrés Kecskeméthy for his advices during our several meetings.

Last but not least, I want to thank all the support provided by my parents, Martial and Nadine, my step father, Moumou, my brothers, Audric, Mathys and Gabin, and two very special people for me, Mickael and Rafa.

Agradecimientos

Una tesis doctoral representa una etapa importante en una vida. De su inicio a su final, las cosas evolucionan y la ayuda de personas ajenas es necesaria para conseguir el éxito de este trabajo personal.

Me gustaría entonces agradecer, en un primer lugar, a mis directores de tesis Javier Cuadrado y Urbano Lugrís por transmitirme parte de sus conocimientos y haber dirigido este trabajo de la mejor manera. También quiero agradecer al resto de mis compañeros de trabajo del Laboratorio de Ingeniería Mecánica de la Universidad de A Coruña por su ayuda y ofrecer un buen ambiante de trabajo: Emilio, David, Amelia, Daniel, Alberto, Lolo, Urbano, Francisco González, Francisco Mouzo y Antonio. Sin olvidarme de los ultimos integrados: Borja, Sarath, Álvaro, Mario y Alejandro. Me gustaría destacar la gran ayuda recibida de Alberto para solucionar problemas de programación, la de Emilio con la redacción de mi tesis y Amelia por su ayuda general a lo largo de mi tesis.

También pude disfrutar de la ayuda de gente de otras universidades, especialmente durante mi estancia en la Universidad de Rice en Houston, donde el supervisor de mi estancia, Benjamin J. Fregly y Mohammad S. Shourijeh contribuyeron a la realizacíon de una parte de esta tesis. Agradezco igualmente la ayuda de Andrés Kecskeméthy por sus consejos a lo largo de nuestros encuentros.

Por último, pero no menos importante, quiero agradecer todo el apoyo proporcionado por parte de mis padres, Martial y Nadine, mi padastro, Moumou, mis hermanos, Audric, Mathys y Gabin, y dos personas muy especiales para mí, Mickael y Rafa.

Remerciements

Une thèse doctoral représente une étape importante dans une vie. Du début à la fin, les choses évoluent et l'aide d'autres personnes est nécessaire au succès de ce travail personnel.

Je voudrais tout d'abord remercier mes directeurs de thèse, Javier Cuadrado et Urbano Lugrís, de m'avoir transmis une partie de leurs connaissances et d'avoir dirigé ce travail de la meilleure façon possible. Je souhaite également remercier le reste de mes collègues du laboratoire d'ingénierie mécanique de l'Université de La Corogne pour leur aide et me permettre de travailler dans une bonne ambiance : Emilio, David, Amelia, Daniel, Alberto, Lolo, Urbano, Francisco González, Francisco Mouzo et Antonio. Sans oublier les derniers intégrés : Borja, Sarath, Alvaro, Mario et Alejandro. Je voudrais souligner la grande aide reçue par Alberto pour résoudre les problèmes de programmation, celle d'Emilio lors de la rédaction de ma thèse et celle d'Amelia pour son aide générale tout au long de ma thèse.

J'ai également pu bénéficier de l'aide de personnes d'autres universités, en particulier lors de mon séjour à l'université de Rice à Houston, où le superviseur de mon séjour, Benjamin J. Fregly et Mohammad S. Shourijeh, ont contribué à la réalisation d'une partie de cette thèse. Je souhaite également remercier l'aide d'Andrés Kecskeméthy pour ses conseils lors de nos rencontres.

Enfin, je tiens à remercier tout le soutien fourni par mes parents, Martial et Nadine, mon beau-père, Moumou, mes frères, Audric, Mathys et Gabin, et deux personnes très spéciales pour moi, Mickael et Rafa.

Abstract

Spinal-cord-injured (SCI) subjects with some level of hip actuation but with no or very weak actuation at knee and ankle levels can often walk with the assistance of knee-ankle-foot orthoses (KAFO) and crutches. However, since knees are kept extended at all times, even during the swing phase, gait becomes very uncomfortable as the hip must be raised for the swing, thus leading to a high energetic cost which makes fatigue appear quickly. Moreover, the use of crutches leads to high loads in some joints, particularly shoulders, which may produce injuries in the long term. The result is that many patients prefer to use the wheelchair, thus losing the benefits of walking for rehabilitation and for their general health state. To alleviate these problems, active orthoses have been proposed that detect swing intention and launch a knee flexion-extension cycle, thus approaching healthy gait, which can make gait more comfortable and increase the actual chances of walking for users. Some magnitudes, as joint reactions or energetic cost, may serve as indicators to evaluate the effect of assistive devices in a specific user and, hence, the likeliness of their actual use in the long term. The combined use of motion-force-EMG capture and personalized neuromusculoskeletal models enables to estimate the mentioned magnitudes, without the need for long and tiring experimental tests which could hardly be undergone by these subjects. Therefore, the present work is devoted, on the one hand, to review, select, adapt, improve and/or develop, and validate, all the necessary methods and tools which are required for this purpose: (i) personalized musculoskeletal models; (ii) methods for analysis at skeletal and musculoskeletal levels; (iii) methods for energetic cost estimation. And, on the other hand, to apply them to two SCI subjects, bilateral and unilateral, respectively, and to compare a new active KAFO with a conventional passive one. Results show that the evaluation of device impact through the mentioned indicators is effective, and that the new active system objectively streamlines walking to users.

Resumo

Os lesionados medulares con algunha capacidade de actuación en cadeira pero con pouca ou nula capacidade de actuación en xeonllo e nocello, poden en moitos casos camiñar coa axuda de órteses de xeonllo-nocello-pé e muletas. Con todo, dado que os xeonllos se manteñen estendidos en todo momento, mesmo durante a fase de abalo, a marcha resulta moi incómoda, pois a cadeira debe levantarse para permitir o abalo da perna, o que supón un alto custo enerxético que fai aparecer a fatiga rapidamente. Ademais, o uso de muletas produce cargas elevadas nalgunhas articulacións, especialmente nos ombreiros, o que pode xerar lesións a longo prazo. O resultado é que moitos pacientes prefiren usar a cadeira de rodas, perdendo así os beneficios de camiñar para a súa rehabilitación e para o seu estado de saúde xeral. Para paliar estes problemas, propuxéronse órteses activas que detectan a intención de dar o paso e lanzan un ciclo de flexión-extensión de xeonllo, aproximando así a marcha normal, o que pode facer a marcha máis cómoda e aumentar as posibilidades reais de camiñar para os usuarios. Algunhas magnitudes, como as reaccións nas articulacións ou o custo enerxético, poden servir como indicadores para avaliar o efecto dos dispositivos de asistencia nun usuario específico e, polo tanto, a probabilidade do seu uso real a longo prazo. O uso combinado da captura de movemento-forza-EMG e os modelos neuromusculoesqueléticos personalizados permite estimar as magnitudes mencionadas, sen a necesidade de longas e esgotadoras probas experimentais que dificilmente poderían afrontar estes pacientes. Polo tanto, o presente traballo está dedicado, por unha banda, a revisar, seleccionar, adaptar, mellorar e/ou desenvolver, e validar, todos os métodos e ferramentas necesarios que se requiren para este propósito: (i) modelos músculoesqueléticos personalizados; (ii) métodos de análises a nivel esquelético e musculoesquelético; (iii) métodos de estimación de custo enerxético. E, doutra banda, a aplicalos a dous lesionados medulares, bilateral e unilateral, respectivamente, e a comparar unha nova órtese activa cunha pasiva convencional. Os resultados mostran que a avaliación do impacto do dispositivo a través dos indicadores mencionados é efectiva, e que o novo sistema activo facilita certamente camiñar aos usuarios.

Resumen

Los lesionados medulares con alguna capacidad de actuación en cadera pero con poca o nula capacidad de actuación en rodilla y tobillo, pueden en muchos casos caminar con la ayuda de órtesis de rodilla-tobillo-pie y muletas. Sin embargo, dado que las rodillas se mantienen extendidas en todo momento, incluso durante la fase de balanceo, la marcha resulta muy incómoda, pues la cadera debe levantarse para permitir el balanceo de la pierna, lo que conlleva un alto coste energético que hace aparecer la fatiga rápidamente. Además, el uso de muletas produce cargas elevadas en algunas articulaciones, especialmente en los hombros, lo que puede generar lesiones a largo plazo. El resultado es que muchos pacientes prefieren usar la silla de ruedas, perdiendo así los beneficios de caminar para su rehabilitación y para su estado de salud general. Para paliar estos problemas, se han propuesto órtesis activas que detectan la intención de dar el paso y lanzan un ciclo de flexión-extensión de rodilla, aproximando así la marcha normal, lo que puede hacer la marcha más cómoda y aumentar las posibilidades reales de caminar para los usuarios. Algunas magnitudes, como las reacciones en las articulaciones o el coste energético, pueden servir como indicadores para evaluar el efecto de los dispositivos de asistencia en un usuario específico y, por lo tanto, la probabilidad de su uso real a largo plazo. El uso combinado de la captura de movimiento-fuerza-EMG y los modelos neuromusculoesqueléticos personalizados permite estimar las magnitudes mencionadas, sin la necesidad de largas y agotadoras pruebas experimentales que difícilmente podrían afrontar estos pacientes. Por lo tanto, el presente trabajo está dedicado, por un lado, a revisar, seleccionar, adaptar, mejorar y/o desarrollar, y validar, todos los métodos y herramientas necesarios que se requieren para este propósito: (i) modelos músculoesqueléticos personalizados; (ii) métodos de análisis a nivel esquelético y musculoesquelético; (iii) métodos de estimación de coste energético. Y, por otro lado, a aplicarlos a dos lesionados medulares, bilateral y unilateral, respectivamente, y a comparar una nueva órtesis activa con una pasiva convencional. Los resultados muestran que la evaluación del impacto del dispositivo a través de los indicadores mencionados es efectiva, y que el nuevo sistema activo facilita ciertamente caminar a los usuarios.

Résumé

Les personnes souffrant d'une lésion médullaire conservant une bonne mobilité au niveau de la hanche mais ayant une mobilité nulle ou très faible au niveau du genou et de la cheville ont la possibilité de marcher avec l'aide d'orthèses de genou-cheville-pied et de béquilles. Cependant, comme les genoux sont maintenus en extension tout au long du cycle de marche, même pendant la phase du swing, le mouvement de marche devient très inconfortable car il demande une élévation additionnelle du bassin durant le swing, entraînant ainsi un coût énergétique élevé qui fait apparaître rapidement la fatigue. De plus, l'utilisation de béquilles entraîne des charges élevées dans certaines articulations, en particulier les épaules, susceptibles de provoquer des blessures à long terme. Il en résulte que de nombreux patients préfèrent utiliser leur fauteuil roulant, perdant ainsi les avantages de la marche pour leur rééducation et leur état de santé général. Afin d'atténuer ces problèmes, des orthèses actives ont été proposées pour détecter la phase du swing et lancer un cycle de flexion-extension du genou, simulant ainsi le mouvement normal d'une personne saine, ce qui peut rendre la démarche plus confortable et augmenter les chances réelles de marcher pour les utilisateurs. Certaines grandeurs, telles que les forces de réaction des articulations ou le coût énergétique peuvent servir d'indicateurs pour évaluer l'effet des dispositifs d'assistance sur un utilisateur spécifique et, par conséquent, la probabilité de son utilisation réelle à long terme. L'utilisation combinée de la capture de mouvement, de forces et d'EMG et de modèles neuromusculosquelettiques personnalisés permet d'estimer les grandeurs mentionnées, sans recourir à des tests expérimentaux longs et fatigants que ces sujets pourraient difficilement réaliser. Par conséquent, le présent travail est consacré, d'une part, à examiner, sélectionner, adapter, améliorer et/ou développer et valider toutes les méthodes et tous les outils nécessaires à cet effet : (i) modèles musculosquelettiques personnalisés ; ii) méthodes d'analyse aux niveaux squelettique et musculosquelettique ; (iii) méthodes d'estimation des coûts énergétiques. Et, d'autre part, de les appliquer à deux sujets atteints d'une lésion médullaire, bilatérale pour l'un, et unilatérale pour le second, et de comparer une nouvelle orthèse active avec une originale, passive. Les résultats montrent que l'évaluation de l'impact du dispositif à l'aide des indicateurs mentionnés est efficace et que la nouvelle orthèse active offre objectivement des facilités pour marcher aux utilisateurs.

Contents

List of Figures

List of Tables

Acronyms

CMC computed muscle control. 9, 48–50, 52, 78, 102

CNS central nervous system. 2, 3, 5, 6, 33, 34, 42

CSA co-simulation approximated. 52, 78, 102

CSS co-simulation standard. 52, 78, 102

CTC computed torque control. 26, 49, 78

DAE differential-algebraic equations. 24

EMG electromyography. 2, 5, 9, 30, 33, 40–43, 45, 68, 71, 72, 74, 78, 102

FPL force plate. 28, 29

IMU inertial measurement unit. 63

KAFO knee-ankle-foot orthoses. 1, 2, 7–9, 63, 64, 67, 71–74

LEMS lower extremity muscle score. 7, 67, 71, 74, 75

LHS left-hand side. 24

MBD multibody dynamics. 23, 25, 27, 29

NMF non-negative matrix factorization. 42, 44, 45

SCI spinal cord injured. 1, 7–10, 28, 57, 63, 65, 67, 71, 72, 74, 75, 77–79

SO static optimization. 34, 41, 43–45

SynO synergy optimization. 43–45, 77, 79, 101

List of symbols

The symbols used all along the document are defined here. The symbols employed in small parts of the document are defined locally.

$F^{MT}_{i,max}$ Maximum feasible musculotendon force of the muscle i. 33, 34, 37, 38

$F^{MT}_{i,min}$ Minimum feasible musculotendon force of the muscle i. 33, 34, 37, 38

F^{MT} Force of the musculotendon. 15, 18–22, 33, 34, 37, 39, 49–51

F^{M}_{0} Maximum isometric force. 18–22, 40, 58, 60, 92, 93

F^{M}_{CE} Active force exerted by the contractile element. 18, 58, 60

F^{M}_{PE} Passive force exerted by the passive elastic component. 18, 19, 40

J Jacobian matrix of muscular moment arms. 15, 33, 34, 37, 39, 45, 49–51

$\%FT$ Percentage of fast twitch. 58, 59

$\bar{\mathbf{M}}$ Mass matrix projected over the independent coordinates. 25–28, 49, 50

$\bar{\mathbf{Q}}$ Vector of generalized forces projected over the independent coordinates. 25

$\ddot{\mathbf{\Phi}}$ Second time derivative of the constraints vector. 24

$\ddot{\mathbf{q}}$ Vector of dependent accelerations. 24, 25

$\ddot{\mathbf{z}}$ Vector of independent accelerations. 24–28, 34, 39, 48–51

$\dot{E}$ Total rate of energy consumption. 57, 58, 60

$\dot{F}^{MT}$ Derivative of the force of the musculotendon. 19, 20

$\dot{H}$ Heat rate. 57

$\dot{W}$ Mechanical work. 57

$\dot{\mathbf{\Phi}}$ Time derivative of the constraints vector. 24

$\dot{\mathbf{R}}$ Time derivative of the velocity projection matrix R. 25

$\dot{\mathbf{q}}$ Vector of dependent velocities. 24, 25, 29

$\dot{\mathbf{y}}^{*}$ Vector of Cartesian velocities. 28, 29

$\dot{\mathbf{z}}^{*}$ Estimated vector of generalized virtual velocities. 28, 29

$\dot{\mathbf{z}}$ Vector of independent coordinates. 24–26, 28, 29, 34, 39, 48–51

$\dot{a}$ Muscle activation derivative. 17, 18, 20

$\dot{h}_{A}$ Activation heat rate. 57–60

$\dot{h}_{M}$ Maintenance heat rate. 57–60

$\dot{h}_{AM}$ Activation and maintenance heat rate. 58

$\dot{h}_{SL}$ Shortening/lengthening heat rate. 57, 58, 60

$\dot{w}_{CE}$ Mechanical work rate of the contractile element. 57, 58, 60

$\mathbf{0}$ Null matrix. 23–25

$\mathbf{D}$ Projection matrix. 24, 25

$\mathbf{M}$ Mass matrix. 24, 25

$\mathbf{Q_c}$ Vector grouping all the remaining generalized forces. 26, 27

$\mathbf{Q_m}$ Vector of generalized motor forces. 26–30

$\mathbf{Q_u}$ Vector of the inputs provided by the controllers. 26

$\mathbf{Q_{GR}}$ Vector of ground reactions forces. 34, 39, 49, 51

$\mathbf{Q}$ Vector of generalized forces. 24, 25

$\mathbf{R}$ Velocity projection matrix, such as $\dot{\mathbf{q}} = \mathbf{R}\dot{\mathbf{z}}$. 24, 25, 29

$\mathbf{S}$ Transformation matrix for rheonomous constraints. 24, 25

$\mathbf{T}$ Set of forces and moments. 28–30

α Pennation angle. 16–19, 38, 40, 92, 93

$\mathbf{q}$ Vector of dependent coordinates. 23–25, 29

$\mathbf{w_{GR}}$ Ground reactions measurements from force plates. 34, 39, 49, 51

$\mathbf{z}$ Vector of independent coordinates. 23, 25, 26, 28, 34, 39, 48–51

$\mathcal{T}^{MT}$ Joint torques driven by muscles. 15, 33, 34, 37, 39, 44, 45, 48

$\mathcal{T}$ Joint torques. 28, 30, 49, 51

τ_{act} Time constant for buildup in activation. 17, 18, 40

τ_{deact} Time constant for relaxation of activation. 17, 18, 40

$\tilde{l}^M$ Normalized muscle fiber length. 18–21, 38–40, 59

$\tilde{v}^M$ Normalized muscle fiber velocity. 18, 19, 21, 22, 38, 40, 58

ε^T Tendon strain. 19, 22, 23, 38

a Muscle activation. 17–20, 36, 38, 40, 49, 51, 59

f_l Dimensionless force-length relationship. 18–21, 38, 40

f_v Dimensionless force-velocity relationship. 18, 19, 21, 22, 38, 40

f_{PE} Dimensionless force-length relationship of the passive elastic component. 19, 21

f_T Dimensionless force-strain relationship. 19, 20, 22, 23, 38

k^T Tendon stiffness. 19, 22

l^{MT} Musculotendon length. 14, 16, 20, 38, 39, 45

l_0^M Optimal muscle fiber length. 17, 19, 20, 38, 58, 92, 93

l^M Tendon length. 16, 17, 19, 21, 38, 39, 58

l_S^T Slack tendon length. 19, 20, 22, 38, 39, 92, 93

l^T Muscle fiber length. 16, 19, 20, 39

u Neural excitation. 17, 20, 40, 59

w Constant distance between the aponeurosis of the origin of the muscle and its insertion during the muscle contraction. 17, 20, 39

$\mathbf{\Phi_q}$ Jacobian of the constraints vector wrt the coordinates. 23–25

$\mathbf{\Phi}$ Vector of constraints. 23–25

$\boldsymbol{\lambda}$ Vector of Lagrange multipliers. 24, 25

v^{MT} Musculotendon velocity. 15, 19, 20, 39, 45

v^{M} Muscle fiber velocity. 19, 39, 58, 60

v^{T} Tendon velocity. 19

Chapter 1

Introduction

1.1 Motivation

Advances in the care of spinal cord injured (SCI) subjects have resulted in an increased life expectancy among this population [1]. Standing up and walking regularly has huge benefits for the general health state of these subjects, since it reduces the negative consequences of sedentarism. An example is osteoporosis [2], i.e. bone loss due to skeletal mechanical unloading. While muscle plasticity or muscle electric stimulation attenuate muscle atrophy, none of them preserves bone mass [3]. Therefore, achieving adherence to assisted gait is important, but there is a risk of abandoning due to several issues, as pain, fatigue or very low speed, which can make the subject return to solely use the wheelchair.

SCI subjects with some level of hip actuation but with no or very weak actuation at knee and ankle levels can often walk with the assistance of knee-ankle-foot orthoses KAFO and crutches [4] [5]. However, since knees are kept extended at all times, even during the swing phase, gait becomes very uncomfortable as the hip must be raised for the swing, thus leading to a high energetic cost which makes fatigue appear quickly. Moreover, the use of crutches leads to high loads in some joints, particularly shoulders, which may produce injuries in the long term. The result is that many patients prefer to use the wheelchair [6], thus losing the benefits of walking for rehabilitation and for their general health state. To alleviate these problems, active orthoses have been proposed that detect swing intention and launch a knee flexion-extension cycle [7], thus approaching healthy gait, which can make gait more comfortable and increase the actual chances of walking for users. Some magnitudes, as joint reactions or energetic cost, may serve as indicators to evaluate the effect of assistive devices in a specific user and, hence, the likeliness of their actual use in the long term. The combined use of motion-force-EMG capture and personalized neuromusculoskeletal models enables to estimate the mentioned magnitudes, without the need for long and tiring experimental tests which could hardly be undergone by these subjects. Therefore, the present work is devoted, on the one hand, to review, select, adapt, improve and/or develop, and validate, all the necessary methods and tools which are required for this purpose: (i) personalized musculoskeletal models; (ii) methods for analysis at skeletal and musculoskeletal levels; (iii) methods for energetic cost estimation. And, on the other hand, to apply

them to SCI subjects to compare a new active KAFO with a conventional passive one.

1.2 Background

Biomechanics is an interdisciplinary science that studies the concepts of mechanics applied to life sciences [8]. It evolves on the border between biology and mechanics by appropriating the knowledge of many other scientific disciplines.

The study of the movement of the human body and its interaction with the environment in which it evolves is the main objective of this discipline. The human body can be seen as a multibody system, composed by solids linked by joints and actuated by internal motors, the muscles. The central nervous system (CNS) manage the control of this complex mechanism [9]. For its full understanding, knowledge and experience from different scientific disciplines is necessary.

Among the different applications of biomechanics, the study of locomotion is one of the main topics of investigation, firstly in the case of healthy people and more and more in the case of people with motor problems.

Determination of muscle forces during gait (or any other exercise) is of great interest to extract the principles of the CNS control [10] (assessment of pathological gait from muscular activation abnormalities, diagnosis of neuromuscular disorders), or to estimate the loads on bones and joints [11] (prevention of injuries in sports, surgical planning to reconstruct diseased joints). The invasive character of in vivo experimental measurements, and the uncertain relation between muscle force and electromyography (EMG) , makes computer modeling and simulation a useful substitutive approach [12].

1.2.1 Gait analysis

Walking is the natural mode of locomotion of the adult human being, allowing him to combine the maintained standing equilibrium and the propulsion [13]. It involves combining and alternating the two lower limbs. Schematically, walking consists of putting one foot in front of the other alternatively and repeatedly. Walking is characterized by a succession of double supports and unipodal supports, the body remaining permanently in contact with the ground by at least one unilateral support.

The repeated movement composed by a support phase and a swing phase is called gait cycle. In this work, the following gait cycle has been considered: it starts with the initial heel contact of the right foot and ends with the new contact of the same foot on the ground. The support phase corresponds to the entire period when the foot is in contact with the ground. Its beginning corresponds to the initial contact (contact of the foot with the ground) and its end to the detachment of toes (loss of contact of the foot with the ground) [14]. It ranges from 0 to 60% of the walking cycle, a duration of 60% of the walking cycle. The swing phase corresponds to the entire phase when the foot is no longer in contact with the ground and which allows the advancement of the lower limb. Its beginning corresponds to the detachment of the toes and its end to the new ground contact of the same foot. It extends from 60

to 100% of the walking cycle, i.e. a duration of 40% of the walking cycle. A more detailed description of the gait cycle can be observed in Figure 1.1.

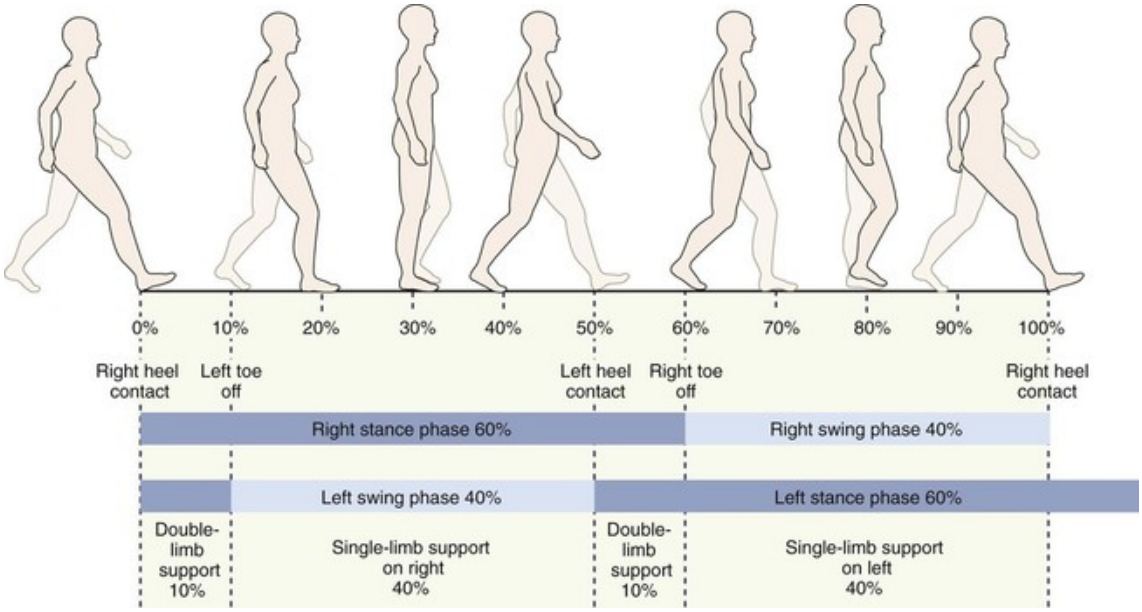

Figure 1.1 – Gait cycle [15].

The gait analysis and pattern of the human body movement represents a fundamental part of the assessment of the individual by correlating their changes due to alterations in the different body systems. Over time, many investigations have been conducted in order to determine the normality values in the various parameters that shape or determine the particular characteristics of gait pattern in specific diseases or specific population groups. According to the interest, the analysis can focus on the kinematics, the dynamics, the muscular activity or the energy consumption during the locomotion activity [16].

Crutch-assisted gait is a particular case because of the intensive use of the upper limbs. Ground contacts are more complicated due to the additional support offered by the crutches [17]. The gait cycle will depend on the type of crutch gait employed by the subject.

1.2.2 Neuromusculoskeletal models

Movement of the human body is controlled by the CNS, which generates neural commands to activate the contractile apparatus of the muscles. Muscles generate forces which combine with the inertia and external forces acting on the body, resulting in observable movements. Complete models of the musculoskeletal mechanics must represent the dynamics of muscle force production and the dynamics of movement in the skeletal system [18].

The skeletal system is composed of bones (considered as rigid bodies) that are connected to each other via articulations or joints. The articulated bodies form a multibody system whose motion is influenced by external forces (applied by muscles, gravity, and the environment) and constraints imposed by joints. The configuration

of the body segments and the types of articulations determine all possible movements that a skeletal system is capable of performing.

Motion within the degree(s) of freedom allowed by a joint type is usually constrained by mechanical stops and elastic ligaments associated with the construction of the anatomical joint, which can be modeled as joint angle-dependent internal forces acting on the skeleton. Environmental forces arise when the skeletal system contacts the environment such as foot-ground and hand-tool contacts. These forces are modeled by equations that represent the dynamics of the contact between the body segment and the environment. The calculation and the application of a given muscle force is more complicated. The correct calculation and application of muscle force to the skeletal system requires knowledge of the correct path of the muscle from its origin to its insertion [19].

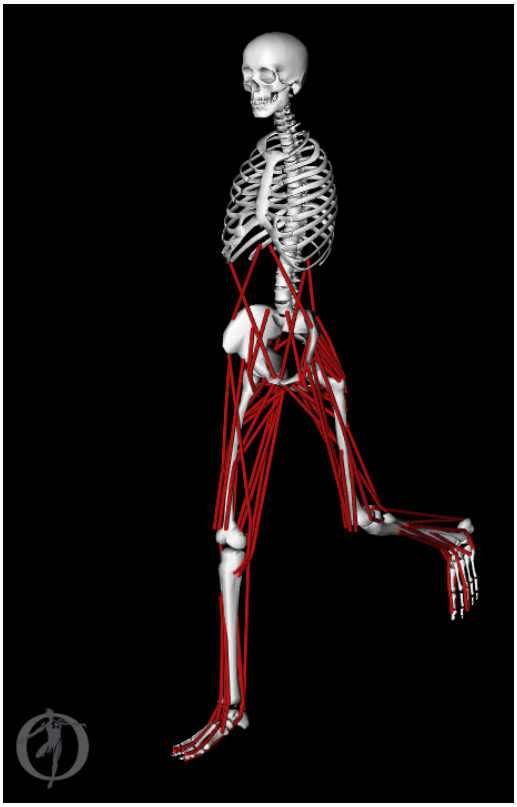

Figure 1.2 – 3D Opensim gait musculoskeletal model 2392.

As the muscles stretch from its origin to its insertion, they commonly wrap around multiple complex anatomical obstacles such as bones and neighboring tissue, thus most muscle paths cannot be represented adequately by straight lines. Therefore, a broad variety of muscle model wrapping approaches has been reported in the literature. Finite element algorithms [20] provide the highest level of detail because they allow for considering muscle deformations and use realistic bone geometry for wrapping, but they are computationally expensive. In the majority of musculoskeletal models, muscle paths are approximated by wrapping around geometric obstacle surfaces representing bone and tissue [21] [22] or simply by plural straight lines via several points [23]. Commercial musculoskeletal models can be

found as, for example, Anybody [24] or SIMM [25], but researchers commonly use the open-source software Opensim [26] (Figure 1.2) or develop their own model.

In addition of the different geometries, muscle modeling can consider the muscle physiology, providing the feasible muscle forces according to the complex relation with the muscle length, muscle contraction velocity and activation state. Hill-type muscle model [19] is commonly used to consider these restrictions. However, the high stiffness of the tendon generates some computational difficulties and drive the authors to consider it as rigid [27] or to directly neglect the physiological constraints [28]. Quantitative models of muscle contraction are crucial for understanding neural control of movement.

1.2.3 Central nervous system strategy

A large set of muscles is commanded in a precise sequence by the CNS. The fundamental problem is that there are more muscles serving each degree of freedom of the system than those strictly necessary from the mechanical point of view, which implies that, in principle, an infinite number of recruitment patterns are acceptable. This problem is often referred to as the redundancy problem of the muscle recruitment [29] or the force-sharing problem [30]. Experimental studies [31] and EMG collections [32] suggest that a specific strategy of muscle coordination is chosen by the CNS to perform a given motor task. The actual strategy selected from this set will likely depend on factors such as metabolic energy consumption, whose minimization is clearly advantageous for survival.

A popular mathematical approach for solving the muscle recruitment problem is the optimization method, which can be associated to inverse or forward dynamics [33]. These methods minimize or maximize some criterion (objective function or cost function) which reflects the mechanism used by the CNS to recruit muscles for the movement considered. The proper cost function is not known a priori, so the adequacy of the chosen function must be validated according to the obtained results [34]. Many criteria have been proposed in the literature to predict muscular activations.

Activity patterns appear to be different for each muscle, although certain features are common to many muscles. In fact, there is analytical evidence that many muscles may share certain activity patterns. In the last decades, some authors determined whether the main features of the EMG patterns could be described by a few underlying components [35], [36] and [37]. Later, by applying other mathematical methods, researchers demonstrated that the CNS use muscle synergies in order to simplify the muscular control [38] [39].

1.2.4 Energy consumption

Physiological energy expenditure estimation has proven to be a reliable method of quantitatively assessing the penalties imposed by gait disability [40]. While energy consumption is generally experimentally based on the oxygen consumption (VO_2) measured with gas analyzer [41] [40] [42] or estimated by heart rate monitoring [43] [41] [44], these processes require maintaining a constant activity during several

minutes and wearing uncomfortable devices which can be a limitation for some activities or subjects.

So, use of musculoskeletal models to estimate the energy consumption shows a great interest to avoid the previous limitation. In the last decades, several methods have been proposed to computationally estimate the human energy expenditure during gait [45] [46] [47], and some of them were compared in [48].

As energy expenditure computational methods are directly linked with the muscular activity, the force-sharing problem needs to be solved first by optimization, regardless of whether it is an inverse or forward dynamics approach [49]. By the way, Hill-type muscle parameters are extracted from this step to be used as input of the mentioned methods to computationally estimate the human energy expenditure during gait. Accuracy of the neuromusculoskeletal model chosen is consequently fundamental.

1.2.5 Spinal-cord-injured subjects

The spinal cord is the part of the CNS that lies inside the spine. It is an essential structure to the sensations coming from our body and to the motor functions. A spinal cord injury cuts off communication between the brain and the body and causes total or partial paralysis of the limbs and trunk. The extent of paralysis depends on the location of the wound in the spine and its severity (Figure 1.3) [50]. A low lesion causes paraplegia, that is, paralysis of the lower limbs, while a high lesion in the cervical vertebrae, for example, causes quadriplegia, the paralysis of the four limbs.

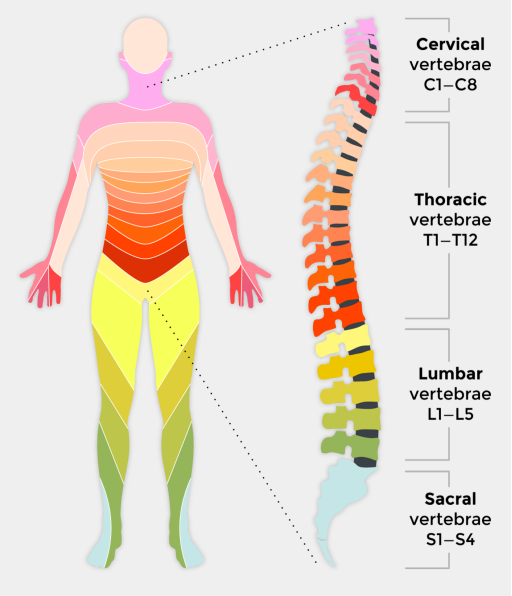

Figure 1.3 – Spinal cord injury levels.

However, the level of the injury is not enough to determine the associated damage. The same injury can have different consequences on subjects. For this reason,

the American Spinal Injury Association (ASIA) published the International Standards for Neurological Classification of Spinal Cord Injury (ISNCSCI) to evaluate the motor scores [50]. At lower extremities, the lower extremity muscle score (LEMS) is used to evaluate SCI subjects. Muscles function grading of Figure 1.4 are defined as follows:

- 0 = total paralysis,
- 1 = palpable or visible contraction,
- 2 = active movement, full range of motion (ROM) with gravity eliminated,
- 3 = active movement, full ROM against gravity,
- 4 = active movement, full ROM against gravity and moderate resistance in a muscle specific position,
- 5 = (normal) active movement, full ROM against gravity and full resistance in a functional muscle position expected from an otherwise unimpaired person,
- 5* = (normal) active movement, full ROM against gravity and sufficient resistance to be considered normal if identified inhibiting factors (i.e. pain, disuse) were not present,
- NT = not testable (i.e. due to immobilization, severe pain such that the patient cannot be graded, amputation of limb, or contracture of $> 50\%$ of the normal ROM).

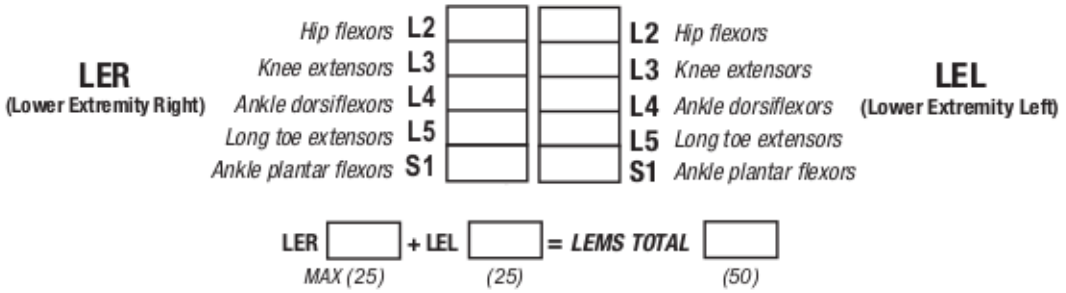

Figure 1.4 – LEMS evaluation.

In addition to reducing motor function, the lesion in most cases affects the functioning of organs below the level of the lesion, including the bladder and intestines. It also deprives the spinal cord injured of its sensitivity in areas of the body whose nerves are connected to the spinal cord below the site of the lesion. Spinal cord injuries are often the result of accidents: road accidents, falls, diving accidents, accidents at work, etc.

Because the spinal cord controls the functioning of the lower and upper limbs, SCI people often have to use a wheelchair [6]. Subjects selected for our experiments were able to walk with crutches but required in addition the assistance of passive KAFO (Figure 1.5), commonly referred to with the term "caliper" few years ago. Advances in both material science and orthotic design have resulted in improved functional outcomes for individuals who require lower limb orthoses [51]. However, KAFO provokes a biomechanical problem for the normal gait pattern. By locking the knee to allow subjects to stand and ambulate safely, subjects are unable to clear the floor during swing phase, which causes an abnormal gait pattern, with either

hip hiking, abducted swing, or excessive heel rise (vaulting) on the contralateral side, all combined with higher loads in upper extremities by using crutches which create other long-term problems for the patient [52]. With technical advancements controlling how and when the knee locks and unlocks during stance and swing phase (active orthoses), it is expected that more patients who are bound to wheelchairs will be able to ambulate with fewer complications.

Figure 1.5 – KAFO.

Because of the mentioned difficulties, the two subjects of this study mainly used a wheelchair to move in daily life, and resorted to the crutch-assisted gait with KAFO only occasionally and during short periods of time.

In order to apply the analysis methods used in healthy people to SCI subjects, neuromusculoskeletal models have to be personalized to each subject due to the uniqueness of each injury and its consequences.

1.3 Objectives

The objective of this work is to evaluate the effect of orthotic devices on SCI subjects and the likeliness of its long-term use, through the estimation of some indicators as joint reactions and energetic cost, which in turn require the estimation of muscular activations and forces. To this end, some partial goals are set:

- Selection of a neuromusculoskeletal model for healthy subjects and adaptation to SCI subjects.
- Comparison, at accuracy and efficiency levels, of several methods for the solution of the muscle recruitment problem, and proposal of use criteria depending on the application.
- Validation of two methods for energetic cost estimation in healthy gait.
- Application of the previously selected models and methods to the crutch-orthosis-assisted gait of SCI subjects and comparison between a passive and an active orthotic device.

1.4 Contributions

The contributions of this thesis can be summarized as follows:

— A synergy-based approach is presented for the inverse-dynamics based analysis of human gait at neuromusculoskeletal level, which calculates synergies by applying non-negative matrix factorization to the activations coming from a static optimization. This approach is compared with other synergy-based approach proposed in the literature, and with EMG measurements.

— A co-simulation algorithm is shown for the forward-dynamics based analysis of human gait at neuromusculoskeletal level, which enables to separately integrate the equations of motion and the muscular dynamic equations, thus allowing to use codes for general multibody-dynamics simulation. This algorithm is compared with the popular computed muscle control (CMC) algorithm.

— An extensive comparison is carried out, both in terms of accuracy and efficiency, among several variants of inverse- and forward-dynamics based approaches for the analysis of human gait at neuromusculoskeletal level. Criteria of use are then drawn based on the comparison results.

— Two methods proposed in the literature for the estimation of energetic cost are validated in healthy gait with experimental results and results from literature, and indications are given for their application.

— A neuromusculoskeletal model is proposed for SCI subjects walking with the help of KAFO and crutches, along with a way to personalize the model to a particular subject.

— The gait of a bilateral SCI subject is analyzed, by application of the techniques previously developed in the thesis, when wearing a pair of conventional passive orthoses. Results of the muscular force-sharing problem are assessed by comparison with EMG measurements, and reaction forces at shoulders are estimated. Furthermore, gait improvement is studied at kinematic level when wearing active orthoses.

— The gait of a unilateral SCI subject is analyzed, by application of the techniques previously developed in the thesis, when wearing either a pair of passive or active orthoses. Results of the muscular force-sharing problem are assessed by comparison with EMG measurements. Both reaction forces at shoulders and energetic cost are estimated for the two types of orthotic devices, and improvement provided by the active system is studied at kinematic and dynamic levels.

1.5 Thesis outline

The remainder of this thesis is organized as follows:

Chapter 2 introduces musculoskeletal model, the muscle model and the mutibody-dynamics formulation used in this thesis.

Chapter 3 compares several optimization methods for estimating muscle forces in human gait using inverse- and forward-dynamics approaches.

Chapter 4 presents two methods from the literature to estimate the muscular energy expenditure: Umberger's and Bhargava's methods.

Chapter 5 shows the application of the methods proposed in previous chapters to two SCI subjects walking with two types of orthotic devices and compares their effect on the subjects' gait.

Chapter 6 draws the conclusions and indicates future research lines.

Chapter 2

Human models, multibody formulation and data collection

2.1 Subjects and models

2.1.1 Subjects

Five voluntary healthy subjects whose characteristics are presented in Table 2.1 were recorded during walking for the experimental validation of the different methods treated in this work.

2.1.2 Skeletal model

The human body is modeled as a 3D multibody system formed by rigid bodies, as shown in Figure 2.1. It consists of 18 anatomical segments: two hindfeet, two forefeet, two shanks, two thighs, pelvis, torso, neck, head, two arms, two forearms and two hands. The segments are linked by ideal spherical joints, thus defining a model with 57 degrees of freedom. The global axes are defined as follows: x-axis in the antero–posterior direction, y-axis in the medio–lateral direction, and z-axis in the vertical direction. The computational model is defined with 228 mixed (natural + angular) coordinates. The subset of natural coordinates comprises the three Cartesian coordinates of 22 points, and the three Cartesian components of 36 unit vectors, thus making a total of 174 variables. The points correspond to the positions of all the spherical joints (white dots in Figure 2.1, left and center), along

	Subjects				
	1	**2**	**3**	**4**	**5**
Gender	Male	Male	Male	Female	Male
Age	28	26	58	30	28
Weight (kg)	86	74	96	50	99
Height (cm)	187	182	190	165	180
Speed (m/s)	1,18	1,29	1,14	0,92	1,20

Table 2.1 – Characteristics of the five healthy subjects.

with points of the five distal segments -head, hands and forefeet- (black dots in Figure 2.1). Each one of the 18 bodies is defined by its proximal and distal points, plus two orthogonal unit vectors aligned at the antero–posterior and medio–lateral directions, respectively, when the model is in a standing posture. The remaining 54 variables are the 18 sets of 3 angles that define the orientation of each body with respect to the inertial frame.

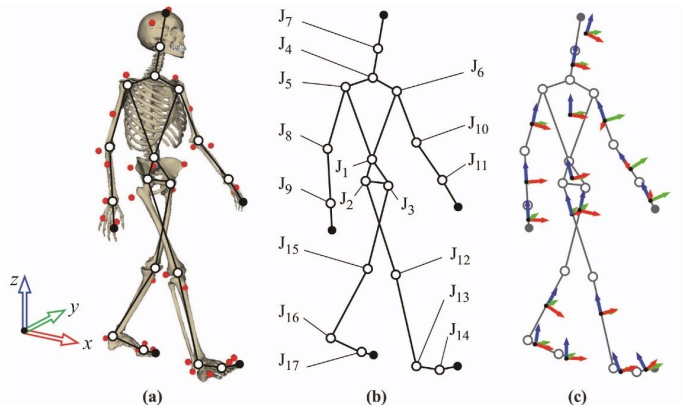

Figure 2.1 – 3D human model.

The geometric and inertial parameters of the model are obtained, for the lower limbs, by applying correlation equations from a reduced set of measurements taken on the subject, following the procedures described in [53].

For the upper part of the body, data from standard tables [33] is scaled according to the mass and height of the subject. In order to adjust the total mass of the subject, a second scaling is applied to the inertial parameters of the upper part of the body.

The kinematic information of the motion is obtained from the trajectories of the 37 markers attached to the subject's body (red dots in Figure 2.1, left), which are captured at 100 Hz frequency by means of the 12 infrared cameras. Position data are filtered using an algorithm based on Singular Spectrum Analysis (SSA) [54] and the natural coordinates of the model are calculated using algebraic relations. Afterwards, a minimization procedure ensures the kinematic consistency of the natural coordinates. From that information, the histories of a set of 57 independent coordinates -as many as the system degrees of freedom- formed by the Cartesian coordinates of the position vector of the lumbar joint and the 18 x 3 angles that define the absolute orientation of each body, are kinematically obtained and approximated by using B-spline curves. Analytical differentiation yields the corresponding velocity and acceleration histories. More detail about the treatment of the captured data can be found in [17].

2.1.3 Musculoskeletal model

Gait studies for healthy people focus on lower limbs. 43 muscles have been considered in each leg of the model plus 6 muscles in the pelvis (Figure 2.2). Geometries and properties of the muscles have been taken from OpenSim [26], which are defined for the OpenSim reference model. According to the aim of the studies the number of

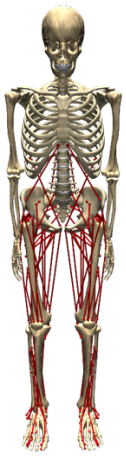

Figure 2.2 – Musculoskeletal model.

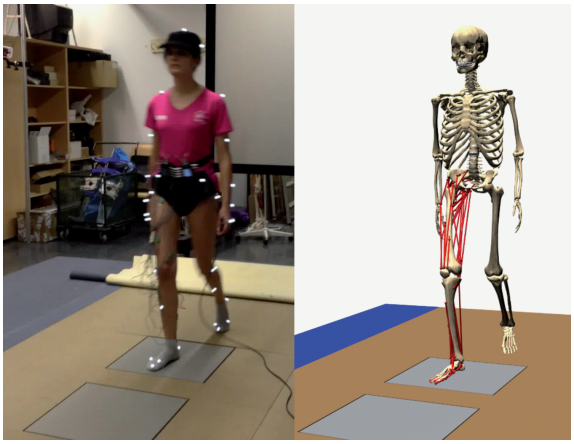

Figure 2.3 – Gait of healthy subject: acquired motion (left); computational model (right).

muscles can be reduced. For example, to estimate the muscular forces during gait, muscles on the right leg have only been considered due to the symmetric behaviour (Figure 2.3), whereas to estimate the whole energy consumption all the muscles of the lower limb have been take into account.

A scale factor is derived for each segment by comparing its dimensions with those of the reference model. This factor is applied to obtain the corrected location of the origin and insertion points in the segment. Then, lengths of muscles are calculated from the standing position and compared with their counterparts in the reference model, thus yielding a scale factor for each muscle. This scale factor is applied to muscle parameters as the tendon slack length and the optimal muscle fiber length. However, no recommendation has been found in the literature on how to scale the muscle maximum isometric force, which could be expected to significantly vary among different subjects.

2.2 Musculoskeletal geometry

The musculotendon length, musculotendon velocity, and moment arms of a muscle depend directly on the musculoskeletal geometry as well as on body segment configurations. These variables play an important role in generating joint torques.

2.2.1 Muscle paths

Muscles are modeled as a single or a plural straight line with several points. These points correspond to the attachment of musculotendon to bone and are defined as origin (i.e., proximal attachment) or insertion (i.e., distal attachment). Local coordinates of this points have been obtained from [26] for the lower limb and [55] for the upper limb. For musculotendon actuators with more than one single straight line, effective origins and insertions are defined when the straight path from the actual origin to the actual insertion passes through bones during certain body configurations (see Figure 2.4).

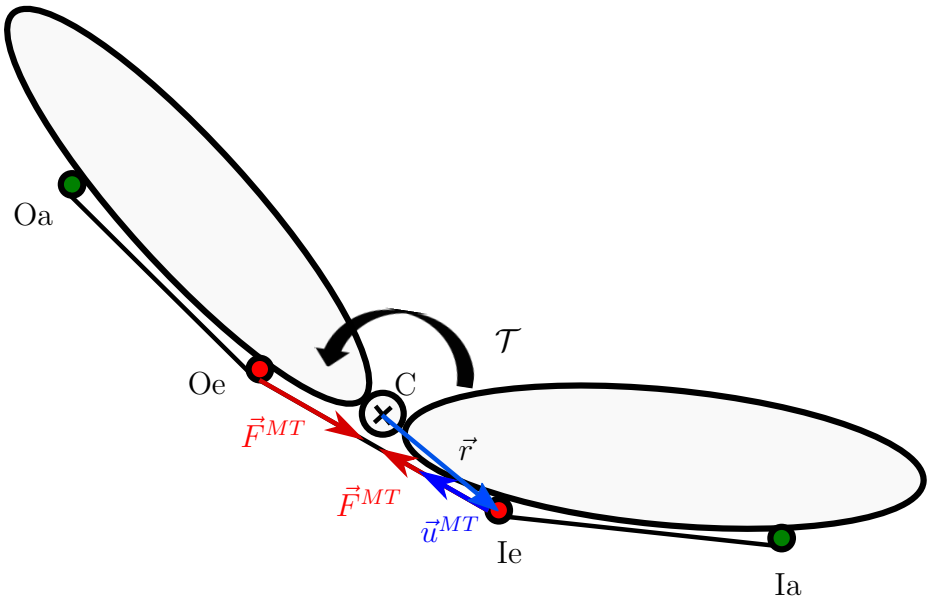

Figure 2.4 – Muscle path and line of action. O and I refer to origin and insertion, and the subscripts a and e denote actual and effective origin and insertion points, respectively.

The musculotendon length is the summation of the lengths of muscle segments that connect the points defining the muscle path. If a muscle path is defined by n points, the musculotendon length is given by

$$l^{MT} = \sum_{i=1}^{n-1} s_i \tag{2.1}$$

where s_i is the length of ith muscle segment. The musculotendon velocity is the time derivative of the musculotendon length, i.e.,

$$v^{MT} = \sum_{i=1}^{n-1} \dot{s}_i \tag{2.2}$$

The musculotendon force vector can be expressed as the unit vector $\vec{u}$ (see Figure 2.4) directed along the line of action of the muscle multiplied by the force magnitude F^{MT}, i.e.,

$$\vec{F}^{MT} = F^{MT}\vec{u}^{MT} \tag{2.3}$$

The unit vector of the line of action of the muscle is given by

$$\vec{u}^{MT} = \frac{\vec{r}_{Ie} - \vec{r}_{Oe}}{\|\vec{r}_{Ie} - \vec{r}_{Oe}\|} \tag{2.4}$$

where $\vec{r}_{Oe}$ and $\vec{r}_{Ie}$ are the locations of the effective origin and insertion of the muscle, respectively.

2.2.2 Calculation of the Jacobian of muscle moment arms

Muscle forces provide the joint torques $\mathcal{T}^{MT}$ at the multiple joints crossed by the muscle. Musculotendon forces are transformed into muscular moments by this relation:

$$\mathcal{T}^{MT} = J^{\top} F^{MT} \tag{2.5}$$

where $J^{\top}$ is the transpose of the Jacobian matrix J which is called the Jacobian matrix of muscle moment arms. There are two methods to determine J: one is the velocity-based determination method [56] and the other is the force-based determination method. In this work, the force-based determination method is used to determine the Jacobian of muscle moment arms, where, for each muscle and each joint, the moment arm vector $\vec{d}$ is obtained by the following relation:

$$\vec{d} = \vec{u}^{MT} \wedge \vec{r} = [d_x d_y d_z]^{\top} \tag{2.6}$$

$J^{\top}$ can be written as

$$J^{\top} = [\vec{d}_1 ... \vec{d}_i ... \vec{d}_m] \tag{2.7}$$

where $\vec{d}_i = [d_{1i}, ..., d_{ni}]^{\top}$ represents the ith column of $J^{\top}$ and is called the moment arm vector of muscle i, m is the number of muscles, n is the number of the muscle-driven generalized coordinates.

If the Jacobian matrix J of moment arms is a square matrix and has full rank, a unique solution exists. Normally, there are more musculotendon actuators than joint DOFs, i.e., $m > n$. In this case, $J^{\top}$ is rectangular, and its inverse is not defined. This is called actuator redundancy. This problem is resolved by optimizing an objective function that represents some neural strategy.

2.3 Musculotendon actuator dynamics

The dynamics of musculotendon actuators can be divided into activation dynamics and contraction dynamics [19]. Activation dynamics refers to the transformation of a neural excitation into an activation of the contractile apparatus, while contraction dynamics refers to the transformation of the activation to a muscle force. Thus, according to the Hill's muscle model, muscle dynamics are represented by two first-order dynamical processes which are cascaded and decoupled from each other [19]. This summary of the musculotendon actuator dynamics is provided by [57].

2.3.1 Hill's muscle model

Muscles are composed by a set of fibers and tissues, called tendons, which make the connection to the bone. Fibers, oriented either parallel to the tendon (a parallel-fibered muscle) or at an acute angle $\alpha > 0$ to the tendon (a pennated muscle, see Figure 2.6), are considered equally long. The fibers of a pennated muscle are connected to the aponeurosis of the muscle, which is the internal portion of the tendon. The properties of the internal and external portions of the tendon are assumed identical. Muscle fibers contain contractile filaments as well as non-contractile fiber strands [19].

In this study, a Hill-type model [19] is used to estimate the force generated by a musculotendon actuator. The simplified mechanical model of a musculotendon (see Figure 2.5) consists of an active contractile element (CE), a parallel passive elastic element (PE), and a serial elastic element (SE). For a pennated muscle, a relationship among the musculotendon length l^{MT} , the muscle fiber length l^{M}, the tendon length l^{T} , and the pennation angle α is given by

$$l^{MT} = l^{M} \cos\alpha + l^{T}. \tag{2.8}$$

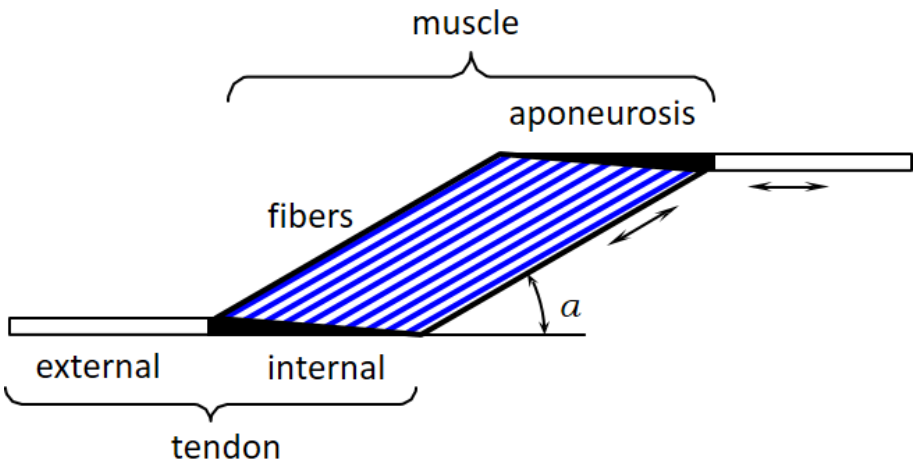

Figure 2.5 – Architecture of a pennated muscle.

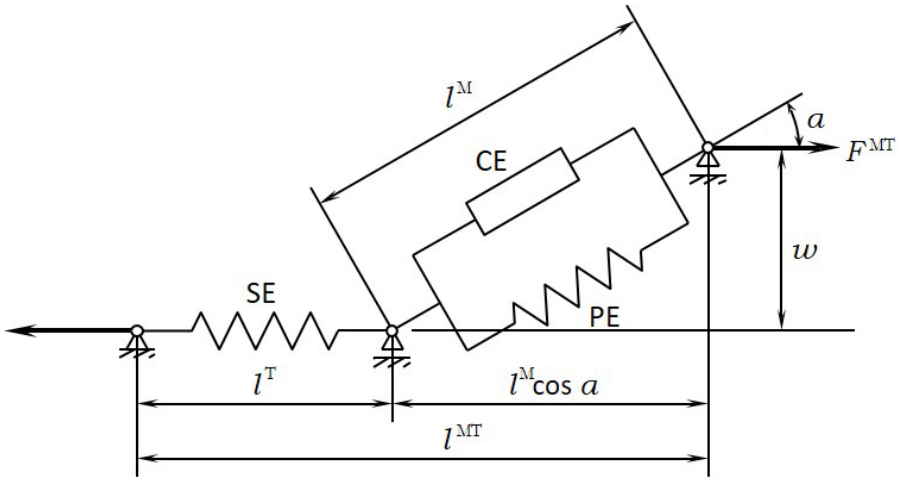

Figure 2.6 – Hill-type muscle model. The muscle fibers are modeled as an active contractile element (CE) in parallel with a passive elastic component (PE). These elements are in series with a nonlinear elastic tendon (SE). The pennation angle α denotes the angle between the muscle fibers and the tendon [19]. Superscripts MT, M, and T indicate musculotendon, muscle fiber, and tendon, respectively.

If the distance between the aponeuroses of the origin and the insertion of the muscle remains constant during the contraction of the muscle, it follows that

$$w = l_0^M \sin\alpha_0 = l^M \sin\alpha = const \tag{2.9}$$

where l_0^M is the optimal muscle fiber length and α_0 is the pennation angle corresponding to l_0^M. From Eq. (2.8) and Eq. (2.9), a velocity relationship can be obtained

$$v^{MT} = \left(\frac{v^M}{\cos\alpha}\right) + v^T. \tag{2.10}$$

2.3.2 Activation dynamics

Activation dynamics is described by an first-order ordinary differential equation [58] that contains the relationship among the muscle activation $a = a(t)$, its derivative $\dot{a} = \dot{a}(t)$, and the neural excitation $u = u(t)$ as

$$\dot{a} = (u-a)\frac{u}{\tau_{act}} + [u - (a - a_{min}) - (u-a)u]\frac{1}{\tau_{deact}} \tag{2.11}$$

where τ_{act} is the time constant for buildup of activation when the muscle is fully excited, i.e., $u(t) = 1$, and τ_{deact} is the time constant for relaxation of activation when the muscle is deactivated, i.e., $u(t) = 0$; a_{min} is a lower bound imposed on the muscle activation to deal with the problem associated with inverting the force-velocity curve of the muscle (mathematically expressed in Eq. (2.30)) at low activation levels. The ratio of τ_{act} to τ_{deact} is constant and ranges from 0 to 1 [19]. Regardless of the difference between slow and fast fibers, all muscles are assumed to have the same

activation dynamics. In this work, the activation and deactivation time constants τ_{act} and τ_{deact} are set to 15 ms and 50 ms, respectively [59] [60]; and a_{min} is set to 0.001. Figure 2.7 shows the time response of the muscle activation $a(t)$ to an excitation $u(t)$ which is switched on to $u(t) = 1$ for the time period $0.1s \leq t \leq 0.2s$ and is zero otherwise. When the muscle is fully excited, the activation goes up asymptotically from the initial value a_{min} to the maximum value 1. When the muscle is deactivated, the activation falls gradually to a_{min}.

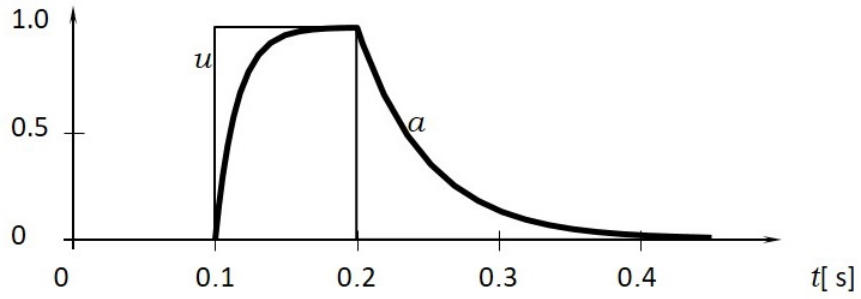

Figure 2.7 – Excitation (thin line) and its response (thick line).

The activation dynamics in Eq. (2.11) can be expressed as

$$\dot{a}(t) = f(a(t), u(t)). \tag{2.12}$$

2.3.3 Musculotendon contraction dynamics

A muscle and its tendons work together as an actuator. The contraction dynamics of the musculotendon actuator is a first-order process which follows another first-order process (activation dynamics) [19]. Due to the interaction between the contraction dynamics of musculotendon and the dynamics of body segments, the musculotendon contraction dynamics is more complex than the activation dynamics. The following describes contraction dynamics for the Hill's muscle model. For simplification, all muscle elements are assumed massless and friction is neglected. The force equilibrium equation for a muscle can be written as

$$F^{MT} = (F^M_{CE} + F^M_{PE}) \cos \alpha. \tag{2.13}$$

where F^M_{CE} and F^M_{PE} are the active and passive forces exerted by CE and PE, respectively, and F^{MT} is the tendon force which is also referred to as the force of the muscle and tendon complex. The force produced by the contractile element depends on the muscle fiber length and velocity and the activation level. It is expressed as

$$F^M_{CE} = F^M_0 \cdot a \cdot f_l(\tilde{l}^M) \cdot f_v(\tilde{v}^M) \tag{2.14}$$

where F^M_0 is the maximum isometric muscle force, $\tilde{l}^M$ is the normalized muscle fiber length, $\tilde{v}^M$ is the normalized muscle fiber velocity, and f_l and f_v are dimensionless force-length and force-velocity relationships, respectively. The normalized muscle fiber length $\tilde{l}^M$ is defined as

$$\tilde{l}^M = \frac{l^M}{l_0^M} \tag{2.15}$$

The normalized muscle fiber velocity is defined as

$$\tilde{v}^M = \frac{v^M}{v_{max}} \tag{2.16}$$

where v^M is the muscle fiber velocity and v_{max} is the maximum contraction velocity defined as $v_{max} = l^M/\tau_c$. τ_c is called the time-scaling parameter. For simplification, a standard value of $\tau_c = 0.1s$ is used for all muscle types [57]. The force of the parallel passive element F_{PE}^M and the tendon force F^{MT} can be formulated, respectively, as

$$F_{PE}^M = F_0^M \cdot f_{PE}(\tilde{l}^M) \tag{2.17}$$

and

$$F^{MT} = F_0^M \cdot f_T(\varepsilon^T) \tag{2.18}$$

where f_{PE} and f_T are the dimensionless force-length relationship and the dimensionless force-strain relationship, respectively; ε^T is the tendon strain defined as the amount of the tendon stretch relative to the tendon slack length l_S^T, i.e.,

$$\varepsilon^T = \frac{l^T - l_S^T}{l^T} \tag{2.19}$$

The rate of change of tendon force with respect to time, i.e., $\dot{F}^{MT} = dF^{MT}/dt$, is proportional to the tendon velocity v^T and is given by

$$\dot{F}^{MT} = k^T v^T \tag{2.20}$$

where k^T is the tendon stiffness which is defined as

$$k^T = \frac{dF^{MT}}{dl^T} \tag{2.21}$$

If the tendon force F^{MT}, the normalized muscle fiber length $\tilde{l}^M$, and the activation a are given, the normalized muscle velocity $\tilde{v}^M$ can be derived from Eq. (2.13), Eq. (2.14) and Eq. (2.17), and expressed as

$$\tilde{v}^M = f_v^{-1}\left(\frac{F^{MT}/\cos\alpha - F_0^M \cdot f_{PE}(l^M)}{F_0^M \cdot a \cdot f_l(l^M)}\right) \tag{2.22}$$

where ${f_v}^{-1}$ denotes the inverse of the force-velocity relationship. From Eq. (2.10), Eq. (2.16), and Eq. (2.22), the tendon velocity v^Tcan be obtained as

$$v^T = v^{MT} - \frac{v_{max}}{\cos\alpha} f_v^{-1}\left(\frac{F^{MT}/\cos\alpha - F_0^M \cdot f_{PE}(l^M)}{F_0^M \cdot a \cdot f_l(l^M)}\right). \tag{2.23}$$

Substituting Eq. (2.23) into Eq. (2.20) yields

$$\dot{F}^{MT} = k^T\left[v^{MT} - \frac{v_{max}}{\cos\alpha} f_v^{-1}\left(\frac{F^{MT}/\cos\alpha - F_0^M \cdot f_{PE}(l^M)}{F_0^M \cdot a \cdot f_l(l^M)}\right)\right]. \tag{2.24}$$

The normalized muscle fiber length $\tilde{l}^M$ in Eq. (2.24) is unknown and can be derived from Eq. (2.8), Eq. (2.9), and Eq. (2.15) as

$$\tilde{l}^M = \frac{1}{l_0^M}\sqrt{(l^{MT} - l^T)^2 + w^2} \tag{2.25}$$

Furthermore, the tendon length l^T can be obtained from Eq. (2.18) and Eq. (2.19) as follows:

$$l^T = l_S^T \left[1 + {f_T}^{-1}\left(\frac{F^{MT}}{F_0^M}\right)\right] \tag{2.26}$$

where ${f_T}^{-1}$ denotes the inverse of the force-strain relationship of the tendon. In summary, the differential Eq. (2.24) describes the contraction dynamics of the musculotendon. Its time function can be abbreviated as

$$\dot{F}^{MT}(t) = f\left(F^{MT}(t), l^{MT}(t), v^{MT}(t), a(t)\right) \tag{2.27}$$

If the musculotendon length l^{MT}, the musculotendon velocity v^{MT}, and the activation a are input to the musculotendon actuator, then a tendon force F^{MT} is produced via the contraction dynamics. The musculotendon length l^{MT} and velocity v^{MT} depend on the position and velocity of the body segments and, in turn, the generated tendon force F^{MT} affects the motion of the body segments. Thus, there exists interaction between muscles and body segments. The complete musculotendon dynamics can be represented by a block diagram, as depicted in Figure 2.8.

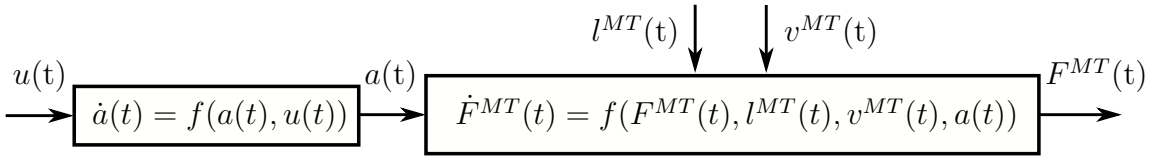

Figure 2.8 – Dynamics of the musculotendon actuator [19]

2.3.4 Muscle and tendon properties

Force-length curve

The force-length relationship of the active contractile element of a muscle can be given by [61]

$$f_l(\tilde{l}^M) = e^{-[(\tilde{l}^M - 1)/\gamma]^2} \tag{2.28}$$

where γ is a parameter that denotes the half-width of the curve at $f_l = 1/e$ (see Figure 2.9). A value of 0.45 is selected for γ^2 to approximate the force-length relationship of individual sarcomeres [59].

The force-length relationship of the passive elastic element of a muscle can be written as

$$f_{PE}(\tilde{l}^M) = \frac{e^{k_{PE}(\tilde{l}^M - 1)/\varepsilon_0^M} - 1}{e^{k_{PE}} - 1} \tag{2.29}$$

where k_{PE} is an exponential shape factor, and ε_0^M is the passive muscle strain if $F^{MT} = F_0^M$. k_{PE} is set equal to 5.0, while ε_0^M is different for young and old adults and thus is set equal to 0.6 (for young adults). $f_l(\tilde{l}^M)$ and $f_{PE}(\tilde{l}^M)$ are illustrated together in Figure 2.9.

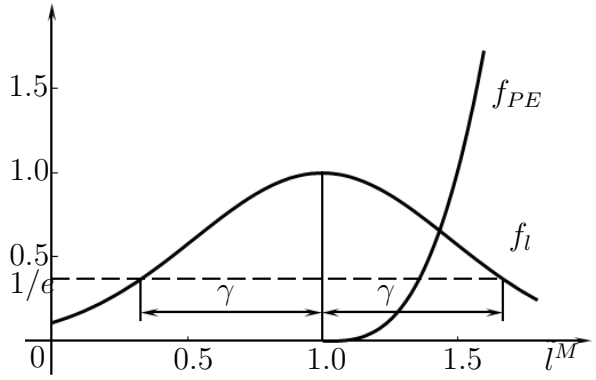

Figure 2.9 – Isometric force-length curves $f_l(l^M)$ and $f_{PE}(l^M)$ of the active contractile (CE) and passive elastic (PE) elements of the muscle.

Force-velocity curve

The force-velocity relationship is different when the muscle is shortening (i.e., $\tilde{v}^M \leq 0$) or lengthening (i.e., $\tilde{v}^M > 0$) (see Figure 2.10), and it is given by

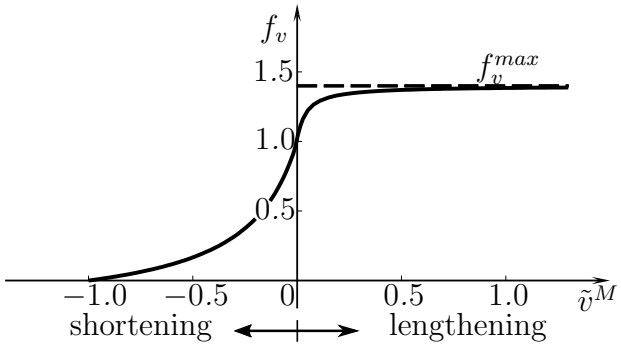

Figure 2.10 – Force-velocity curve $f_v(\tilde{v}^M)$ of the active contractile element (CE) of the muscle.

$$f_v(\tilde{v}^M) = \begin{cases} 0 & if \quad \tilde{v}^M \leq -1, \\ \dfrac{1+\tilde{v}^M}{1-\tilde{v}^M/k_{CE1}} & if \quad -1 < \tilde{v}^M \leq 0, \\ \dfrac{1+\tilde{v}^M f_v^{max}/k_{CE2}}{1+\tilde{v}^M/k_{CE2}} & if \quad \tilde{v}^M \geq 0 \end{cases} \tag{2.30}$$

where k_{CE1} and k_{CE2} are the force-velocity shape factors [62]. k_{CE1} indicates how fast the force converges to zero when the muscle is shortening; k_{CE2} indicates how fast the force converges to the maximum force when the muscle is lengthening. f_{max} is the maximum normalized achievable muscle force when the muscle is lengthening, i.e.,

$$f_v^{max} = \lim_{\tilde{v}^M \to +\infty} f_v(\tilde{v}^M). \tag{2.31}$$

In Eq. (2.30), k_{CE1} is set to 0.25 and f_v^{max} is set to 1.4 for young adults [59]. Under isometric conditions, the slop of the force-velocity curve during lengthening is about two times that during shortening [63], i.e,

$$\frac{df_v}{d\tilde{v}^M}\Big|_{\tilde{v}^M=0^+} = 2\frac{df_v}{d\tilde{v}^M}\Big|_{\tilde{v}^M=0^-}. \tag{2.32}$$

From Eq. (2.30) and Eq. (2.32) , k_{CE2} can be obtained as follows:

$$k_{CE2} = \frac{f_v^{max}-1}{2}\frac{k_{CE1}}{1+k_{CE1}}. \tag{2.33}$$

Force-strain curve

The normalized force-strain relationship of tendon (Figure 2.9) is represented by an exponential function during an initial nonlinear toe region and by a linear function thereafter, and it is given by [64]

$$f_T(\varepsilon^T) = \begin{cases} 0.10377(e^{91\varepsilon^T - 1}) & for \quad 0 \leq \varepsilon^T < 0.01516, \\ 37.526\varepsilon^T - 0.26029 & for \quad 0.01516 \leq \varepsilon^T < 0.1 \end{cases} \tag{2.34}$$

The linear region begins at strain $\varepsilon^T = 0.01516$ and fails at $\varepsilon^T = 0.1$ [19]. The strain in the tendon is termed ${\varepsilon^T}_0$ for $F^{MT} = F_0^M$, and thus $\varepsilon_0^T = 0.0336$ can be found. From Eq. (2.19) and Eq. (2.21), it follows that

$$k^T = \frac{dF^{MT}}{df_T}\frac{df_T}{d\varepsilon^T}\frac{d\varepsilon^T}{dl_S^T} = \frac{F_0^M}{l_S^T}\frac{df_T}{d\varepsilon^T} \tag{2.35}$$

Substituting Eq. (2.34) into Eq. (2.35) yields

$$k^T = \begin{cases} 9.44307\frac{F_0^M}{l_S^T}e^{91\varepsilon^T} & for \quad 0 \leq \varepsilon^T < 0.01516, \\ 37.526\frac{F_0^M}{l_S^T} & for \quad 0.01516 \leq \varepsilon^T < 0.1 \end{cases} \tag{2.36}$$

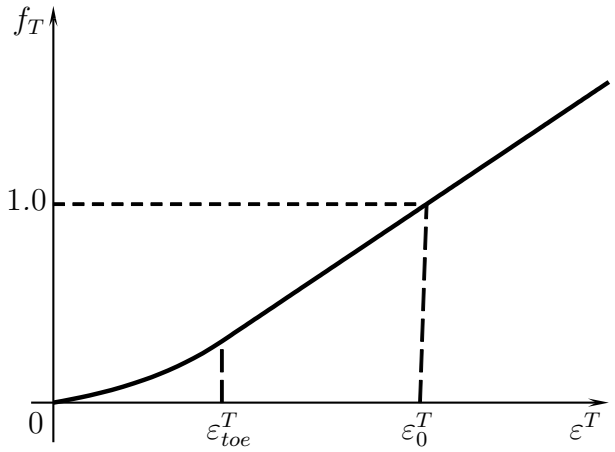

Figure 2.11 – Force-strain curve $f_T(\varepsilon^T)$ of the tendon.

2.4 Multibody dynamics (MBD)

Several options can be used for the motion description of multibody systems but, in general, a set of dependent coordinates is needed to write the dynamic equations of complex systems. Classical parameterizations in multibody dynamics are reference point coordinates [65], natural coordinates [66], or relative (joint) coordinates [67, 68, 69]. In this work, mixed coordinates (natural and relative) were used.

Matrix-R formulation was applied to set the equations of motion, and employed both in inverse- and forward-dynamics approaches. This formulation was implemented in the in-house-developed library MBSLIM [70], programmed in FORTRAN language.

2.4.1 Kinematics

The multibody approach to kinematic problems is introduced in this section. A more detailed discussion can be seen in [66]. The first step is solving the position problem. That is, obtaining the value of all the coordinates ($\mathbf{q}$) which fulfill the constraint equations once the values of the degrees of freedom ($\mathbf{z}$) are known. To do that, the constraint equations are written as follows:

$$\mathbf{\Phi} = \mathbf{0} \tag{2.37}$$

where $\mathbf{\Phi}$ is the vector of the constraint equations. The constraint equations are, in general, nonlinear equations, hence an iterative method is used to solve the problem. Usually, the Newton-Raphson method, which is based on a linearization, is employed:

$$\mathbf{\Phi}(\mathbf{q}, t) \approx \mathbf{\Phi}(\mathbf{q}_0, t) + \mathbf{\Phi}_\mathbf{q}(\mathbf{q}_0, t)(\mathbf{q} - \mathbf{q}_0) = \mathbf{0} \tag{2.38}$$

where $\mathbf{\Phi}_\mathbf{q}$ is the Jacobian matrix of the constraints with respect to the coordinates. Rearranging the terms of this equation, the next iterative expression is obtained:

$$\mathbf{\Phi}_\mathbf{q}(\mathbf{q}_i, t)(\mathbf{q}_{i+1} - \mathbf{q}_i) = -\mathbf{\Phi}(\mathbf{q}_i, t) \tag{2.39}$$

where the values corresponding to the degrees of freedom are not modified. This system must be solved until the position problem converges to the desired accuracy.

The next kinematic problem to be solved is the velocity problem. Similarly to the position problem, the velocity problem consist in finding the vector of dependent velocities $\dot{\mathbf{q}}$ which fulfill the velocity constraints, given a position $\mathbf{q}$ of the system, and the velocity of the degrees of freedom, $\dot{\mathbf{z}}$. The velocity constraints $\dot{\mathbf{\Phi}}$ can be expressed as follows:

$$\dot{\mathbf{\Phi}} = \mathbf{\Phi_q}\dot{\mathbf{q}} + \mathbf{\Phi}_t = \mathbf{0} \quad \Rightarrow \quad \mathbf{\Phi_q}\dot{\mathbf{q}} = -\mathbf{\Phi}_t \tag{2.40}$$

where $\mathbf{\Phi}_t$ is the partial derivative of $\mathbf{\Phi}$ with respect to time t. This problem is linear, so the unknown values of $\dot{\mathbf{q}}$ are obtained in one step. Again, the values of the degrees of freedom are known, so they are not modified.

The last problem in kinematics is the acceleration problem: provided a position vector $\mathbf{q}$ and a velocity vector $\dot{\mathbf{q}}$ which fulfill the constraints at position and velocity respectively, and given the acceleration $\ddot{\mathbf{z}}$ of the degrees of freedom of the mechanism, the vector of dependent accelerations $\ddot{\mathbf{q}}$ which fulfill the acceleration constraints is obtained. The constraints at acceleration level can be written as:

$$\ddot{\mathbf{\Phi}} = \dot{\mathbf{\Phi}}_\mathbf{q}\dot{\mathbf{q}} + \mathbf{\Phi_q}\ddot{\mathbf{q}} + \dot{\mathbf{\Phi}}_t = \mathbf{0} \quad \Rightarrow \quad \mathbf{\Phi_q}\ddot{\mathbf{q}} = -\mathbf{\Phi}_t - \dot{\mathbf{\Phi}}_\mathbf{q}\dot{\mathbf{q}} \tag{2.41}$$

Again, this problem is linear, so the unknown values of $\ddot{\mathbf{q}}$ are obtained from the previous equation by solving the linear system.

2.4.2 Matrix-R formulation

The equations of a multibody system in their most general form can be expressed as a system of index-3 differential-algebraic equations (DAE):

$$\mathbf{M}\ddot{\mathbf{q}} + \mathbf{\Phi_q}^\top\boldsymbol{\lambda} = \mathbf{Q} \tag{2.42a}$$

$$\mathbf{\Phi} = \mathbf{0} \tag{2.42b}$$

where $\mathbf{M}$ is the mass matrix, $\boldsymbol{\lambda}$ is the vector of Lagrange multipliers, and $\mathbf{Q}$ is the vector of external forces. The term $-\mathbf{\Phi_q}^\top\boldsymbol{\lambda}$ represents the reaction forces. To solve this system of equation, a method based on a projection matrix, called matrix $\mathbf{R}$, and described in [66] is used.

First, a constant matrix projection matrix $\mathbf{D}$ is considered. The independent velocities $\dot{\mathbf{z}}$ are given by the projection of the dependent velocities $\dot{\mathbf{q}}$ over the rows of this matrix:

$$\dot{\mathbf{z}} = \mathbf{D}\dot{\mathbf{q}} \tag{2.43}$$

Writing Eqs. (2.40) and (2.43) together in matrix form yields:

$$\begin{bmatrix}\mathbf{\Phi_q}\\ \mathbf{D}\end{bmatrix}\dot{\mathbf{q}} = \begin{bmatrix}-\mathbf{\Phi}_t\\ \dot{\mathbf{z}}\end{bmatrix} \tag{2.44}$$

The rows of the $\mathbf{D}$ matrix are linearly independent from the rows of the Jacobian matrix of the constraints $\mathbf{\Phi_q}$. Hence, the matrix on the left-hand side (LHS) of the equation can be inverted, leading to:

$$\dot{\mathbf{q}} = \begin{bmatrix}\mathbf{\Phi_q}\\ \mathbf{D}\end{bmatrix}^{-1}\begin{bmatrix}-\mathbf{\Phi}_t\\ \dot{\mathbf{z}}\end{bmatrix} \equiv \begin{bmatrix}\mathbf{S} & \mathbf{R}\end{bmatrix}\begin{bmatrix}-\mathbf{\Phi}_t\\ \dot{\mathbf{z}}\end{bmatrix} = -\mathbf{S}\mathbf{\Phi}_t + \mathbf{R}\dot{\mathbf{z}} \tag{2.45}$$

where the term $\mathbf{R}\dot{\mathbf{z}}$ represents the general solutions of the homogeneous velocity equation, and the term $-\mathbf{S}\boldsymbol{\Phi}_t$ represents a particular solution of the complete equation.

Differentiating Eq. (2.44) with respect to time, and rearranging the terms yields:

$$\begin{bmatrix} \boldsymbol{\Phi}_\mathbf{q} \\ \mathbf{D} \end{bmatrix} \ddot{\mathbf{q}} = \begin{bmatrix} -\dot{\boldsymbol{\Phi}}_t - \dot{\boldsymbol{\Phi}}_\mathbf{q}\dot{\mathbf{q}} \\ \ddot{\mathbf{z}} \end{bmatrix} \tag{2.46}$$

Solving for $\ddot{\mathbf{q}}$ and introducing the matrices $\mathbf{S}$ and $\mathbf{R}$ defined in Eq. (2.45),

$$\ddot{\mathbf{q}} = \begin{bmatrix} \boldsymbol{\Phi}_\mathbf{q} \\ \mathbf{D} \end{bmatrix}^{-1} \begin{bmatrix} -\dot{\boldsymbol{\Phi}}_t - \dot{\boldsymbol{\Phi}}_\mathbf{q}\dot{\mathbf{q}} \\ \ddot{\mathbf{z}} \end{bmatrix} = \mathbf{S}\left(-\dot{\boldsymbol{\Phi}}_t - \dot{\boldsymbol{\Phi}}_\mathbf{q}\dot{\mathbf{q}}\right) + \mathbf{R}\ddot{\mathbf{z}} \tag{2.47}$$

Substituting Eq. (2.47) in Eq. (2.42a), and premultiplying by $\mathbf{R}^\top$,

$$\mathbf{R}^\top \left\{ \mathbf{M}\left[\mathbf{S}\left(-\dot{\boldsymbol{\Phi}}_t - \dot{\boldsymbol{\Phi}}_\mathbf{q}\dot{\mathbf{q}}\right) + \mathbf{R}\ddot{\mathbf{z}}\right] + {\boldsymbol{\Phi}_\mathbf{q}}^\top \boldsymbol{\lambda} \right\} = \mathbf{R}^\top \mathbf{Q} \tag{2.48}$$

Rearranging, and keeping in mind that the matrix $\mathbf{R}$ is the orthogonal complement of the Jacobian of the constraints $\boldsymbol{\Phi}_\mathbf{q}$, hence $\boldsymbol{\Phi}_\mathbf{q}\mathbf{R} = \mathbf{0}$:

$$\mathbf{R}^\top \mathbf{M}\mathbf{R}\ddot{\mathbf{z}} = \mathbf{R}^\top \mathbf{M}\mathbf{S}\left(\dot{\boldsymbol{\Phi}}_t + \dot{\boldsymbol{\Phi}}_\mathbf{q}\dot{\mathbf{q}}\right) + \mathbf{R}^\top \mathbf{Q} \tag{2.49}$$

$$\mathbf{R}^\top \mathbf{M}\mathbf{R}\ddot{\mathbf{z}} = \mathbf{R}^\top \left[\mathbf{Q} + \mathbf{M}\mathbf{S}\left(\dot{\boldsymbol{\Phi}}_t + \dot{\boldsymbol{\Phi}}_\mathbf{q}\dot{\mathbf{q}}\right)\right] \tag{2.50}$$

For scleronomous systems, $\boldsymbol{\Phi}_t = \mathbf{0}$, thus some simplifications can be introduced:

$$\dot{\mathbf{q}} = \mathbf{R}\dot{\mathbf{z}} \tag{2.51}$$

$$\ddot{\mathbf{q}} = \dot{\mathbf{R}}\dot{\mathbf{z}} + \mathbf{R}\ddot{\mathbf{z}} \tag{2.52}$$

leading to the following equation of motion:

$$\mathbf{R}^\top \mathbf{M}\mathbf{R}\ddot{\mathbf{z}} = \mathbf{R}^\top \left[\mathbf{Q} - \mathbf{M}\dot{\mathbf{R}}\dot{\mathbf{z}}\right] \tag{2.53}$$

Matrix $\mathbf{R}$ can be calculated symbolically in some simple cases, but it is usually calculated numerically at every time step from a velocity analysis: the i^{th} column of $\mathbf{R}$ is the vector of dependent velocities when the i^{th} degree of freedom has a unit velocity and all the others null velocity.

The term $-\mathbf{S}\left(\dot{\boldsymbol{\Phi}}_t + \dot{\boldsymbol{\Phi}}_\mathbf{q}\dot{\mathbf{q}}\right)$, which becomes $\dot{\mathbf{R}}\dot{\mathbf{z}}$ in scleronomous systems, represents the vector of velocity-dependent accelerations, hence it can be calculated numerically by doing an acceleration analysis in which all the degrees of freedom have a null acceleration.

Therefore, the equations of motion Eq. (2.53) can be written in a compact form as,

$$\bar{\mathbf{M}}\ddot{\mathbf{z}} = \bar{\mathbf{Q}} \tag{2.54}$$

with and the mass matrix and vector of generalized forces referred to $\mathbf{z}$, respectively. The number of equations in Eq. (2.54) is 57, as many as the number of degrees of freedom of the model.

For the forward-dynamics analysis, the equations of motion (Eq. (2.54)) were numerically integrated in time by means of the single step, fixed time step, trapezoidal rule.

2.4.3 Inverse dynamics

The inverse-dynamics analysis (IDA) of the experimentally measured motion allows to obtain the net joint torques and ground reactions. The histories of positions, velocities and accelerations of the independent coordinates, and of the dependent coordinates, are already known from the processing of the motion capture data. Then, writing the equations of motion Eq. (2.54) as,

$$\bar{\mathbf{M}}\ddot{\mathbf{z}} = \mathbf{Q_m} + \mathbf{Q_c} \tag{2.55}$$

where $\mathbf{Q_m}$ is the vector of generalized motor forces and $\mathbf{Q_c}$ is the vector grouping all the remaining generalized forces (centrifugal and Coriolis forces), the unknown vector can be obtained as,

$$\mathbf{Q_m} = \bar{\mathbf{M}}\ddot{\mathbf{z}} - \mathbf{Q_c} \tag{2.56}$$

which provides the net joint torques and the ground reactions that produced the acquired motion, taking the pelvis as the base body.

2.4.4 Forward dynamics: Computed Torque Control

Forward-dynamics analysis (FDA) of the acquired gait motion consists of using trajectory tracking controllers associated to all the system degrees of freedom. This implies assuming that there exist actuators not only at joint level, which is indeed the case, but also for the six degrees of freedom of the base body, which does not obviously correspond to reality.

The equations of motion Eq. (2.54) are written again as,

$$\bar{\mathbf{M}}\ddot{\mathbf{z}} = \mathbf{Q_u} + \mathbf{Q_c} \tag{2.57}$$

where $\mathbf{Q_u}$ is the vector of the inputs provided by the controllers and $\mathbf{Q_c}$ is the vector of the remaining generalized forces with the pelvis as the base body.

The actuation provided by the so-called computed torque control (CTC) is used as input of the FDA [71]. Then, the inputs provided by the controllers are,

$$\mathbf{Q_u} = \bar{\mathbf{M}}\left[\ddot{\mathbf{z}}_{ref} + \mathbf{K}_D(\dot{\mathbf{z}}_{ref} - \dot{\mathbf{z}}) + \mathbf{K}_P(\mathbf{z}_{ref} - \mathbf{z})\right] - \mathbf{Q_c} \tag{2.58}$$

where $\mathbf{z}_{ref}$ is the vector containing the reference signals of the controllers, which are the measured values of the independent coordinates, and $\mathbf{z}$ is the vector containing the actual values of the independent coordinates. The gains of the controllers are gathered in the diagonal matrices $\mathbf{K}_D$ and $\mathbf{K}_P$, whose values, k_{Di} and k_{Pi} are associated to each independent coordinate.

As explained in [71], the error dynamics of this control method is represented by a system of second order differential equations, having $\mathbf{K}_D$ and $\mathbf{K}_P$ as coefficients of the proportional and first derivative terms, respectively. Therefore, imposing the relation,

$$k_{Di} = 2\sqrt{k_{Pi}} \tag{2.59}$$

between the gains associated to a certain coordinate, critical damping is achieved, so that only one gain value should be tuned by coordinate.

2.4.5 Splitting of the equations of motion

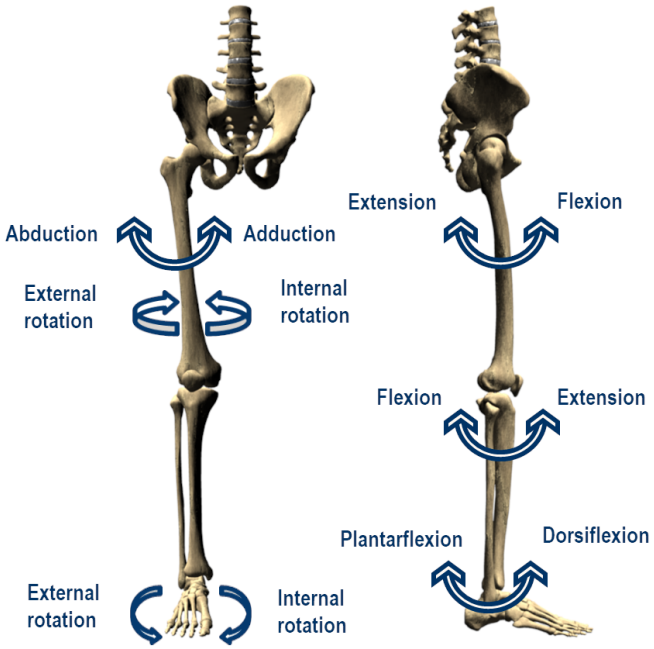

Figure 2.12 – Degrees of freedom considered as actuated by muscles at the leg.

It has been said when describing the human model that spherical kinematic pairs have been considered for all the joints. This means that three joint drive torques are obtained at each joint from the dynamic analysis. However, the motion of all the degrees of freedom is not due to muscle actuation. For example, it is clear that the abduction/adduction torque at the knee is not provided by muscles, but rather by other joint structures as condyles and ligaments, being more a reaction moment than a drive torque. Therefore, the following joint drive torques have been selected in this work: the three torque components at the trunk and the hip, the flexion/extension torque at the knee, and the plantarflexion/dorsiflexion and external/internal rotation torques at the ankle (Figure 2.12). A discussion on how the modeling of the joints and the torques considered in the optimization affect to the results can be found in [72]. Starting from the general multibody formulation, Eq. (2.56), muscle driven (md) joints were separated from the other guided degrees of freedom (gui) to solve the muscle force sharing problem as follows:

$$\begin{bmatrix} \mathbf{Q_m}^{gui} \\ \mathbf{Q_m}^{md} \end{bmatrix} = \begin{bmatrix} \bar{\mathbf{M}}_{11} & \bar{\mathbf{M}}_{12} \\ \bar{\mathbf{M}}_{21} & \bar{\mathbf{M}}_{22} \end{bmatrix} \begin{bmatrix} \ddot{\mathbf{z}}_{gui} \\ \ddot{\mathbf{z}}_{md} \end{bmatrix} - \begin{bmatrix} \mathbf{Q_c}^{gui} \\ \mathbf{Q_c}^{md} \end{bmatrix} \tag{2.60}$$

From equation Eq. (2.60), the equation of motion with respect to the muscle driven degrees of freedom can be obtained as follows:

$$\mathbf{Q_m}^{md} = \bar{\mathbf{M}}_{22}\ddot{\mathbf{z}}_{md} + \bar{\mathbf{M}}_{21}\ddot{\mathbf{z}}_{gui} - \mathbf{Q_c}^{md} \tag{2.61}$$

and simplified as:

$$\mathbf{Q_m}^{md} = \bar{\mathbf{M}}_{22}\ddot{\mathbf{z}}_{md} + H(\mathbf{z}, \dot{\mathbf{z}}, \ddot{\mathbf{z}}). \tag{2.62}$$

2.4.6 Multiple support

The obtained ground reactions and net joint torques either with IDA or FDA correspond to the ones considering the pelvis as the base body. However, joint torques produced by muscles correspond to the internal torques $\mathcal{T}$ when the feet are considered as the base body, since the external reactions act on the feet, not on the pelvis.

Fortunately, the torques obtained with the pelvis as the base body can easily be transformed to their counterparts when the supporting foot is considered as the base body, thus yielding the proper values of external reactions and net joint torques. However, when the two feet are contacting the ground, the external reactions must be distributed between them. In this work, this was done in the same proportion shown by the reactions measured by the force plate (FPL), following the approach presented in [73].

As long as there is only one foot in contact with the ground, as it happens in normal gait during the swing phase, the joint torques can be obtained without the aid of FPL measurements, since the actual ground reaction has six components. However, it is common to have more than one contact with the ground, especially in the case of an SCI subject walking with the assistance of a pair of crutches. When more than one ground contact exists, the ID provides the resultant of all the external reaction forces, but there is no information on how it is shared among the contacting elements. It is possible to calculate an estimate during normal gait if the double support phase is short, but complex gait patterns such as those of SCI subjects will always require ground reaction measurements to solve the indeterminacy, since the net external reaction can be the resultant of up to 18 ground reaction components, namely three force and three moment components at each foot, and three force components at each crutch.

If all the ground reactions are measured, the problem becomes overdetermined, since the net ground reaction can be obtained by following two independent paths: it can be derived from the ID, or obtained as the resultant of the ground reaction measurements.

A simple and fast optimization was proposed to obtain a set of forces and moments $\mathbf{T}$ which were fully consistent with the captured motion, while keeping the ground reactions as close as possible to the measured ones. In order to maintain the forces and moments in $\mathbf{T}$ consistent with the measured motion, their virtual power $\mathbf{W}^*$ for any set of generalized virtual velocities $\dot{\mathbf{z}}^*$ must be equal to that of the generalized forces, which is directly obtained as

$$\mathbf{W}^* = \dot{\mathbf{z}}^{*\top}\mathbf{Q_m} \tag{2.63}$$

$\mathbf{T}$ is composed by three types of magnitudes: $\mathbf{F}_{ext}$ the external forces, $\mathbf{M}_{ext}$ the external moments and the internal torques $\mathcal{T}$ expressed in the local axes of the proximal body of the corresponding joint. In order to calculate the virtual power of $\mathbf{T}$, a vector of Cartesian velocities $\dot{\mathbf{y}}^*$ is defined such that

$$\mathbf{W}^* = \dot{\mathbf{y}}^{*\top}\mathbf{T} \tag{2.64}$$

The vector $\dot{\mathbf{y}}^*$ is composed of the corresponding velocities of the points where ground forces $\mathbf{F}_{ext}$ are applied, the absolute angular velocities of the segments at which the external moments $\mathbf{M}_{ext}$ are acting, and the relative angular velocities at the joints (in local coordinates of the proximal segment, in order to be consistent with the joint torques). The relationship between the independent velocities $\dot{\mathbf{z}}$ and the velocities used to calculate the virtual power of the ground reactions and joint torques $\dot{\mathbf{y}}$ can be expressed by obtaining a position-dependent velocity transformation matrix $\mathbf{B}$ such that

$$\dot{\mathbf{y}} = \mathbf{B}\dot{\mathbf{z}} \tag{2.65}$$

Analogously to what happens to matrix $\mathbf{R}$, the jth column of matrix $\mathbf{B}$ contains the $\dot{\mathbf{y}}$ velocities obtained when the jth generalized coordinate is given a unit velocity while the rest of them remain static. Since the velocities can be easily derived from $\mathbf{q}$ and $\dot{\mathbf{q}}$, and the latter are already contained within the columns of $\mathbf{R}$, the $\mathbf{B}$ matrix is calculated at a very small computational cost. The relationship between dependent and independent velocities shown in Eq. (2.65) can be introduced into Eq. (2.64) which, in turn, is combined with Eq. (2.63) to yield

$$\dot{\mathbf{z}}^{*\top}\mathbf{Q}_\mathbf{m} = \dot{\mathbf{z}}^{*\top}\mathbf{B}^\top\mathbf{T} \tag{2.66}$$

which means that the following condition can be established for the Cartesian forces $\mathbf{T}$ to be equivalent to $\mathbf{Q}_\mathbf{m}$

$$\mathbf{B}^\top\mathbf{T} = \mathbf{Q}_\mathbf{m}. \tag{2.67}$$

Any given set of forces and moments $\mathbf{T}$ that fulfils this condition will produce the same virtual power as $\mathbf{Q}_\mathbf{m}$, regardless of the virtual velocities chosen, thus guaranteeing that is fully consistent with the captured motion.

In order to have a unique solution for Eq. (2.67), the number of unknowns in $\mathbf{T}$ must be equal to the number of degrees of freedom. Since the net external reaction has six components, and $\mathbf{T}$ can contain up to 18 external reactions, the ID problem without ground reaction measurements is underdetermined.

As explained above, since there may be up to 12 unknowns in excess, directly introducing the 18 measured reactions $\mathbf{T}_j$ as known values would render the system overdetermined, with no solution unless the measurements were fully consistent with the ID. A unique solution can be obtained if a minimization problem is stated, in order to find, among the infinite sets of forces and torques $\mathbf{T}$ which fulfil the virtual power constraint, the solution with the minimum deviation with respect to the external reactions measured by the instrumented crutches and FPLs

$$\underset{\mathbf{T}}{\text{minimize}} \quad g(\mathbf{T}) = \frac{1}{2}\sum_{j=1}^{18} w_j(\mathbf{T}_j - \mathbf{T}_j^*)^2 \tag{2.68}$$

where w_j are the weights assigned to each deviation in the cost function $g(\mathbf{T})$. Since this is a minimization problem with a quadratic cost function and linear constraints,

it can be efficiently solved in one single step by means of the Lagrange multipliers method.

$$\begin{pmatrix} \mathbf{W} & \mathbf{B} \\ \mathbf{B}^\top & 0 \end{pmatrix} \begin{Bmatrix} \mathbf{T} \\ \sigma \end{Bmatrix} = \begin{Bmatrix} \mathbf{W}\mathbf{T}^* \\ \mathbf{Q_m} \end{Bmatrix} \tag{2.69}$$

In this way, the value of internal torques $\mathcal{T}$ can be obtained in $\mathbf{T}$ from $\mathbf{Q_m}$.

In the other hand, with the FDA, $\mathcal{T}$ has to be revert in net joint torques correspond to considering the pelvis as the base body. The conversion can be easily obtained using Eq. (2.67).

This method requires to know, at each instant, the ground reactions in the various contacts so as to share the external reactions between them. So, to study a complete gait cycle, at least three force plates should be required. The gait lab used was equipped with only two force plates but, anyway, the complete gait cycle has been studied using this strategy: when a foot has not ground contact, all the external reactions are considered acting on the other foot. Without the third force plate, it is needed to use an additional information (obtained from kinematics) when a foot leaves the ground contact. In such a situation, the shared external reactions are considered acting on one foot only. Due to some residuals error, discontinuities are obtained during this change. The discontinuity period is replaced using a spline method to reconstruct the data. In that way, the data of a third force plate could be estimated and used to study a complete gait cycle.

2.5 Data collection

The experimental method is applied by measuring the kinematics of the body segments, the ground reactions, and the EMG signals of the muscles. As shown in Figure 2.13, the gait laboratory used is equipped with an optical camera tracking system composed of 12 infrared cameras (Natural Point, OptiTrack FLEX:V100 sampling at 100 Hz) that compute the position of 37 optical markers plus 3 for each crutch (Figure 5.3), 2 force plates (AMTI, AccuGait, sampling at 100 Hz) and an EMG telemetry system (BTS FREEEMG, this counts up to 16 wireless sensors sampling at 1 kHz) which are synchronized together. EMG signals were rectified, filtered by SSA with a window length of 250 (equivalent to the common forward and reverse low-pass 5th order Butterworth filter with a cut-off frequency of 15 Hz) and then normalized with respect to its maximal value [74]. To analyze crutch-assisted gait, a couple of crutches instrumented for ground contact force measurement were used too. For the experimental measurements of energy consumption, which require that the subject maintains a constant activity during at least 5 min, so a running track and a portable gas analyzer (Cortex MetaMax 3B) were used.

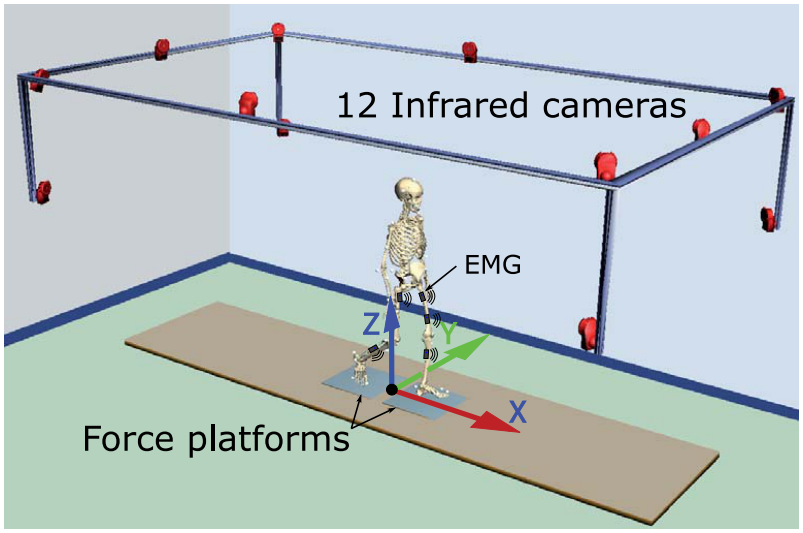

Figure 2.13 – Gait laboratory.

Chapter 3

The muscle force-sharing problem

The fundamental problem is that there are more muscles serving each degree of freedom of the system than those strictly necessary from the mechanical point of view, which implies that, in principle, an infinite number of recruitment patterns are acceptable. This problem is often referred to as the redundancy problem of the muscle recruitment [29] or the force-sharing problem [30]. Experimental studies [31] and EMG collections [32] suggest that a specific strategy of muscle coordination is chosen by the CNS to perform a given motor task. A popular mathematical approach for solving the muscle recruitment problem is the optimization method, which can be associated to inverse or forward dynamics [33]. These methods minimize or maximize some criterion (objective function or cost function) which reflects the mechanism used by the CNS to recruit muscles for the movement considered. The proper cost function is not known a priori, so the adequacy of the chosen function must be validated according to the obtained results [34]. Many criteria have been proposed in the literature to predict muscle forces.

3.1 Inverse-dynamics based optimization

As illustrated in Figure 3.1, the histories of positions, velocities and accelerations of the dependent coordinates and ground reactions are already known from the processing of the motion capture data and provide the dynamic information by using formulations presented in Section 2.4. Then, an optimization is needed to estimate the muscles forces which correspond to the calculated joint torques.

3.1.1 Static optimization

In order to determine the muscle forces at each time-point, the inverse optimization problem can be formulated in general form as:

$$\text{minimize or maximize} \quad C \tag{3.1}$$

$$\text{subject to} \quad \mathcal{T}^{MT} = J^{\top} F^{MT} \tag{3.2}$$

$$F^{MT}_{i,min} < F^{MT} < F^{MT}_{i,max} \quad i = 1, ..., m \tag{3.3}$$

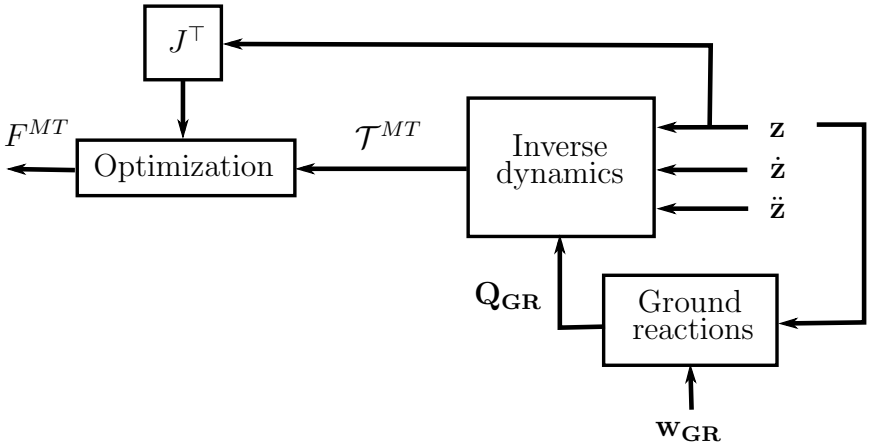

Figure 3.1 – Block diagram illustrating the inverse problem.

where C is an objective function associated with decision variables, $F^{MT}_{i,min}$ and $F^{MT}_{i,max}$ are the instantaneous minimum and maximum allowed forces in muscle i, respectively. For static optimization (SO), the values of the limits of the system are the following: $F^{MT}_{i,min} = 0$ and $F^{MT}_{i,max} = F^{M}_{i,0}$.

Expression of the objective function C depends of the muscle recruitment criteria used. In the literature, several muscle recruitment criterion have been suggested to represent the CNS behavior. In this work, four of them have been considered for static optimization.

Nonlinear polynomial criterion

The polynomial criterion can be written as

$$\text{minimize} \quad \sum_{i=1}^{m} \left(\frac{F_i^{MT}}{\kappa_i} \right)^p \tag{3.4}$$

where κ_i denotes a positive weighting factor and p the power of the polynomial. According to Crowninshield and Brand [75], the muscle force prediction by minimizing the sum of muscle stresses raised to a power p coincides with maximizing the endurance of activity. Furthermore, experimental studies demonstrated that the power p varies between individual subjects and individual muscles due to fiber types, fiber orientations, etc., and has a range from 1.4 to 5.1.

In this study, we choose to compare three polynomial criteria which are most used in literature and took $p = 2$:

Criterion I - *minimization of the sum of the squares of muscle forces*

$$\text{minimize} \quad \sum_{i=1}^{m} (F_i^{MT})^2; \tag{3.5}$$

Criterion II - *minimization of the sum of the squares of relative muscle forces*

$$\text{minimize} \quad \sum_{i=1}^{m} \left(\frac{F_i^{MT}}{F_{i,0}^{M}} \right)^2 ; \tag{3.6}$$

Criterion III - *minimization of the sum of the squares of muscle stresses*

$$\text{minimize} \quad \sum_{i=1}^{m} \left(\frac{F_i^{MT}}{PCSA_i} \right)^2 ; \tag{3.7}$$

($PCSA$: physiological cross sectional area).

Min/max criterion

The min/max criterion is based on the idea that the duration for a given loading task, or the sustainable endurance depends more on the endurance of each individual participating muscle. Therefore, the largest endurance for a task means the maximum relative muscle force [76] or the maximum muscle stress [77] is as small as possible. The min/max criterion takes such form

$$\text{minimize} \quad \max \left\{ \frac{F_i^{MT}}{\kappa_i} \right\}, i = 1, ..., m. \tag{3.8}$$

Dealing with the min/max optimization criterion (Eq. (3.8)) in a direct way is quite difficult. By introducing an artificial variable β, the performance criterion in Eq. (3.8) is equivalent to a criterion which has the following form

$$\text{minimize} \qquad \beta \tag{3.9}$$

$$\frac{F_i^{MT}}{\kappa_i} < \beta \quad i = 1, ..., m. \tag{3.10}$$

Both equations, Eq. (3.9) and Eq. (3.10), are linear, and the linear programming algorithm can be used to obtain unique solutions. For this study, the following criterion is used:

Criterion IV - *minimization of the largest relative muscle force*

$$\text{minimize} \quad \max \left(\frac{F_i^{MT}}{F_{i,0}^{M}} \right), i = 1, ..., m. \tag{3.11}$$

3.1.2 Physiological approach

At physiological level, musculotendon dynamics introduces muscle force constraints to the system. Whereas the static optimization approach disregards this constraints in order to simplify the problem, the so-called physiological approach [78] takes it into consideration. This approach applies optimization techniques at each time-point, and prescribes minimal and maximal constraints for the forces by extrapolating the force values from the previous time-point using feasible muscle

activation values. In this way, a fast optimization as well as feasible time histories of the muscle forces are achieved.

Using the Hill's muscle model, the state variables of the ith muscle are denoted by the vector

$$x_i(t) = \begin{bmatrix} a_i(t) \\ F_i^{MT}(t) \end{bmatrix}. \tag{3.12}$$

Thus, the first derivation of the state variables has the form

$$\dot{x}_i(t) = \begin{bmatrix} \dot{a}_i(t) \\ \dot{F}_i^{MT}(t) \end{bmatrix} = \begin{bmatrix} f(a_i(t), u_i(t)) \\ f(a_i(t), F_i^{MT}(t), l_i^{MT}(t), v_i^{MT}(t)) \end{bmatrix}. \tag{3.13}$$

Eq. (3.13) can be written as

$$\dot{x}_i(t) = f(x_i(t), u_i(t), l_i^{MT}(t), v_i^{MT}(t)). \tag{3.14}$$

The time interval T is discretized into N equidistant intervals of width Δt, i.e.,

$$\Delta t = \frac{T}{N}, \tag{3.15}$$

and the excitation of muscle i within an interval Δt is assumed to be constant (see Figure 3.2)

$$u_i(t_{k-1} \leq t \leq t_k) = u_i(t_{k-1}) = u_{i,k-1} \tag{3.16}$$

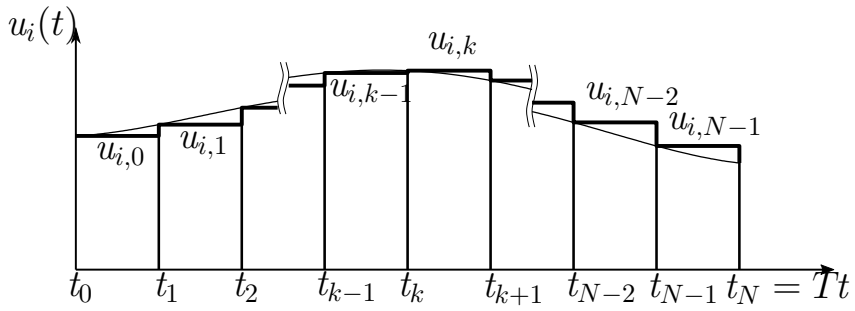

Figure 3.2 – Discretization of the neural control of the ith muscle.

where

$$t_{k-1} = (k-1)\Delta t \quad \text{and} \quad t_k = k\Delta t. \tag{3.17}$$

If the state variables of the ith muscle force at time t_{k-1}, $x_i(t_{k-1})$, are given, the minimum and maximum state variables that could be achieved by the ith muscle at the next time t_k, $x_{i,min}(t_k)$ and $x_{i,max}(t_k)$, can be computed by setting the neural input $u_{i,k-1}$ to 0 and 1, respectively, i.e.,

$$x_{i,min}(t_k) = x_i(t_{k-1}) + \int_{t_{k-1}}^{t_k} f(x_i(t), u_{i,k-1}(t) = 0, l_i^{MT}(t), v_i^{MT}(t))\, dt, \tag{3.18}$$

$$x_{i,max}(t_k) = x_i(t_{k-1}) + \int_{t_{k-1}}^{t_k} f(x_i(t), u_{i,k-1}(t) = 1, l_i^{MT}(t), v_i^{MT}(t))\, dt. \tag{3.19}$$

In this work, all the time integrations of muscle equations have been carried out using the ode23t integrator, which contains the implicit trapezoidal rule. The histories of musculotendon length and velocity corresponding to the set of the sampling time-points for each muscle are precomputed from the measured kinematics and stored in memory arrays. The musculotendon length and velocity at time instant t within two adjacent sampling time points (e.g., $t_{k-1} < t < t_k$) are calculated by using linear interpolation i.e.,

$$l^{MT}(t_{k-1} < t < t_k) = l^{MT}(k-1) + \frac{l^{MT}(k) - l^{MT}(k-1)}{\Delta t}(t - t_{k-1}), \tag{3.20}$$

$$v^{MT}(t_{k-1} < t < t_k) = v^{MT}(k-1) + \frac{v^{MT}(k) - v^{MT}(k-1)}{\Delta t}(t - t_{k-1}) \tag{3.21}$$

where $l^{MT}(k-1)$, $l^{MT}(k)$ and $v^{MT}(k-1)$, $v^{MT}(k)$ denote the musculotendon length and velocity at time t_{k-1} and t_k, respectively.

To determine the individual muscle forces at time-point t_k, the sum of the squares of muscle forces is minimized. In order to obtain a feasible muscle force prediction, the force of muscle i at time t_k is constrained by $F_{i,min}^{MT}(t_k)$ and $F_{i,max}^{MT}(t_k)$ (see Figure 3.3). Thus, applying the physiological approach, the muscle recruitment problem is formulated as

$$\text{minimize} \qquad \sum_{i=1}^{m} F_i^{MT}(t_k)^2 \tag{3.22}$$

$$\text{subject to} \qquad J^{\top}(t_k) F^{MT}(t_k) = \mathcal{T}^{MT}(t_k) \tag{3.23}$$

$$F_{i,min}^{MT}(t_k) < F^{MT}(t_k) < F_{i,max}^{MT}(t_k) \quad i = 1, ..., m. \tag{3.24}$$

Once the individual muscle forces $F^{MT}(t_k)(i = 1, ..., m)$ are determined, an iteration process is run for each muscle to solve the corresponding excitation $u_{i,k-1}(i = 1, ..., m)$ so that the muscle force satisfies the following equation:

$$x_i(t_{k-1}) + \int_{t_{k-1}}^{t_k} f(x_i(t), u_{i,k-1}(t), l_i^{MT}(t), v_i^{MT}(t))\, dt - x_i(t_k) = 0. \tag{3.25}$$

The block diagram in Figure 3.4 makes it easier to understand the procedure using the physiological approach to determine individual muscle forces and neural excitation.

Using the physiological approach, the initial activations and muscles forces are need. The determination of initial activations and muscles forces is based on a

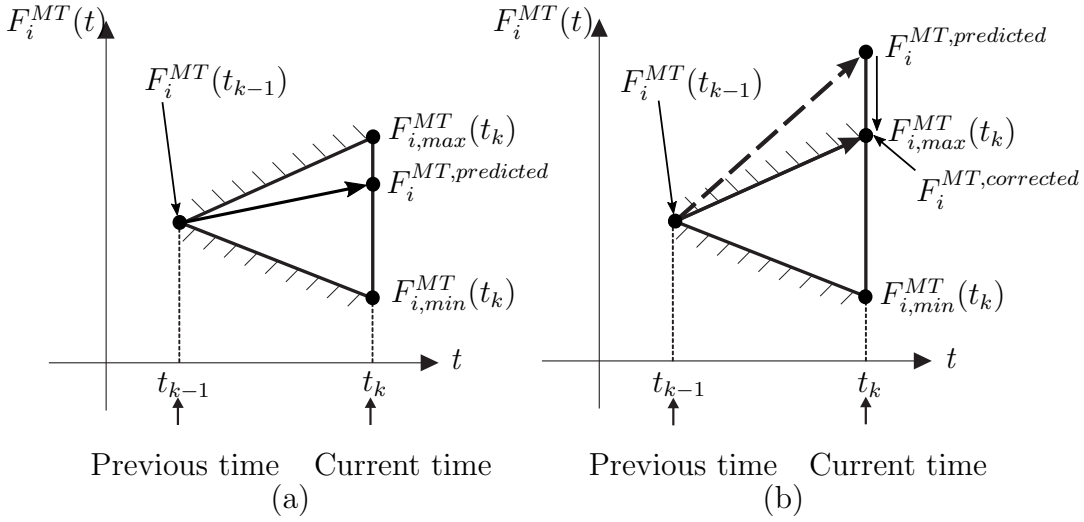

Figure 3.3 – Feasible prediction for the ith muscle force. (a) physiologically feasible case; (b) physiologically infeasible case

static condition in which the initial fiber velocity of each muscle v^M is set to zero, i.e, $f_v(\tilde{v}^M = 0) = 1$. To determine the initial muscle forces, the muscle recruitment problem given by Eq. (3.22) - Eq. (3.24) is solved. However, for this case, each muscle force is constrained by F_{min}^{MT} and F_{max}^{MT} corresponding to $a = 0$ and $a = 1$, respectively. Substituting Eq. (2.14), Eq. (2.17) and Eq. (2.18) into Eq. (2.13) and then rearranging, one obtains

$$(a \cdot f_l(\tilde{l}^M) + f_{PE}(\tilde{l}^M)) \cos\alpha - f_T(\varepsilon^T) = 0. \tag{3.26}$$

For a given activation level a, Eq. (3.26) can be expressed as a function of l^M. Solving l^T from Eq. (2.8) and substituting it in into Eq. (2.19) yields

$$\varepsilon^T = \frac{l^{MT} - l^M \cos\alpha - l_S^T}{l_S^T}. \tag{3.27}$$

Thus, Eq. (3.26) can be rewritten as

$$\left(a \cdot f_l\left(\frac{l^M}{l_0^M}\right) + f_{PE}\left(\frac{l^M}{l_0^M}\right)\right)\cos\alpha - f_T\left(\frac{l^{MT} - l^M\cos\alpha - l_S^T}{l_S^T}\right) = 0. \tag{3.28}$$

Eq. (3.28) is nonlinear and can be iteratively solved to find the solution of l^M. $F_{i,min}^{MT}$ and $F_{i,max}^{MT}$ can then be determined from the corresponding l^M.

After the initial muscle forces have been solved by optimization, the corresponding initial activation for each muscle can be derived from Eq. (3.26).

$$a = \frac{f_{PE}(\tilde{l}^M)\cos\alpha - f_T(\varepsilon^T)}{f_l(\tilde{l}^M)}. \tag{3.29}$$

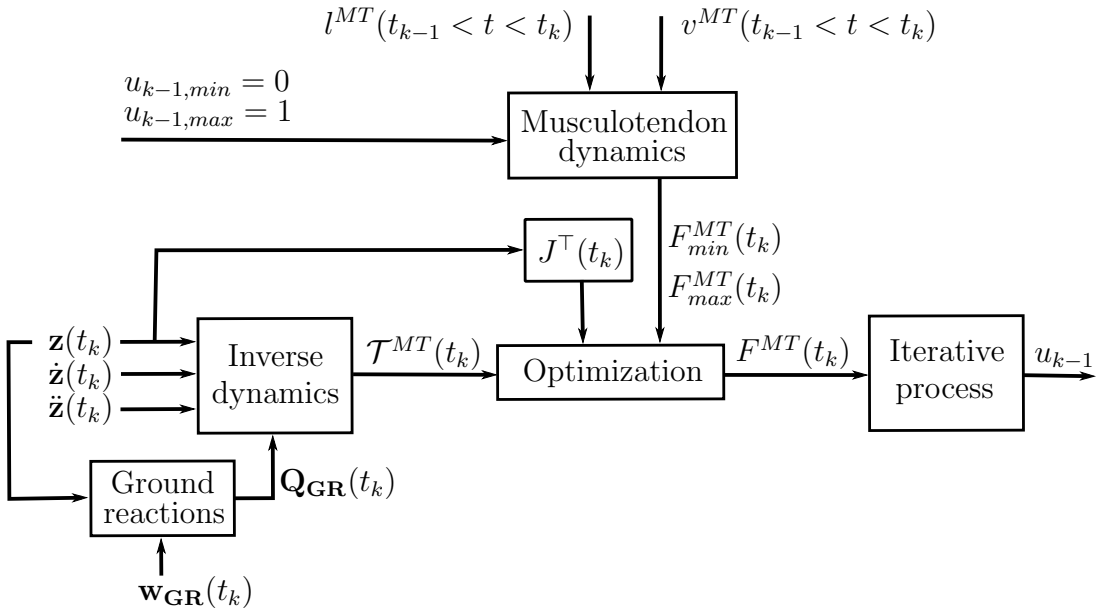

Figure 3.4 – Procedure using physiological approach to determine individual muscle forces at time instant t_k and neural excitations within the time interval $[t_{k-1}, t_k]$.

where the normalized muscle fiber length $\tilde{l}^M$ can be computed from Eq. (2.25) and Eq. (2.26).

Physiological approach with rigid tendon

Optimization and integration are both heavy and slow calculation processes. Moreover, the high tendon stiffness makes really difficult to use this approach. Therefore, in order to simplify the problem while keeping some physiological characteristics, most authors prefer to use a Hill type musculotendon model with a rigid tendon [27] [79].

In this way, the tendon length is constant, $l^T = l_S^T$, and the muscle fiber length l^M can be easily deduced by the following relation:

$$l^M = \sqrt{(l^{MT} - l_S^T)^2 + w^2} \tag{3.30}$$

Consequently, deriving Eq. (2.8) and knowing that

$$\cos\alpha = \sqrt{1 - \left(\frac{w}{l^M}\right)^2}, \tag{3.31}$$

it is obtained :

$$v^M = v^{MT}\cos\alpha \tag{3.32}$$

and the musculotendon force can be derived from Eq. (2.13).

Activation dynamics simplifications

Use of the rigid tendon model avoids the two integrations needed to calculate the limits of the muscle force at each instant, F_{min}^{MT} ($u = 0$) and F_{max}^{MT} ($u = 1$). Then, in order to further reduce the computational burden, the first-order ordinary differential equation (Eq. (2.11)) used to estimate the muscular activation, a, can be simplified as follows:

Time response ignored (Phys. 2) - *direct relation*

Usually, authors who consider the tendon as a rigid element choose to ignore the muscular time response and assume that:

$$a(t_k) = u_k. \tag{3.33}$$

Consequently:

$$F_{min}^{MT} = F_{PE}^{M} \cdot \cos\alpha \tag{3.34}$$

$$F_{max}^{MT} = (F_0^M \cdot f_l(\tilde{l}^M) \cdot f_v(\tilde{v}^M) + F_{PE}^{M}) \cdot \cos\alpha. \tag{3.35}$$

Time response considered (Phys. 3) - *differential equation*

In order to keep the muscular time response relation given by Eq. (2.11), the first-order ordinary differential equation can be converted into:

$$a(t_k) = \begin{cases} u_k + (a(t_{k-1}) - u_k) \cdot e^{(-dt/\tau_{act})} & if \quad a(t_{k-1}) < u_k \\ \\ u_k + (a(t_{k-1}) - u_k) \cdot e^{(-dt/\tau_{deact})} & if \quad a(t_{k-1}) \geq u_k \end{cases} \tag{3.36}$$

Therefore, the minimum and maximum muscle activations, a_{min} ($u = 0$) and a_{max} ($u = 1$) can be obtained, and the muscle force limits become:

$$F_{min}^{MT} = (F_0^M \cdot a_{min} \cdot f_l(\tilde{l}^M) \cdot f_v(\tilde{v}^M) + F_{PE}^{M}) \cdot \cos\alpha \tag{3.37}$$

$$F_{max}^{MT} = (F_0^M \cdot a_{max} \cdot f_l(\tilde{l}^M) \cdot f_v(\tilde{v}^M) + F_{PE}^{M}) \cdot \cos\alpha. \tag{3.38}$$

Results and experimental validation

The different approaches presented in this section have been compared with EMG measurements for the five healthy subjects described in 2.1.1. Normalized muscle activations during a gait cycle of one healthy subject estimated using all the previous approaches are plotted in Figure 3.5 along with the corresponding normalized EMG measurements.

In order to compare the correlation with experimental values and, as there is no clear relationship between EMG amplitude and muscle force [80], the correlation coefficient R ($corrcoeff$ of Matlab) has been calculated to focus on the variations. Mean values R of the five healthy subjects for each muscle and approach are given

in Table 3.1. Surprisingly, the best values are obtained with SO and criterion I, the simplest method. Results show that there are no substantial differences between the six approaches studied. Obtained correlations are acceptable, with values going from 59% to 77%. The physiological criterion, in addition to clearly be the slowest approach, shows the lowest correlations.

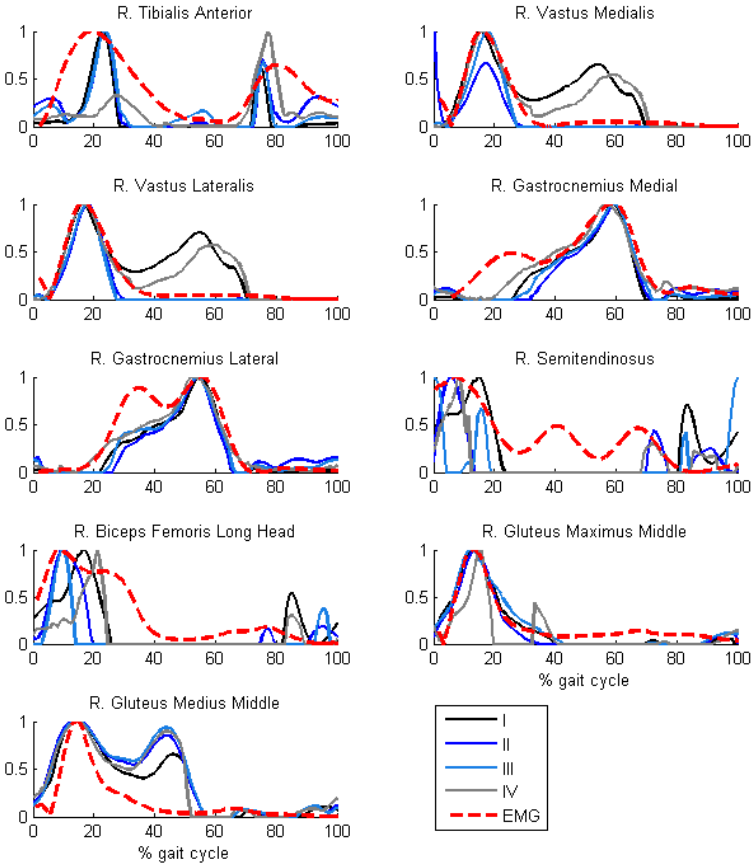

Figure 3.5 – Normalized muscular forces obtained with static optimization (criteria I-IV) vs. normalized EMG for a healthy subject.

3.1.3 Synergy optimization

Muscular synergies

While activity patterns appear to be different for each muscle, although certain features are common to many muscles. In fact, there is analytical evidence that many muscles may share certain activity patterns. First, this was investigated in studies that applied principal component analysis (PCA) to determine whether the main features of the EMG patterns could be described by a few underlying components [35], [36] and [37]. Later, other mathematical methods have been proposed to

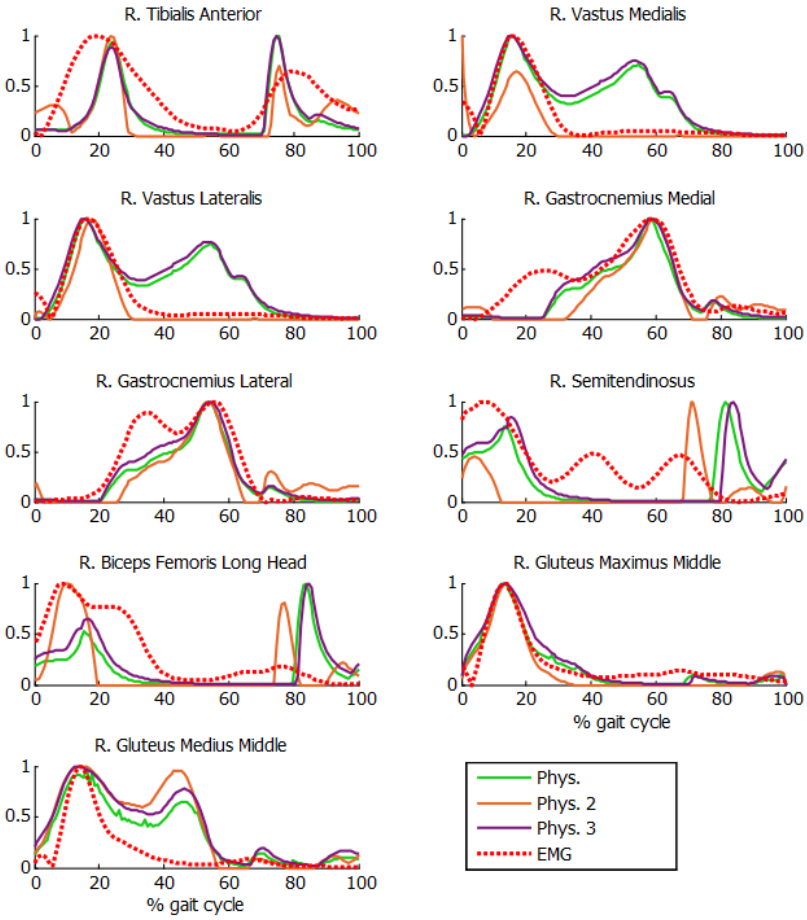

Figure 3.6 – Normalized muscular forces obtained with physiological optimization (original approach and their two simpler alternatives) vs. normalized EMG for a healthy subject (Phys.: Physiological approach, Phys. 2: Physiological approach with rigid tendon and activation's time response ignored and Phys. 3: Physiological approach with rigid tendon and activation's time response considered).

examine the issue of common underlying patterns. For example, Ivanenko [38] applied the factor analysis (FA) to the set of EMG records, and Shourijeh [39] applied the non-negative matrix factorization (NMF). They demonstrated that the CNS use muscle synergies in order to simplify the muscular control.

All of these approaches propose to reduce the m muscles activations obtained for the n time steps $\bar{a}[n \times s]$, into s synergy activations $\bar{A}_{syn}[n \times s]$, using constant synergy vectors $\bar{V}_{syn}[s \times m]$.

$$\bar{a}_{syn} = \bar{A}_{syn} \times \bar{V}_{syn}. \tag{3.39}$$

The objective of this method is to obtain the solution which is closest $\bar{a}_{syn}$ closest to the original values of $\bar{a}$. The results is generally considered good when the correlation is greater than 95%.

	Mean correlation coefficient R values across subjects EMG vs. muscle activations						
	I	**II**	**III**	**IV**	**Phys.**	**Phys. 2**	**Phys. 3**
R. Tibialis Anterior	0,70	0,73	0,63	0,41	0,61	0,71	0,59
R. Vastus Medialis	0,69	0,67	0,83	0,45	0,69	0,69	0,69
R. Vastus Lateralis	0,73	0,71	0,87	0,53	0,71	0,73	0,71
R. Gastrocnemius Medial	0,80	0,65	0,77	0,75	0,80	0,61	0,82
R. Gastrocnemius Lateral	0,73	0,63	0,71	0,65	0,73	0,59	0,74
R. Semitendinosus	0,85	0,85	0,61	0,75	0,76	0,67	0,78
R. Biceps Femoris Long Head	0,81	0,85	0,75	0,72	0,69	0,74	0,74
R. Gluteus Maximus Middle	0,91	0,90	0,92	0,87	0,91	0,91	0,90
R. Gluteus Medius Middle	0,75	0,60	0,57	0,59	0,71	0,49	0,71
Mean	**0,77**	**0,73**	**0,74**	**0,64**	**0,74**	**0,68**	**0,74**
Computational time (sec)	2,2	49,3	26,5	31,9	351,4	2,0	2,6

Table 3.1 – R correlations of EMG with inverse-dynamics based optimization ($R < 0.50$ in red)(Phys.: Physiological approach, Phys. 2: Physiological approach with rigid tendon and activation's time response ignored and Phys. 3: Physiological approach with rigid tendon and activation's time response considered).

Authors diverged on the minimum number of synergies required to reproduce the EMG records of the gait of a healthy subject. While Olree [37] concluded that three synergies were enough, Davis [36] and Ivanenko [38] found respectively that four and five patterns could be necessary. As explained in [81], variations in methodological choices, as unilateral or bilateral analysis, selected muscles, EMG treatment or computational method may lead to these discrepancies.

Synergy parameters have often been used to determine the particular characteristics of gait pattern in specific diseases or specific population groups. Nevertheless, use of muscular synergies is increasing in several applications, as post-stroke rehabilitation through functional electrical stimulation (FES) [82] [83], or computational prediction of subject-specific walking [27]. But, in all these cases, synergies were obtained by statistical analysis from surface EMG measurements. Although this is the most popular approach, it does not consider all the actuating muscles, but only some surface muscles, ignoring deeper ones.

Synergy optimization

The fact that synergies take a high dimensional control space and reduce it to a low dimensional space is potentially useful for reducing the amount of indeterminacy when estimating muscle forces via optimization. For this reason, some authors started to investigate how to include it to solve the muscle force-sharing problem [84].

Recently, Shourijeh and Fregly proposed a computational approach [85], called synergy optimization (SynO), for using muscle synergies to reduce indeterminacy when estimating leg muscle forces during walking. SynO approach is a modified SO approach (developed in Matlab) to estimate leg muscle forces during walking

using synergy-constructed muscle activations. For standard SO, muscle activations are independent between time frames, allowing the optimization to be performed one time frame at a time. In contrast, for the proposed modified SO, muscle activations are coupled via synergies across time frames, requiring the optimization to be performed over all time frames simultaneously.

Muscle synergy quantities were used as the design variables for modified SO. Each muscle activation synergy was composed of a single time-varying synergy activation defined by $p = (n/5)$ (nearest integer, n = number of frames) B-spline nodal points along with a corresponding time-invariant synergy vector defined by m (number of muscles) weights specifying inter-muscle activation coupling. Thus, for s synergies ($s = 2$ through 6), the number of design variables was $s * (p + m)$. Each optimization problem was theoretically over-determined. However, in practice, the problems remained under-determined since neighboring time frames were not independent from one another.

Using these design variables, modified SO problems were formulated as follows. The cost function Eq. (3.40) minimized the sum of squares of relative inverse-dynamics joint moment errors plus the sum of squares of muscle activations over all the time frames simultaneously. Scale factors $\beta = 100$ and $\gamma = 1$ were used to give more importance to minimization of the joint moment errors.

$$\text{minimize} \qquad \beta \sum_{i=1}^{c} \sum_{j=1}^{n} \left[\frac{e_{kj,\mathcal{T}^{MT}}}{max(|\mathcal{T}^{MT}{}_i|)} \right]^2 + \gamma \sum_{k=1}^{m} \sum_{j=1}^{n} a_{kj,syn}^2 \tag{3.40}$$

$$\text{subject to} \qquad \sum_{j=1}^{s} V_{ij,syn} = 1 \quad i = 1, ..., m \tag{3.41}$$

$$0 < N_{bj,syn} \quad b = 1, ..., p \quad and \quad j = 1, ..., s \tag{3.42}$$

$$0 < V_{ij,syn} \quad i = 1, ..., m \quad and \quad j = 1, ..., s \tag{3.43}$$

Linear equality constraints, Eq. (3.41), made the sum of weights within each synergy vector equal to one, which made the synergy construction unique, while lower bound constraints, Eq. (3.42) and Eq. (3.43), made the synergy activation B-spline nodes N and synergy vector weights greater than zero.

A Hill type muscle-tendon model with a rigid tendon was used for calculating muscle forces given synergy-constructed activations. Modified SO problems were solved using Matlab's *fmincon* nonlinear constrained optimization algorithm but the objective function was programmed in a *mex* file (FORTRAN) to reduce the computational time (16 times faster than the original Matlab function).

Extraction of synergies from static optimization

In addition of predicting muscle activations, SynO generates the corresponding muscle synergies for all the considered muscles. Due to the increasing interest in using synergies various applications, this work explored the possibility of extracting muscles synergies through NMF (with two to six synergies) from the estimated activations with SO, instead of extracting the synergies from EMG measurements.

The 43 muscular activations of the right leg estimated by SO (minimizing the sum of squares of muscle activations) were decomposed using NMF into weighted muscle synergies according to Eq. (3.39).

To compare this approach with SynO, the sum of weights within each synergy vector was also made equal to one. Then, using the same Hill-type rigid-tendon muscle model, the reconstructed muscular forces $\bar{F}_{SO}^{MT}$ and corresponding intersegmental joint moments $\bar{\mathcal{T}}_{SO}^{MT}$ were derived from $\bar{a}_{SO}$ (Figure 3.7).

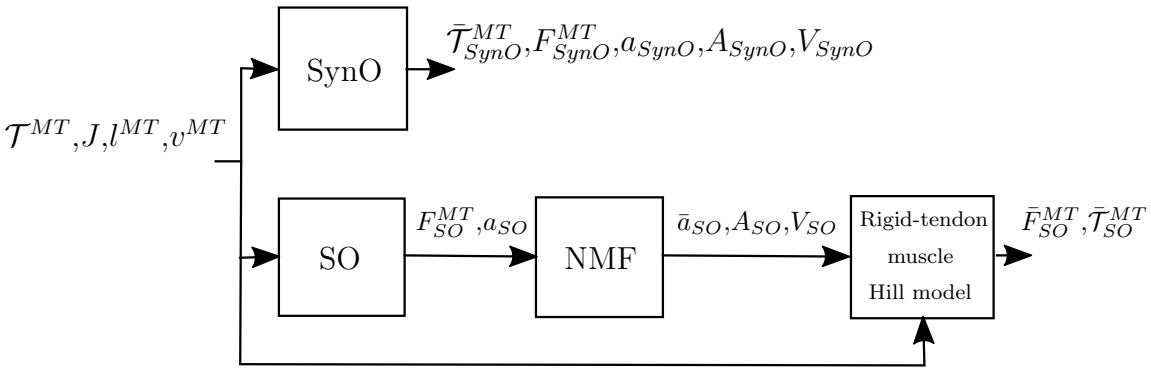

Figure 3.7 – Block diagram of SynO and SO-NMF approaches.

Results and experimental validation

The mean correlation coefficients R^2 obtained for the five healthy subjects between the joint moments calculated through inverse dynamics and the joint moments from SynO are shown in Table 3.2. The worst correlations were observed using only 2 synergies, with a corresponding mean value of 90%. Because its equality constraints, SO reproduced exactly the inverse-dynamics joint moments. However, after applying NMF, the reconstructed intersegmental moments $\bar{\mathcal{T}}_{SO}^{MT}$ matched poorly the reference values, with R^2 mean values varying between 62% and 90%.

Estimated muscle activations varied significantly from 2 to 6 synergies (Figure 3.8). A reduced number of synergies tends to introduce more co-activations and consequently higher joint stiffness. However, coefficient correlations R calculated between EMG and muscle activations for the five healthy subjects (Table 3.3) do not show significant discrepancies between the different synergy cases ($s = 2$ through 6). Mean values were between 60% (with 4 synergies) and 65% (for 3 and 6 synergies). By increasing the number of design variables imply by the number of synergies, the computational time increased significantly. The SynO approach is much slower than SO: applying NMF increased only 2 s the computational time.

	Mean R^2 values across subjects for joint moment matching										
	2 synergies		3 synergies		4 synergies		5 synergies		6 synergies		SO
	SynO	SO-NMF	SynO	SO-NMF	SynO	SO-NMF	SynO	SO-NMF	SynO	SO-NMF	
Hip Abd/Add	0,93	0,76	0,97	0,85	0,99	0,94	0,99	0,97	1,00	0,97	1,00
Hip Flex/Ext	0,94	0,82	0,98	0,95	0,99	0,96	1,00	0,98	1,00	0,98	1,00
Hip Int/Ext rot.	0,94	0,32	0,98	0,37	0,99	0,40	1,00	0,56	1,00	0,54	1,00
Knee Flex/Ext	0,93	0,37	0,97	0,57	0,98	0,87	0,99	0,94	1,00	0,94	1,00
Ankle Int/Ext rot.	0,76	0,55	0,92	0,57	0,98	0,74	1,00	0,83	1,00	0,85	1,00
Ankle Flex/Ext	0,92	0,78	0,96	0,83	0,98	0,87	0,99	0,89	1,00	0,92	1,00
Mean	**0,90**	**0,60**	**0,96**	**0,69**	**0,99**	**0,80**	**1,00**	**0,86**	**1,00**	**0,87**	**1,00**

Table 3.2 – Mean correlation coefficient R^2 values across subjects between moments calculated by inverse dynamics and: i) joint moments from SynO; ii) joint moments from SO with NMF, for n synergies ($n = 2$ through 6) for the 5 subjects. ($R^2 < 0.95$ in red).

	Coeff. corr. R mean values EMG vs. Muscle activations										
	2 Synergies		3 Synergies		4 Synergies		5 Synergies		6 Synergies		SO
	SynO	SO-NMF	SynO	SO-NMF	SynO	SO-NMF	SynO	SO-NMF	SynO	SO-NMF	
R. Tibialis Anterior	0,58	0,52	0,59	0,75	0,56	0,75	0,56	0,74	0,69	0,76	0,69
R. Vastus Medialis	0,84	0,74	0,61	0,84	0,68	0,74	0,68	0,75	0,73	0,76	0,71
R. Vastus Lateralis	0,72	0,74	0,75	0,82	0,65	0,80	0,54	0,78	0,73	0,79	0,74
R. Adductor Magnus Middle	0,48	0,54	0,43	0,71	0,52	0,51	0,57	0,56	0,57	0,56	0,52
R. Gastrocnemius Medial	0,72	0,80	0,87	0,71	0,77	0,67	0,70	0,69	0,75	0,67	0,60
R. Gastrocnemius Lateral	0,57	0,72	0,76	0,77	0,67	0,66	0,70	0,70	0,64	0,71	0,57
R. Semitendinosus	0,36	0,73	0,58	0,89	0,53	0,66	0,66	0,67	0,50	0,60	0,57
R. Biceps Femoris Long Head	0,72	0,69	0,57	0,85	0,51	0,79	0,50	0,80	0,54	0,86	0,84
R. Gluteus Maximus Middle	0,74	0,71	0,71	0,86	0,71	0,90	0,84	0,92	0,87	0,92	0,91
R. Gluteus Medius Middle	0,25	0,39	0,45	0,41	0,36	0,40	0,48	0,42	0,38	0,43	0,44
Mean	**0,60**	**0,66**	**0,63**	**0,76**	**0,60**	**0,69**	**0,62**	**0,70**	**0,64**	**0,71**	**0,66**
Computational time (sec)	80	4	115	4	196	4	317	4	587	4	2

Table 3.3 – R correlations between EMG measurements and muscle activation obtained from SynO and SO-NMF ($R < 0.50$ in red).

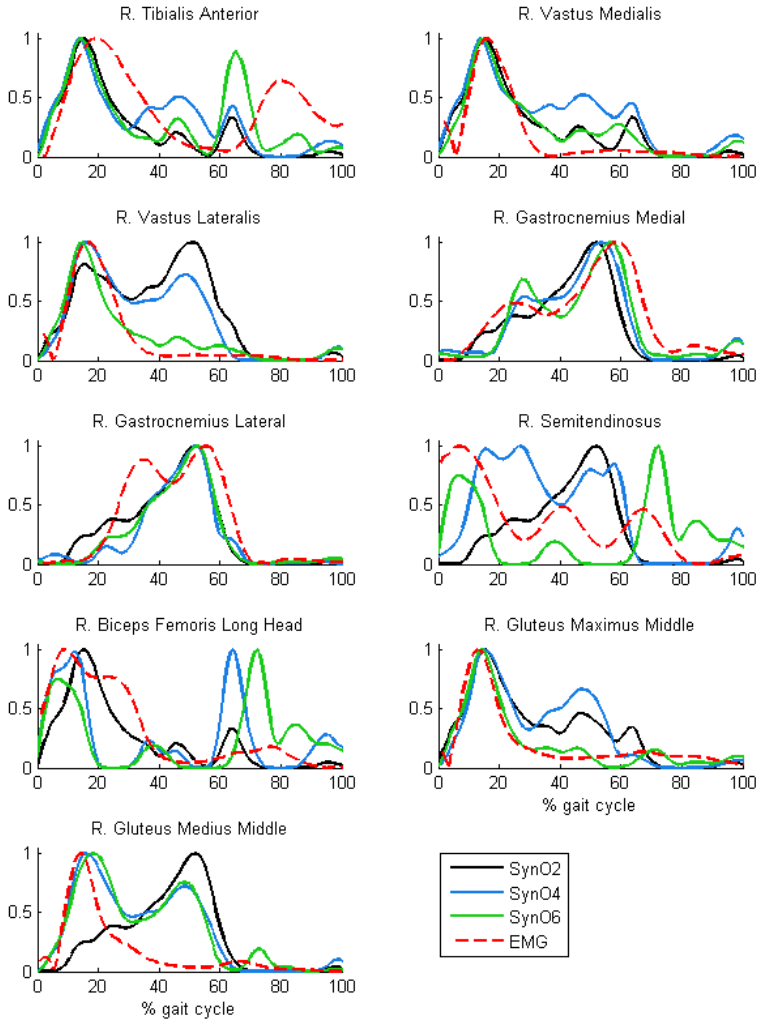

Figure 3.8 – Normalized muscular activations obtained for one subject from SynO and n synergies ($n = 2$ through 6) vs normalized EMG.

3.2 Forward-dynamics based optimization

Because the equations of motion give the relation between motion and forces, they can be used in two directions: solving the forces from the motion (inverse-dynamics) or solving the motion from the forces (forward or direct dynamics). While inverse dynamics is mainly used for analysis of a recorded activity, in some instances it may be practical to use forward dynamics as in the case of model-based control or motion prediction.

A forward-dynamics based approach is proposed in this work, a co-simulation algorithm that allows the separate integration of the multibody and muscular dynamic equations, and the different alternatives for the muscular force-sharing problem that were compared in the previous Section for inverse-dynamics based approaches, are compared here within the proposed co-simulation algorithm. First of all, the new proposed algorithm is compared in a simple case, a simple pendulum actuated by a couple of muscles, with the popular CMC algorithm, as a way of validation. Then, the different alternatives for the muscular force-sharing problem are compared for healthy gait, using the proposed co-simulation algorithm.

3.2.1 Computed muscle control

The CMC was first introduced by Thelen et al. in 2003 [59], and an updated version of the algorithm was presented later in 2006 [86]. The method follows a similar procedure to the physiological approach. The muscle excitations are calculated at discrete intervals and, then, the whole system of equations is integrated one step forward, in a unified scheme, using the previously obtained excitations as inputs (Figure 3.9). However, the calculation of the required joint torques $\mathcal{T}^{MT}$ differs from the physiological approach because the forward integration requires a feedback controller for stabilization. On the other hand, in forward dynamics the positions and velocities at the next time step are unknown, so their values are estimated using information from the desired motion. For obtaining the joint torques, a set of controller accelerations is first calculated:

$$\ddot{\mathbf{z}}^{md}_{CMC}(t_{k+1}) = \ddot{\mathbf{z}}^{md}_{d}(t_{k+1}) + k_v \dot{\varepsilon_k} + k_p \varepsilon_k \tag{3.44}$$

where ε_k and $\dot{\varepsilon_k}$ represent the position and velocity errors at t_k, k_p and k_v are their corresponding feedback gains, and subindex d denotes magnitudes related to the desired (i.e. tracked) motion. The position and velocity errors are defined as:

$$\varepsilon_k = \mathbf{z}^{md}_{d}(t_k) - \mathbf{z}^{md}(t_k) \tag{3.45}$$

$$\dot{\varepsilon_k} = \dot{\mathbf{z}}^{md}_{d}(t_k) - \dot{\mathbf{z}}^{md}(t_k) \tag{3.46}$$

If the velocity gain k_v is set as $2\sqrt{k_p}$ and the accelerations $\ddot{\mathbf{z}}^{md}_{CMC}$ are assumed to be reached, the position error would converge to zero in a critically-damped manner [86].

At the next step, the joint torques producing the $\ddot{\mathbf{z}}_{CMC}$ accelerations can be derived from Eq. (2.62) as:

$$\mathbf{Q_m^{md}}(t_{k+1}) = \bar{\mathbf{M}}_{22}\ddot{\mathbf{z}}_{CMC}^{md}(t_{k+1}) + H(\mathbf{z}(t_{k+1}), \dot{\mathbf{z}}(t_{k+1}), \ddot{\mathbf{z}}(t_{k+1})). \tag{3.47}$$

The obtained joint torques $\mathbf{Q_m^{md}}$ correspond to the ones considering the pelvis as the base body. However, joint torques produced by muscles correspond to the internal torques $\mathcal{T}$ when the feet are considered as the base bodies. Consequently, the procedure described before in Sub-section 2.4.6 was applied to obtain $\mathcal{T}_{CMC}^{MT}$.

Then, the optimal excitations are calculated using the same procedure than in the physiological approach but, as noted above, the desired positions and velocities are used whenever data from the next time step is required.

Finally, the estimated excitations are used as inputs to integrate together the whole system of differential equations (multibody and musculotendon dynamic equations) from t_k to t_{k+1} at a smaller time step.

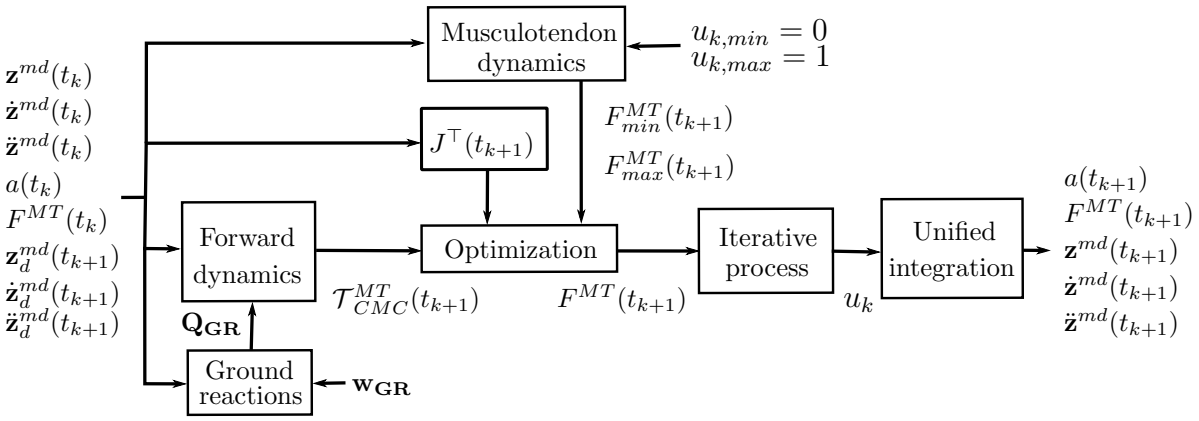

Figure 3.9 – CMC algorithm flowchart.

3.2.2 Co-simulation algorithm

As explained before, the CMC method integrates, in a unified form, the multibody and muscular dynamic equations. Here, a co-integration scheme is presented which allows to generate and integrate the multibody equations by an already existing code, while the muscular dynamics are integrated within a different framework.

An implicit integrator, in a predictor-corrector scheme, was used to integrate the multibody equations. Therefore, the state estimates at step $k+1$ improve after every iteration, and can be used within the corrector loop for performing new muscle optimizations. The required joint torques for the muscle optimizations are calculated at every iteration using a CTC control algorithm:

$$\ddot{\mathbf{z}}_{CTC}^{md}(t_{k+1}) = \ddot{\mathbf{z}}_d^{md}(t_{k+1}) + k_v\dot{\varepsilon}_{k+1} + k_p\varepsilon_{k+1} \tag{3.48}$$

$$\mathbf{Q}^{\mathbf{md}}_{\mathbf{CTC}}(t_{k+1}) = \bar{\mathbf{M}}_{22}\ddot{\mathbf{z}}^{md}_{CTC}(t_{k+1}) + H(\mathbf{z}(t_{k+1}), \dot{\mathbf{z}}(t_{k+1}), \ddot{\mathbf{z}}(t_{k+1})). \tag{3.49}$$

After a muscle optimization has converged, the torques $J^\top F^{MT}$ produced by the optimal forces are introduced in the multibody equations, at the corrector stage. When the corrector loop converges, an iterative process is used as before to obtain the excitations. This method is computationally more expensive than CMC, since several muscle optimizations will potentially be carried out at every time step. However, results are not so different if the optimization is performed only once at the first iteration, using the predictor estimate. This defines a simplified version of the algorithm. Figure 3.10 shows the flowchart, where the rightmost block represents the choice between performing optimization at every iteration or not.

Because the optimization method in this approach does not require to be physiological, all the criteria studied before for inverse dynamics can be used and compared.

Results and experimental validation

Simple pendulum

As explained before, the proposed co-simulation algorithm is compared with the popular CMC as a way of validation. The simple pendulum actuated by two muscles and shown in Figure 3.11 was used for this purpose. The pendulum has a massless bar with a tip mass, and its position is defined by the angle θ with respect to the vertical, which is zero when the pendulum is in equilibrium.

To play the role of the experimentally acquired motion in biomechanical examples, a predefined history of the angle was imposed. The pendulum starts from an inverted position (pointing upwards), i.e. $\theta = \pi$, and performs a one-second-long movement described by a continuous quintic spline through the values shown in Table 3.4.

t(s)	θ **(°)**
0	180
1/3	180-60
2/3	180+60
1	180

Table 3.4 – Pendulum trajectory.

The prescribed motion has zero velocity and acceleration at both $t = 0$ and $t = 1$. The motion is performed with the pendulum in an inverted position, in order to better test the robustness of the controllers. The tests were all programmed in Matlab. In order to accelerate the simulations, the muscle equations and their derivatives were implemented in a vectorized *mex* file. The physiological criterion was used for both approaches: CMC and co-simulation. All the time integrations of muscle equations related to the optimization were carried out using the *ode*23*t* integrator, which contains the implicit trapezoidal rule. In the co-simulation method,

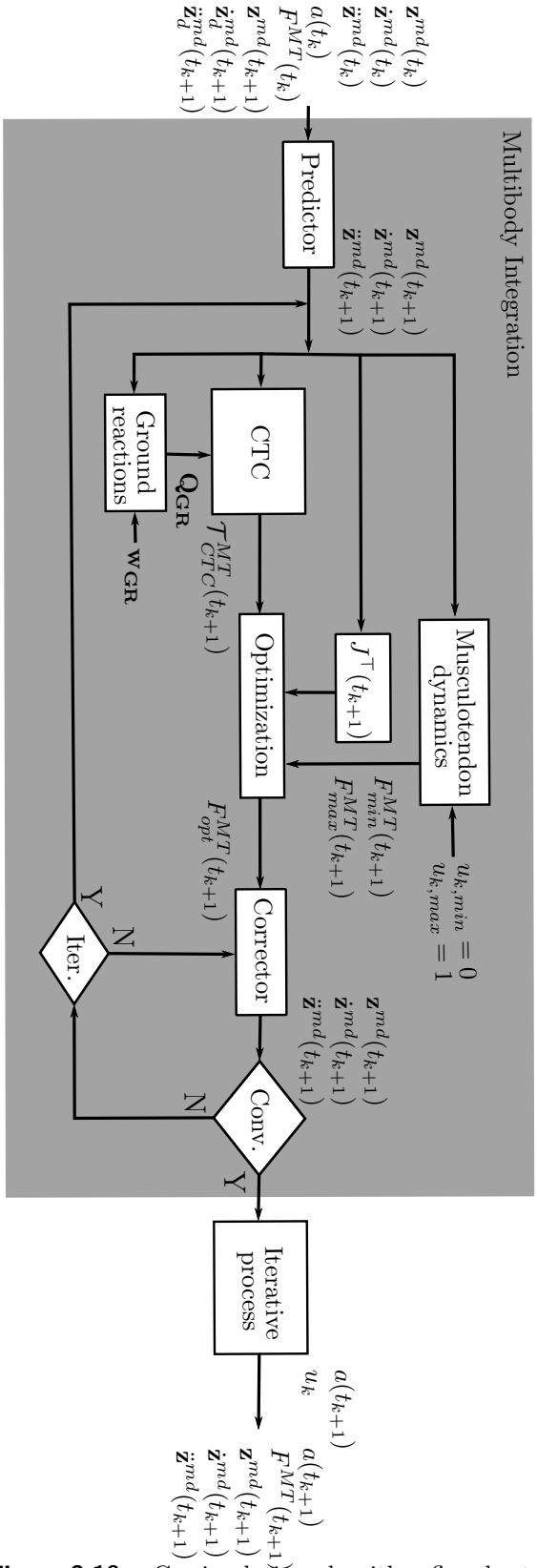

Figure 3.10 – Co-simulation algorithm flowchart.

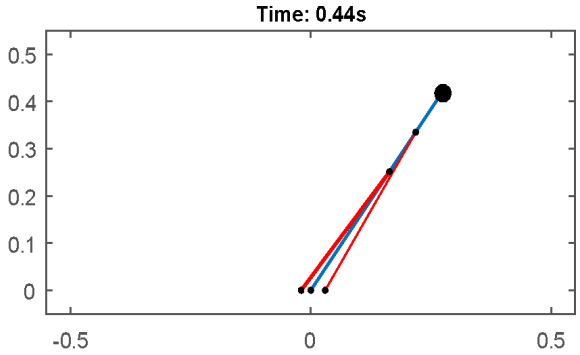

Figure 3.11 – Simple pendulum actuated by two muscles.

the multibody system was integrated with a time step of 10 ms, using an implicit trapezoidal rule with Newton-Raphson iteration.

The CMC method also used the trapezoidal rule, although integrating the multibody and muscle dynamics equations together, and using a time step of 1 ms. The optimization process was repeated every 10 ms.

Method	CPU time (s)	RMS error (deg)
CMC	8.25	0.0025
CSS	23.66	0.0186
CSA	7.85	0.1146

Table 3.5 – Simulation results.

Table 3.5 shows the CPU-time and tracking accuracy obtained for the three methods: CMC, co-simulation standard (CSS), and co-simulation approximated (CSA).

The computational effort to solve the muscle force-sharing problem by optimization every 10 ms is similar for all the methods. However, the simple model analyzed is not totally conclusive, since the multibody equations (in this case a single equation) are too simple and have almost no impact in the computational load. CMC achieved the best accuracy due to the smaller integration time step. Co-simulation can reach even better accuracy at 1 ms, but at the cost of a much higher CPU-time due to the large number of optimizations.

The top plot of Figure 3.12 shows the tracking errors, and the bottom plot compares the excitations obtained with CMC and CSS. CMC excitations are stepped because the integration is performed at 1 ms, but the excitations are calculated every 10 ms. It can be seen that the results at coinciding time steps are very close. If the muscles can always deliver the required torques from Eq. (3.49), all the methods yield very similar excitations (Figure 3.12).

In case the motion is more violent and the muscles cannot follow it accurately, discrepancies between methods increase, due to the different estimations they use for future positions and velocities. This should never happen when analyzing a recorded motion: if the motion actually happened, muscles were capable of producing it. However, this problem can appear in motion prediction.

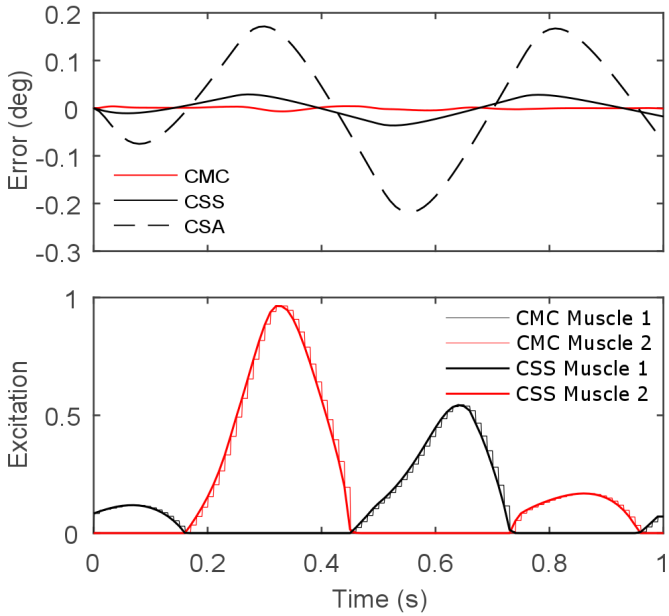

Figure 3.12 – Results comparison between CMC and CS.

Gait analysis

In order to complete the comparison of different ways to estimate muscular forces in healthy gait, the criteria tested with the inverse-dynamics based optimization are compared now using forward dynamics and the co-simulation standard algorithm.

Figure 3.13 illustrates the discrepancies between the muscular activations provided by different criteria and with respect to the EMG measurements too.

Mean values R of the five healthy subjects for each muscle and approach are given in Table 3.6. Once again, the best values are obtained with the first criterion, with a mean correlation of 75%. However, there was no clear differences between the six criterion used. Obtained correlations were acceptable, with values going from 66% to 75%.

No significant differences were observed with respect to the results obtained through the inverse-dynamics approach because the obtained joint moments were similar as the same recorded motions were studied. Therefore, the use of forward dynamics did not improve the results, and the iterative process made the computation slower.

	Mean correlation coefficient R values across subjects EMG vs. muscle activations					
	I	**II**	**III**	**IV**	**Phys.**	**Phys. 3**
R. Tibialis Anterior	0,74	0,73	0,72	0,51	0,69	0,62
R. Vastus Lateralis	0,73	0,74	0,88	0,56	0,85	0,65
R. Adductor Magnus Middle	0,58	0,48	0,39	0,55	0,65	0,61
R. Gastrocnemius Medial	0,80	0,66	0,76	0,75	0,64	0,66
R. Gastrocnemius Lateral	0,72	0,62	0,62	0,67	0,65	0,59
R. Semitendinosus	0,76	0,79	0,79	0,75	0,64	0,67
R. Biceps Femoris Long Head	0,77	0,81	0,84	0,70	0,21	0,56
R. Gluteus Maximus Middle	0,92	0,91	0,93	0,88	0,93	0,93
R. Gluteus Medius Middle	0,75	0,58	0,61	0,59	0,63	0,72
Mean	**0,75**	**0,70**	**0,73**	**0,66**	**0,66**	**0,67**
Computational time (sec)	16,35	360,07	175,77	247,75	1828,71	27,32

Table 3.6 – R correlations in forward-dynamics analysis ($R < 0.50$ in red).

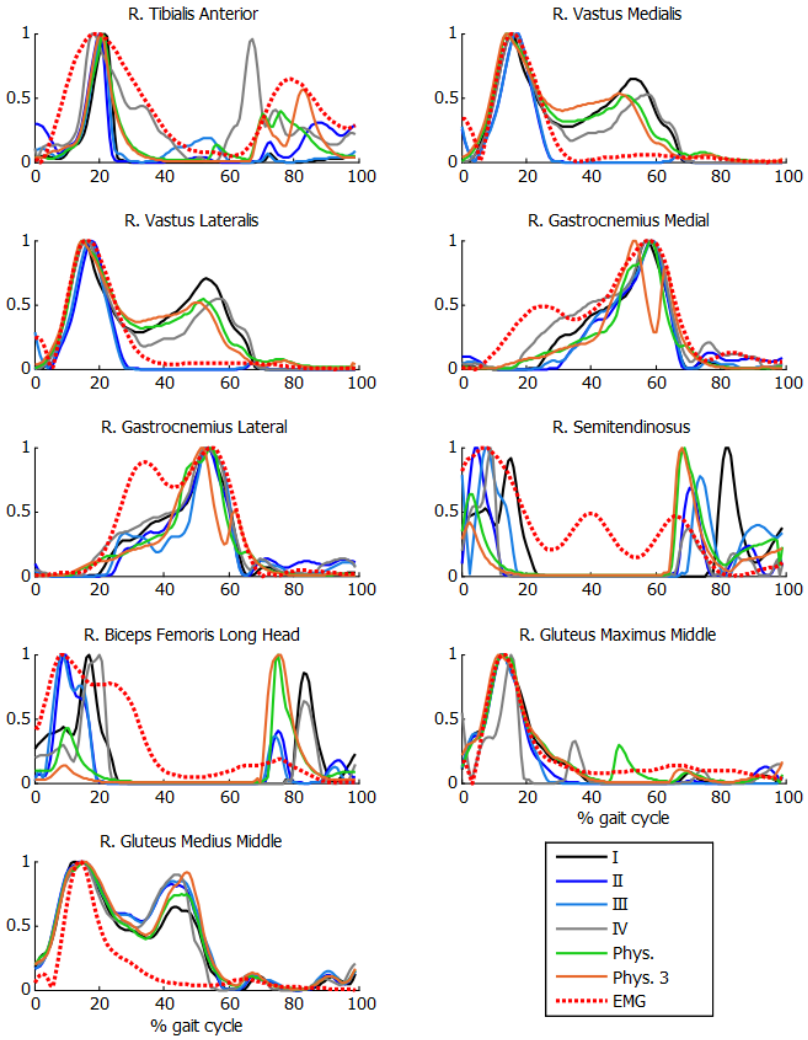

Figure 3.13 – Normalized muscular activations obtained with different criteria in forward-dynamics vs. normalized EMG for a healthy subject.

Chapter 4

Muscle energy expenditure

In the literature, various Hill-based methods to calculate the human muscle energy expenditure can be found [46], [45], [87], [47]. R.H. Miller proposed a comparison of these methods for simulating human walking in [48]. According to his recommendations, the methods of Umberger and Bhargava have been implemented in this work to calculate the energetic cost of healthy subjects in normal gait and of SCI subjects in crutch gait.

Both muscle energy expenditure methods considered, based on the Hill muscle model, need to know some muscular parameters to be used. After obtaining the muscular activity by physiological static optimization method, the activation, the length, the velocity and the muscular force are used as input to the two methods for the estimation of energy expenditure. Both models are based on the first law of thermodynamics. According to this law, the total rate of energy consumption at each instant, $\dot{E}$, is equal to the rate at which heat is liberated, $\dot{H}$, plus the rate at which work is done, $\dot{W}$:

$$\dot{E} = \dot{H} + \dot{W} \tag{4.1}$$

4.1 Umberger

The muscle energy expenditure method of Umberger [46] considers the activation heat rate ($\dot{h}_A$), the maintenance heat rate ($\dot{h}_M$), the shortening/lengthening heat rate ($\dot{h}_{SL}$), and the mechanical work rate of the contractile element of the muscle ($\dot{w}_{CE}$), to determine the total rate of muscle energy expenditure ($\dot{E}$). The relation is given by the sum of this four terms expressed in Eq. (4.2), calculated for each muscle in $W.kg^{-1}$.

$$\dot{E} = \dot{h}_A + \dot{h}_M + \dot{h}_{SL} + \dot{w}_{CE} \tag{4.2}$$

Activation and maintenance heat rate

A combined expression of the activation and maintenance heat rate is used for this first term,

$$\dot{h}_A + \dot{h}_M = \dot{h}_{AM} = 1.28 \times \%FT + 25 \tag{4.3}$$

where represents the percentage of fast twitch which can be found in [88].

Shortening and lengthening heat rate

During CE shortening, the rate of heat production is modeled as the product of a coefficient α_S and v^M , the velocity of the muscular contractile element:

$$\dot{h}_{SL} = \begin{cases} \alpha_{S(ST)}\tilde{v}^M(1 - \%FT/100) - \alpha_{S(FT)}\tilde{v}^M(\%FT/100) & if \quad v^M \leq 0, \\ \alpha_L \tilde{v}^M & if \quad v^M > 0, \end{cases} \tag{4.4}$$

with the constant terms:
$\alpha_{S(ST)} = (4 \times 25)/\tilde{v}^M{}_{(MAX-ST)}$,
$\alpha_{S(FT)} = 153/(\tilde{v}^M{}_{(MAX-FT)})$,
$\alpha_L = 4\alpha_{S(ST)}$,
$\tilde{v}^M{}_{(MAX-FT)} = v^M{}_{MAX}/l_0^M$,
$\tilde{v}^M{}_{(MAX-ST)} = \tilde{v}^M{}_{(MAX-FT)}/2.5$
and $\tilde{v}^M{}_{(MAX-ST)} = l_0^M/0.1$.

Mechanical work rate

The specific mechanical work rate is given by:

$$\dot{w}_{CE} = -(F_{CE}^M v^M)/m \tag{4.5}$$

where m is the muscle mass (kg) related to the physiological cross sectional area (PCSA) by:

$$m = PCSA\rho_m l_0^M \tag{4.6}$$

with $\rho_m = 1059.7\ kg.m^{-3}$, the mammalian muscle density [89].

Total energy expenditure scaled

Eq. (4.2) provides the energy expenditure of the muscle for the case of full activation and optimal muscular length l_0^M of the contractile element. Scaling factors are needed to account for the length and activation dependence of $\dot{h}_{AM}$ and $\dot{h}_{SL}$, and the dependence of the total heat rate on the metabolic working conditions ($S = 1$ for primarily anaerobic conditions, and $S = 1.5$ for primarily aerobic conditions),

$$\dot{E} = \begin{cases} \dot{h}_{AM}A_{AM}S + \dot{h}_{SL}A_{SL}S + \dot{w}_{CE} & if \quad l^M \leq l_0^M, \\ (0.4 \times \dot{h}_{AM} + 0.6 \times \dot{h}_{SL}F_0^M)A_{AM}S + A_{SL}S + \dot{w}_{CE} & if \quad l^M > l_0^M, \end{cases} \tag{4.7}$$

with $A_{AM} = A^{0.6}$, $A_{SL} = A^2$, and

$$A = \begin{cases} u(t) & if \quad u(t) \leq a(t), \\ (u(t) + a(t))/2 & if \quad u(t) > a(t) \end{cases} \tag{4.8}$$

where u and a represent the excitation and activation of the muscle respectively.

4.2 Bhargava

Bhargava's method presents some similarities with the previous one, since both start from equation Eq. (4.2), but details in the terms equations are different.

Activation heat rate

$$\dot{h}_A = \phi f_{FT} \dot{A}_{FT} u_{FT}(t) + \phi f_{ST} \dot{A}_{ST} u_{ST}(t) \tag{4.9}$$

with

$$\phi = 0.06 + exp(-t_{stim} u(t)/\tau_\phi), \tag{4.10}$$

where τ_ϕ is the decay time constant (i.e., 45 ms) and t_{stim} is the amount of time the muscle has been excited above 10%.

$$u_{FT}(t) = 1 - \cos(\frac{\pi}{2} u(t)) \quad and \quad u_{ST}(t) = \sin(\frac{\pi}{2} u(t)), \tag{4.11}$$

and the constant terms: $f_{FT} = \%FT/100$, $f_{ST} = 1 - \%FT/100$, $\dot{A}_{FT} = 133$ and $\dot{A}_{ST} = 40$.

Maintenance heat rate

$$\dot{h}_M = L(\tilde{l}^M) f_{FT} \dot{M}_{FT} u_{FT}(t) + L(\tilde{l}^M) f_{ST} \dot{M}_{ST} u_{ST}(t) \tag{4.12}$$

where $L(\tilde{l}^M)$ is a function that models the dependence on muscle length:

$$L(\tilde{l}^M) = \begin{cases} 0.5 & if \quad \tilde{l}^M \leq 0.5, \\ \tilde{l}^M & if \quad 0.5 < \tilde{l}^M \leq 1 \\ -2(\tilde{l}^M) + 3 & if \quad 1 < \tilde{l}^M \leq 1.5 \\ 0 & if \quad \tilde{l}^M > 1.5 \end{cases} \tag{4.13}$$

and the maintenance heat rate constants: $\dot{M}_{FT} = 111$ and $\dot{M}_{ST} = 74$.

Shortening and lengthening heat rate

During CE shortening, in this method, the rate of heat production is also modeled as the product of a coefficient α_S and v^M,

$$\dot{h}_{SL} = -\alpha_S v^M \tag{4.14}$$

$$\alpha_S = \begin{cases} 0.16F_0^M + 0.18F_{CE}^M & if \quad v^M \leq 0, \\ 0.157F_{CE}^M & if \quad v^M > 0, \end{cases} \tag{4.15}$$

Mechanical work rate

Both authors consider the same expression for the mechanical work rate:

$$\dot{w}_{CE} = -(F_{CE}^M v^M)/m \tag{4.16}$$

Total energy expenditure

$$\dot{E} = \dot{h}_A + \dot{h}_M + \dot{h}_{SL} + \dot{w}_{CE} + \dot{h}_B \tag{4.17}$$

Unlike the first method, the terms are already scaled here, but Bhargava's method proposes in addition a basal metabolic rate $\dot{h}_B$ calculated from a frog skeletal muscle at 0°C and given by:

$$\dot{h}_B = 0.0225. \tag{4.18}$$

4.3 Total energy expenditure during a gait cycle

The total energy expenditure calculated before is for each muscle and each time point. The total energy expenditure during a gait cycle, E_{met}, is obtained as follows:

$$E_{met} = \left(\sum_{i=1}^{n} \left(\frac{\int_{t=0}^{t_{end}} \dot{E}_i(t) \times m_i \, dt}{\Delta t_{cycle}} \right) + k_b \times m_{residual} \right) / m_{subject}, \tag{4.19}$$

with Δt_{cycle} the time of a complete gait cycle ($\Delta t_{cycle} = t_{end} - t_0$), n the number of muscles, and

$$m_{residual} = m_{subject} - \sum_{i=1}^{n} m_{muscle,i}. \tag{4.20}$$

To account for whole body metabolism, the proportion of total body mass not represented by the modeled muscles was assigned an energy rate $k_b = 1.2W.kg^{-1}$, which is the average energy rate for standing [40]. Later, we will see that this constant can be used for model calibration.

4.4 Results and experimental validation

In order to validate the implementation of the two methods presented above, 21 complete gait cycles of a healthy subject (subject 1 in 2.1.1) were recorded at seven different speeds (between his free selected speed and fast speed) for energetic cost estimation. Experimental measurements were obtained by means of a portable gas analyzer during two 5-minute tests at free selected speed and fast speed (Figure 4.1). The obtained linear relation between gait speed and energy expenditure estimations showed a good correlation with experimental measurements and literature [40] (Figure 4.2). However, it's important to highlight that a constant discrepancy of the results was observed with respect to the measured energy values (y-intercept), so the model was calibrated with such a constant ($0.12W.kg^{-1}$ for Umberger's method and $1.9W.kg^{-1}$ for Bhargava's method). This calibration can be considered as an adjustment of the whole-body basal metabolic rate k_b, introduced in Section 4.3.

Figure 4.1 – Energy consumption for a healthy subject: a) motion-force-EMG capture; b) 5-minute test with portable gas analyzer.

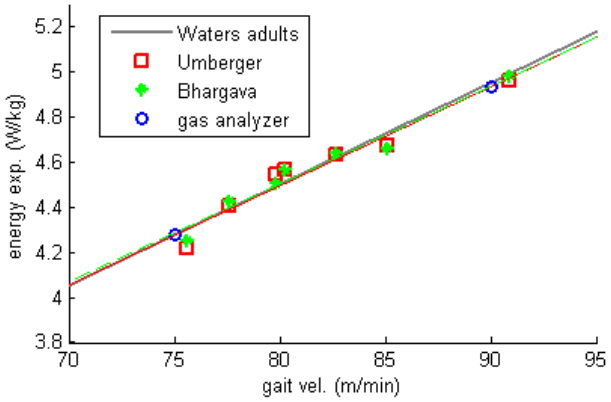

Figure 4.2 – Energy expenditure for a healthy subject.

Chapter 5

Applications to SCI subjects

As explained in the Introduction, the objective of this work is to evaluate the effect of orthotic devices in SCI subjects by means of some indicators which may provide the likeliness of actual use of the device by the subject. Moreover, such indicators will allow the comparison of different orthotic devices.

The mentioned indicators are the joint reactions and the energetic cost. The estimation of both of them requires the previous solution of the muscular problem. Therefore, the methods presented before for healthy gait are applied here to the crutch-assisted gait of SCI subjects.

This thesis was part of an Spanish investigation project with objective to design a research prototype of a low-cost active orthosis for the gait of SCI subjects [7]. The existing methods for gait analysis presented and evaluated before with healthy subjects have been adapted to SCI subjects during crutch-assisted gait. These analyzes allow to compare the efficiency of gait-assistive devices.

5.1 The active KAFO

In this Section, the active KAFO that has been compared with the conventional passive orthosis is described. Starting from a conventional passive KAFO, an electric motor plus Harmonic gearbox are placed at knee level, substituing the external original joint, and an inertial measurement unit (IMU) is placed at shank level in the external upright. The orthoses are complemented by a backpack, carried by the subject, which contains an embedded computer board, the motor drivers and the battery (Figure 5.1).

During gait, when motion intention is detected by the IMU, a swing cycle is launch in order to avoid foot-collision with the ground. With the conventional passive device, the patient needs to perform extra pelvis movements to complete the swing cycle without foot-collision.

The active KAFO also includes an Android application for smartphone that allows to switch on/off the system, enable/disable the gait cycle, and setting the controller parameters.

Figure 5.1 – The low-cost active KAFO.

5.2 The adaptation process

As said before, subjects selected to use the orthotic devices showed partial hip actuation and were able to walk with the conventional passive KAFO and crutches. Gait analysis was carried out with each subject in the gait laboratory (Figure 5.5) to obtain their gait characteristics and estimate the controller parameters of the prototype.

These parameters were adjusted during the training sessions. Subjects needed to get used to the new device, so, initially, they walked with the help of parallel bars for the sake of safety and the swing cycle was progressively introduced in the devices as the patient gained confidence. When the subject was ready, the process was repeated using crutches instead of parallel bars.

To quantify the progress achieved by the patient along the training sessions, some gait cycles were recorded periodically by a portable motion capture system composed by six infrared cameras (Natural Point, OptiTrack FLEX:V100 sampling at 100 Hz). Then, a computer-based application (in-house developed code programmed in Matlab) was used for the subsequent post-processing (Figure 5.2).

Finally, when the subject was able to walk with the aid of the active KAFO and the crutches, a gait analysis was carried out in the lab to obtain motion-force-EMG captures to run and validate musculoskeletal analyses.

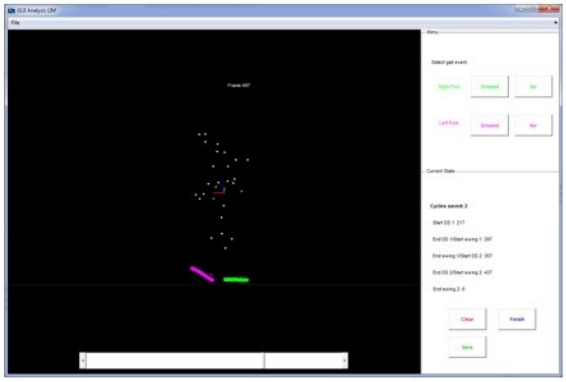

Figure 5.2 – Portable motion capture system and post-processing application.

5.3 Crutch-assisted gait analysis

5.3.1 Skeletal model

The 3D human model for SCI subjects (Figure 5.3) has been modeled in the same way as the healthy skeletal model defined in 2.1.2. The crutches are rigidly connected to the hands and the orthoses are embedded in the corresponding body links (thighs, shanks and feet). The geometric and inertial parameters of the model are the same as those of the healthy subjects previously described. Assistive devices were taken into account by altering the inertia properties of hands (crutches) and thighs, calves and feet (orthoses). Inverse-dynamics analysis was applied to obtain the ground reactions and joint drive torques along the motion [90]. Measurements from the force plates and instrumented crutches were just used to overcome the indeterminacy in the distribution of ground reactions during the multiple-support phases, and to confirm the results from the inverse-dynamics analysis [73]. Therefore, the obtained joint drive torques and external reactions were consistent with the corresponding motion.

5.3.2 Musculoskeletal model

People with SCI have lost some motor functions due to the injury. The SCI subjects participating in this study required crutches and passive orthoses to walk due to the lost of muscular functions in the lower limbs. In such a gait, both lower and upper limbs are solicited so a full body musculoskeletal model is needed. However, as each SCI subject is different, the musculoskeletal model has to be personalized. Therefore, a first step was to carry out local motion tests, designed and supervised by a doctor specialized in sport and exercise, during which surface EMG was measured in muscles of uncertain activity. The subject was asked to perform several hip exercises with the help of parallel bars for stability, as seen in Figure 5.4, to detect active muscles based on EMG results and on how the different motions were performed. Only muscles with detected activity were included in the model.

The whole musculoskeletal model is composed by: 43 muscles in each leg (28 at

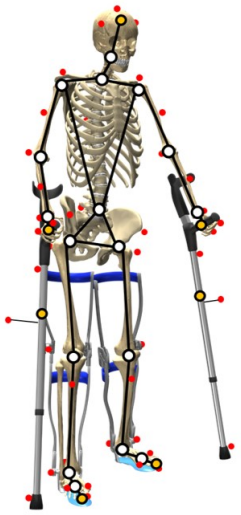

Figure 5.3 – Human multibody model.

Figure 5.4 – Motor test with surface EMG to assess muscle activity.

hip, 5 at knee and 10 at ankle), 6 at the trunk and 26 in each arm (15 at the shoulder and 11 at the elbow). The model is adapted to the subject (eliminating the inactive muscles as explained before) and to the aim of the study (if the gait is symmetric, only one side can be considered). Geometries and properties of the muscles have been taken from OpenSim, which are defined for the OpenSim reference model in [26] for the lower limb and in [55] for the upper limb.

Muscular parameters have been scaled to subjects in the same way as the for healthy subjects.

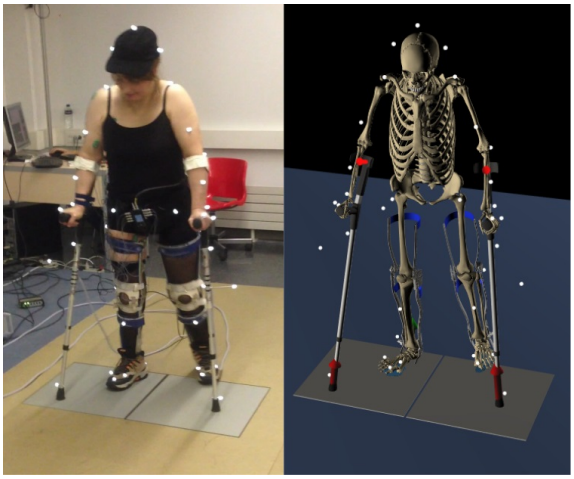

Figure 5.5 – Gait of SCI subject assisted by passive orthoses and crutches: a) acquired motion; b) computational model.

5.4 Results and experimental validations

As commented in 1.2.5, the uniqueness of spinal cord injuries limits the inter-subjects repeatability. Two voluntary SCI subjects have participated in this study.

5.4.1 Case 1: Bilateral SCI subject

Subject

The first subject (Figure 5.5) was an adult female of age 45, mass 65 kg and height 1.52 m, with spinal cord injury at T11 (Figure 1.3). Her injury allowed her a normal motion of the upper extremities and trunk, while partially limiting the actuation at the hips due to partial or no muscular innervation. Her corresponding LEMS is 10/50 (Figure 5.6). Therefore, in order to walk, she required the assistance of a pair of passive KAFO and two crutches. In daily life she mainly used a wheelchair to move and resorted to the mentioned assisted gait only occasionally and during short periods of time.

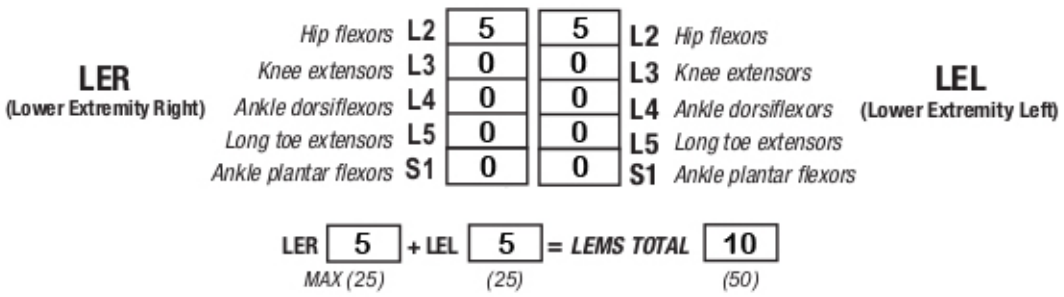

Figure 5.6 – LEMS bilateral SCI subject.

Personalized musculoskeletal model

This subject presented a symmetrical gait pattern, so, only muscles of the right side have been considered. After muscular activity assessment by means of EMG measurements (as explained in Sub-section 5.3.2), inactive muscles at hip level have been removed. The musculoskeletal model (Figure 5.7) was then composed of 53 muscles: 21 muscles at the right hip (only muscles for which EMG activity was detected in the local motion tests), 6 at the trunk, 15 at the right shoulder and 11 at the right elbow.

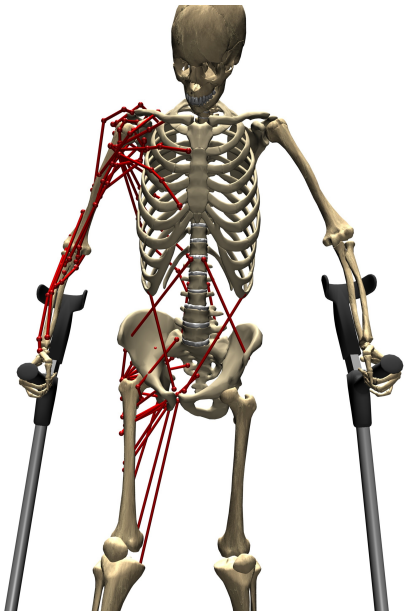

Figure 5.7 – Musculoskeletal model of the bilateral SCI subject.

Estimation of muscle forces during crutch gait

Muscular activation of the 53 muscles were estimated by the physiological inverse-dynamics approach with rigid tendon and the closed-form solution of the activation dynamics (Phys. 3). Results were compared with EMG measurements for 8 muscles and they are represented in Figure 5.8. The corresponding coefficient correlations R between estimations and experimental measurements show acceptable results with a mean correlation of 70% (Figure 5.1).

Walking with crutches produces important joint loads at the upper extremities. Estimated joint reaction forces at the right shoulder show a maximum pick value of 140% of the bodyweight (Figure 5.9). Maximum loads of up to 170% were measured by Westheroff [91] during in-vivo measurements. This explains why 51% of people with spinal-cord injury have shoulder problems [52].

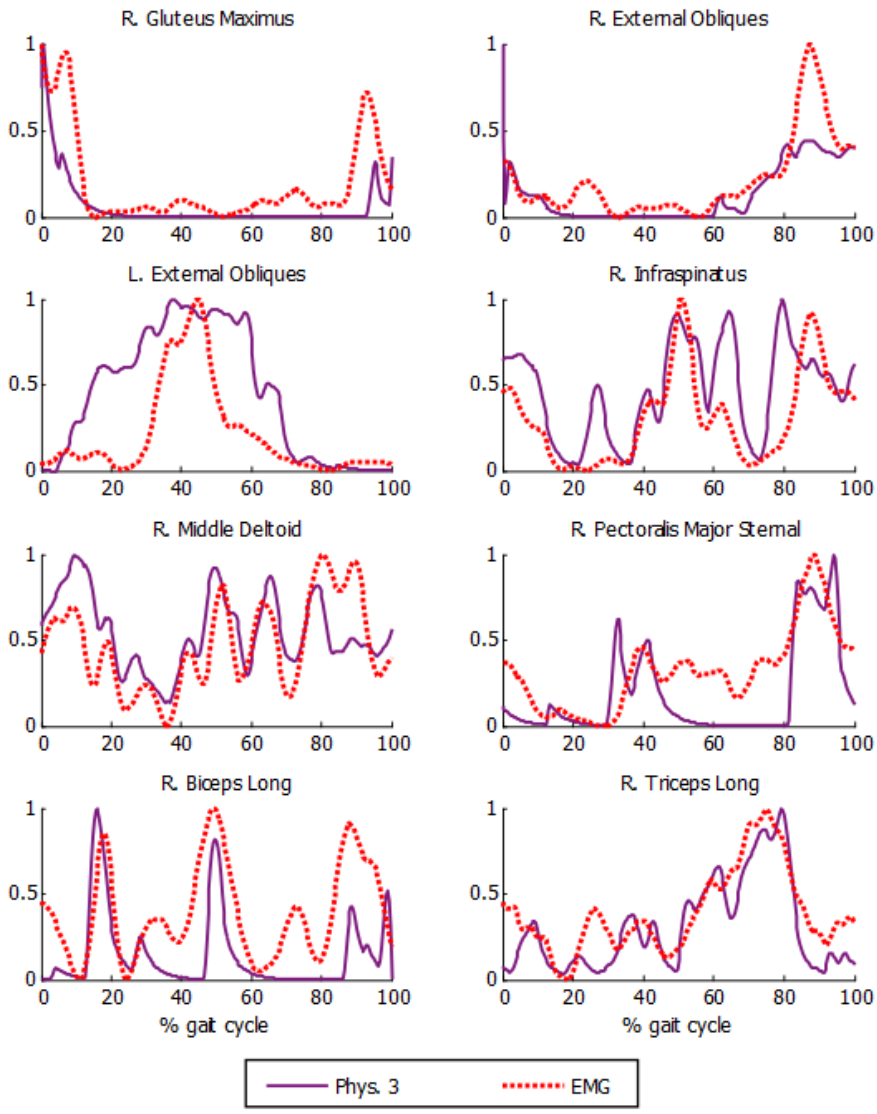

Figure 5.8 – Normalized muscular activations obtained for the bilateral SCI subject vs normalized EMG.

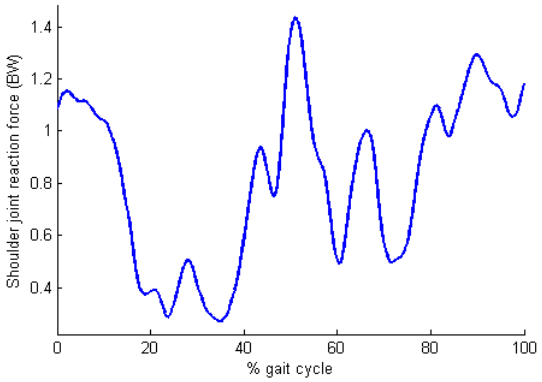

Figure 5.9 – Right shoulder joint reaction force of the bilateral SCI subject during crutch gait.

	Correlation coefficient R EMG vs. muscle activations
R. Gluteus Maximus Posterior	0,68
R. External Obliques	0,89
L. External Obliques	0,76
R. Infraspinatus	0,63
R. Middle Deltoid	0,57
R. Pectoralis Major Sternal	0,75
R. Biceps Long	0,50
R. Triceps Long	0,86
Mean	**0,70**

Table 5.1 – R correlations obtained for the first SCI subject.

Evolution using active orthoses

After some training sessions, the patient was adapted to the use of the active orthoses (Figure 5.10). Gait cycles using the new devices were recorded by the portable motion capture system (Figure 5.2) and gait parameters are compared in Figure 5.11. Significant improvements were noticed thanks to motor actuation in both knees. She was able to walk faster by using a longer stride and a higher cadence. Her gait pattern changed significantly, with reduced pelvis movements which led to a lower lateral displacement of the center of mass (COM).

Unfortunately, the subject couldn't continue to use the active orthoses due to cervical arthritis (resulting of sedentarism and the important use of wheelchair). Motion capture in the gait laboratory for a complete analysis couldn't be done, so comparison of the devices has been limited to the kinematic part for this subject.

Figure 5.10 – Patient using the active orthoses with crutches.

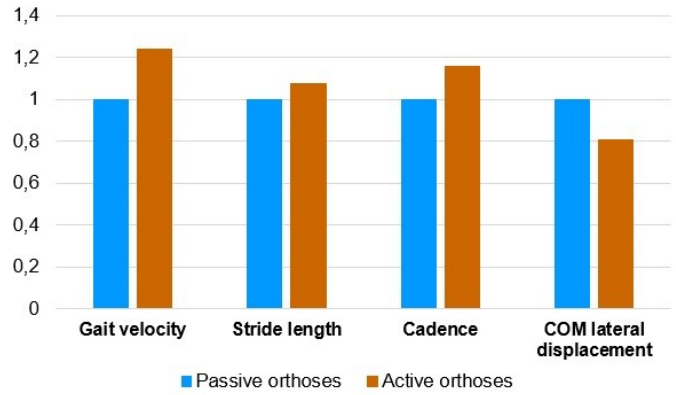

Figure 5.11 – Gait comparisons: passive vs. active orthoses.

5.4.2 Case 2: Unilateral SCI subject

Subject

The second SCI subject was an adult male of mass 82 kg and height 1.85 m, with injury corresponding to LEMS of 13/50 (Figure 5.12). Like the first subject, his injury affects only his lower extremities. However, in this case limitations at the lower limbs are non symmetrical, since the injury allows knee actuation at the right leg in addition to hip actuation. He required the assistance of a passive KAFO at the left leg, a passive ankle-foot orthosis at the right leg, and two crutches. Despite possessing higher capacity than the first subject, he also used mainly a wheelchair to move and resorted to the mentioned assisted gait during short periods of time.

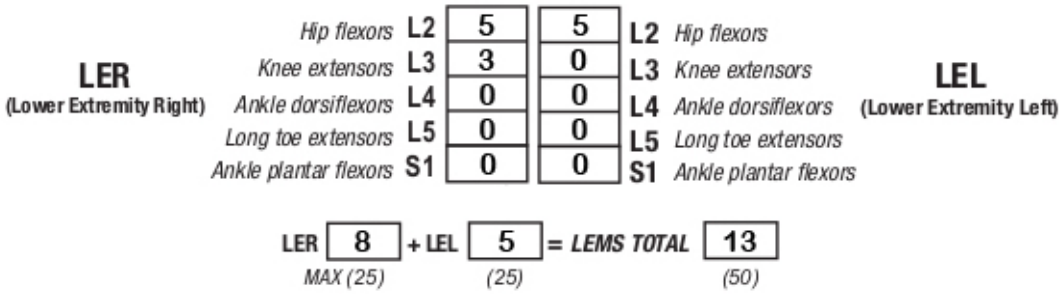

Figure 5.12 – LEMS bilateral SCI subject.

Personalized musculoskeletal model

The second subject presented non symmetrical limitations at the lower limbs, so a bilateral analysis was required. The musculoskeletal model of the full body was customized to the SCI subject according to his muscle activity (previously measured through EMG, as explained in Sub-section 5.3.2). The musculoskeletal

model (Figure 5.13) was composed of 112 muscles for the whole body: 28 at the right hip, 5 at the right knee, 21 at the left hip, 6 at the trunk, 15 at each shoulder and 11 at each elbow.

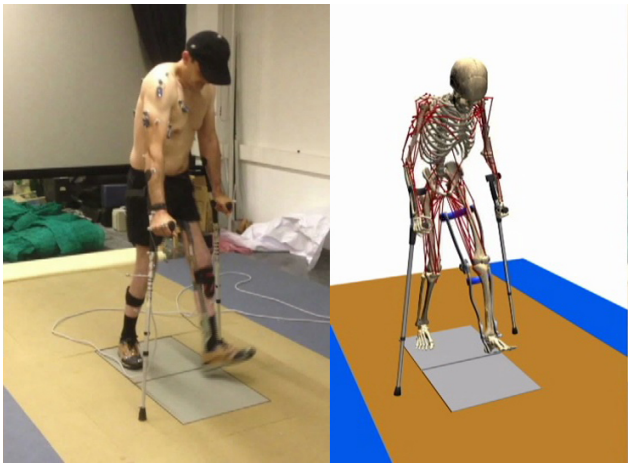

Figure 5.13 – Gait of SCI subject assisted by passive orthoses and crutches: a) acquired motion; b) musculoskeletal model.

Estimation of muscle forces during crutch gait

Muscle forces were estimated by the physiological inverse-dynamics approach with rigid tendon and the closed-form solution of the activation dynamics (Phys3). Results were validated with EMG measurements for 10 muscles, and are represented in Figure 5.14. A mean coefficient correlation R of 56% between experimental measurements and muscle activations was obtained, which is considered acceptable.

Comparison of gait-assistive devices

After some few training sessions, the SCI subject was able to walk with confidence wearing the active KAFO. So three gait cycles were compared for the SCI subject: i) passive orthosis owned by the subject; ii) active orthosis with motor locking the knee; iii) active orthosis with motor moving the knee.

While the walking speed was the same in the three cases, some kinematic differences could be observed (Table 5.2). First, the step length, of 45 cm and 66 cm for the right and left legs respectively using the original KAFO, changed to 58 cm for both sides when using the active KAFO with motor moving the knee. The initial circumduction of the left foot (KAFO's leg) of 11.5 cm with the original KAFO was reduced to 7.25 cm thanks to the actuated knee flexion. Pelvic maximum rotations were reduced from -27.6º and 44.8º to -22.5º and 35.3º in the transverse plane, and from 19.18º to 15.23º in the frontal plane. Finally, the mediolateral COM displacement was significantly reduced from 13.48 cm to 11.54 cm, while the vertical displacement was almost the same in the three cases.

Instrumented crutch measurements did not show significant differences between devices. A mean load of 20% of the bodyweight was observed during the gait cycle,

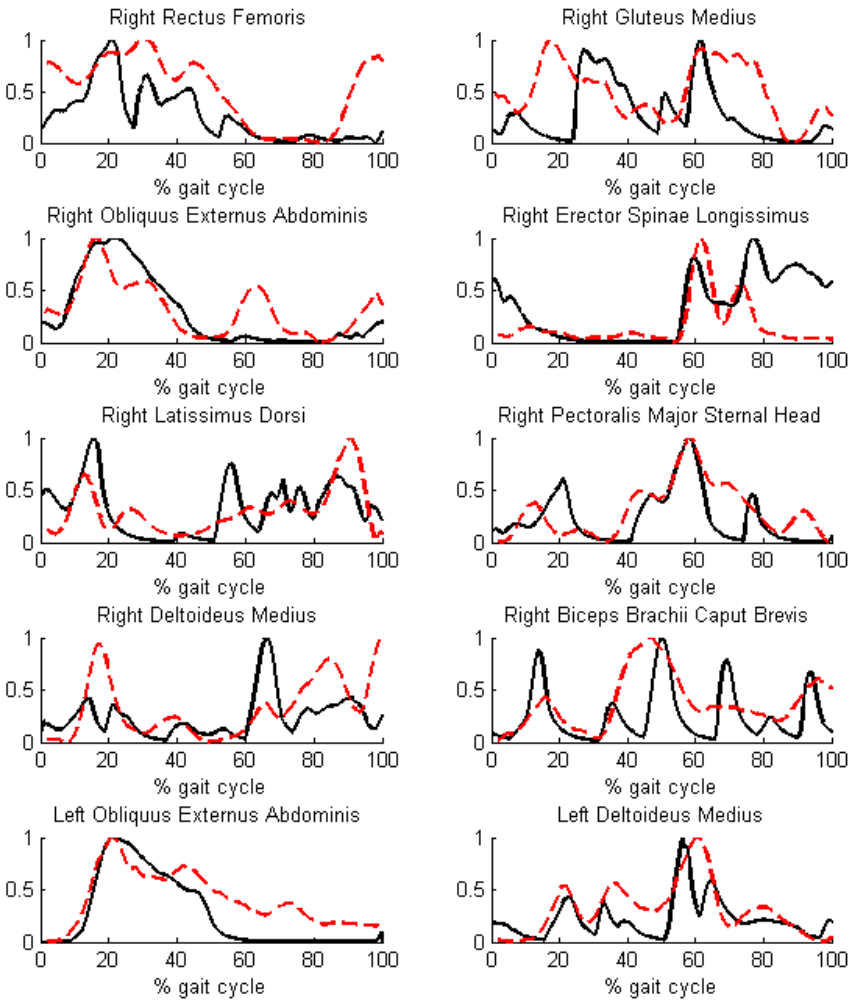

Figure 5.14 – Normalized muscle activations obtained for the unilateral SCI subject (black) vs normalized EMG (red).

with peaks of 55% (left crutch) and 40% (right crutch) at swing start. Estimated joint reaction forces at shoulder were similar too, with peaks between 190% and 225% (left shoulder) of the bodyweight.

The energy cost obtained with the original KAFO was 3.49 $W.kg^{-1}$ for Umberger's model, and 3.11 $W.kg^{-1}$ for Bhargava's. Wearing the active KAFO with motor locking the knee, it was 3.56 $W.kg^{-1}$ and 3.13 $W.kg^{-1}$. Finally, wearing the active KAFO with motor moving the knee, the energy cost was 3.28 $W.kg^{-1}$ and 3.02 $W.kg^{-1}$.

		passive KAFO	active KAFO (locked knee)	active KAFO (moving knee)
Gait velocity (m/min)		33	33	33
Vertical COM displacement (cm)		3.47	3.79	4.11
Mediolateral COM displacement (cm)		13.48	13.42	11.54
Step length (cm)	**Right**	0.45	0.52	0.58
	Left	0.66	0.62	0.58
Left circumduction (cm)		11.52	9.10	7.25
Range pelvic rotations in frontal plane (°)		[-4.81; 19.18]	[-4.56; 16.93]	[-4.86; 15.23]
Range pelvic rotations in transverse plane (°)		[-28.74; 42.87]	[-28.32; 37.93]	[-24.36; 31.83]
Energy cost(W/kg)	**Umberger**	3.49	3.56	3.28
	Bhargava	3.11	3.13	3.02

Table 5.2 – Comparison of the three gait-assistive devices.

Discussion

The self-selected gait velocity achieved by the SCI subject with the three devices was of 33 m/min, which is higher than the velocity corresponding to his LEMS (20.2 m/min) according to [40]. This discrepancy can be explained by the moderately strong linear relationship ($R = 0.64$) between walking speed and LEMS, and by the fact that the subject was tall and athletic.

The SCI subject carried out few training sessions with the active KAFO, and probably needed more experience to show a significant evolution with respect to the passive device, as observed in [92]. However, some improvements of the gait pattern thanks to the knee actuation provided by the KAFO were already detected, as symmetry in the step lengths, reduced circumduction and reduced pelvic rotation. COM displacements are generally used as indicators of balance control to reflect the whole body motion during gait. While the vertical displacement was almost the same for the three cases and was close to that of healthy subjects (3.61 cm at 1 m/s [93]), the mediolateral displacement reflected differences in gait pattern and with respect to healthy subjects (5.96 cm at 1 m/s [93]).

Ground force reactions measured by the instrumented crutches did not highlight any differences between the devices used, likely because of the short training period with the new device. However, the obtained values showed the demanding use of the upper extremities, which are primarily not prepared to walk and to put up with such loads.

Same observations can be done regarding the joint reaction force at shoulders, with estimated peaks greater than 220% of the bodyweight. Westerhoff [91] reported maximum loads of up to 170% during in vivo measurement of shoulder loads during crutch-assisted walking, but subjects were not suffering from any lower limb disability. The highest peaks at the left shoulder were observed during the left-leg swing (leg wearing the KAFO), likely because the subject needed to compensate the instability of the left foot and the lack of force in the right leg, and to avoid the foot contact with the ground.

Correlations observed between EMG measurements and muscle activations for the SCI subject were acceptable and allow trusting in the input used to calculate the energy cost.

Regarding the energetic cost, 5-minute tests are too demanding for SCI subjects and simpler experimental tests are not accurate. Therefore, the obtained results were compared with results from bibliography. First of all, to have a reference, Waters [40] showed that a healthy subject should consume $2.385\,W.kg^{-1}$ at the speed developed by the SCI subject (33 m/min). Continuing with Waters' references for SCI subjects, for a LEMS of 13, the subject should consume 149.8% more than a healthy subject at the same speed. This would correspond to an energy consumption of $3.57\,W.kg^{-1}$, which is close to the values obtained with Umberger for the two first cases ($3.49\,W.kg^{-1}$ and $3.56\,W.kg^{-1}$). In the third case, the motor actuation produces the knee flexion/extension, so that the LEMS could be increased to 14. Then, the corresponding energy consumption increase should be of 145.5% with respect to a healthy subject, thus leading to a consumption of $3.47\,W.kg^{-1}$, versus the $3.28\,W.kg^{-1}$ obtained with Umberger. However, as shown in Section 4.4, results obtained for a healthy subject needed calibration to estimate the correct basal consumption. For the SCI subject, while results obtained without calibration are closer to the mentioned references for Umberger's method, slopes (energy cost vs. LEMS) are closer (gradient of -0.1) using Bhargava's method (gradient of -0.11) than Umberger's (gradient of -0.28).

Chapter 6

Conclusions and future work

6.1 Conclusions

This thesis had the objective of evaluating the effect of orthotic devices on SCI subjects along with the likeliness of its long-term use, through the estimation of some indicators as joint reactions and energetic cost, which in turn require the estimation of muscular activations and forces. Therefore, from the academic point of view, the thesis was focused on the analysis of human gait by computer modeling at musculoskeletal level. The work can be divided into two main parts. In the first part, methods were applied, validated and compared for healthy subjects. In the second part, methods selected in the first part were applied to two clearly different SCI subjects walking with crutches and two types of orthotic devices which were compared.

In the first part, several optimization methods for estimating muscle forces were applied and compared for five healthy subjects. Four static and three physiological inverse-dynamics based optimization approaches were compared first, and showed similar results. However, it must be pointed out that higher complexity of the method does not guarantee better results, as the best correlations with experimental values were obtained with the simplest and most common criterion. The physiological inverse-dynamics approach was hard to implement and presented the longest computational time among all the compared inverse-dynamics based approaches, while its simplified form ran more than 100 times faster and showed almost the same results.

Same conclusions can be drawn for the synergy optimization approach studied in this thesis. The consideration of synergy effects to solve the muscular force-sharing problem complicated the programming and led to slower algorithms. However, the obtained correlations did not show any improvement with respect to non-synergy-based approaches. The positive aspect was that the SynO approach can extract muscular synergies and offer a reasonable prediction of muscular activations and matching of the joint torques for the full leg. However, the proposed combination of SO with NMF showed poor results regarding the joint torques matching. Therefore, the SynO approach could result useful for application to functional electrical stimulation, motion control and prediction, as it reduces the dimensional control space.

Another practical approach for motion control or prediction is forward based. In this work, forward-dynamics based methods were used for recorded motions in order to compare them with the previously inverse-dynamics based approaches. A new method, based on CTC was proposed. It consists of a co-simulation algorithm where the multibody equations and the muscular dynamics are simulated within a different framework, allowing to use existing multibody codes. Two versions of the algorithm were suggested: (i) the standard approach (CSS), which required the solution of the muscular force-sharing problem at each iteration; (ii) the approximated approach (CSA), which limited the solution of the muscular force-sharing problem to the first iteration. These algorithms were compared with a reference method, the popular Computed Muscle Control (CMC), for the case of a simple pendulum actuated by two muscles. The CSS was the slowest approach due to its numerous optimizations and integrations. However, CSA showed better computational performance than CMC but its accuracy was affected. A compromised could be find by optimizing the CPU time and the accuracy. Then, the co-simulation standard algorithm was applied to the gait analysis of the five healthy subjects and several optimization criteria were compared. The obtained results presented the same conclusions as the inverse-dynamics analysis: the simplest criterion was the most efficient and the physiological one was much slower and did not improve the correlations.

However, despite of its disadvantages, the inverse-dynamics based physiological approach resulted useful to implement the two Hill-based energy expenditure methods because it is the only approach which provides the required muscular variables as inputs. If the simplified form with rigid tendon is used, the mechanical work rate gives almost zero due to the small length variations of the muscle's contractile part. Results obtained with the two energy expenditure methods were validated for one healthy subject during various gait cycles at different speeds. Good correlations were obtained with both approaches, but results showed that a subject-calibration of whole-body basal metabolic rate is necessary. Nevertheless, the slopes (energy cost vs. gait speed) obtained with both methods were coincident and agreed with those from literature, which is the essential point to compare two activities performed by the same subject and using the same method.

Afterwards, the same methodology used for the healthy subject was applied to study the crutch-assisted gait of two SCI subjects in order to evaluate the efficiency of an active orthosis with respect to the classical passive one. For each subject, a personalized musculoskeletal model was used due to the uniqueness of each injury.

The first subject showed significant improvements thanks to the motor actuation in both knees: she was able to walk faster by using a longer stride and a higher cadence. Her gait pattern changed significantly, with reduced pelvis movements yielding a lower lateral displacement of the center of mass (COM). Reasonable estimation of muscular activations were obtained for this subject, which supports the methodology used.

Motion-force-EMG captures were carried out with the second subject using either the passive as the active orthosis, allowing a more complete comparison of the devices. Acceptable matching between EMG measurements and estimated muscle activations validated the inputs provided to the energetic cost calculations. Improved gait pattern and reduced energy consumption were the results of using the

actuated gait-assistive device, while no significant reduction was found in the reaction forces at shoulders.

Therefore, it was shown that computer modeling and analysis can provide valuable indicators, as joint reactions and energy consumption, to assess the effect of assistive devices in patients without the need for long and tiring experimental tests.

6.2 Future work

The research done in this thesis leaves some unexplored topics which can become future research lines.

The first one is to make a comparison between the results obtained from the motion-force-EMG capture of the five healthy subjects by the in-house developed methods and the reference software OpenSim. Although, in this thesis, the OpenSim muscle geometry was used, models and methods are different. Comparison should be performed for the kinematics, joint torques and estimated muscular activations.

Then, it was noticed that energy expenditure could be estimated using the rigid tendon model. It will be interesting to validate this observation and try other optimization methods to estimate the whole body consumption, as for example the SynO approach.

Regarding the studies with SCI subjects, some limitations were suffered in this work. The first limitation was that only two SCI subjects were studied due to the difficulties experimented in finding valid candidates, and the expensive and time-consuming process required for building the customized devices. The second limitation was that the SCI subjects performed few training sessions with the active orthotic device; it would had been desirable to continue the study for a longer period and see the evolution of the joint reactions and the energetic cost as users became more acquainted with the new devices. Future works could go in the direction of overcoming these limitations. Repeating the study for more SCI subjects and spanning longer periods.

Finally, the acquired knowledge and the developed software could be applied to different activities and/or subjects suffering from other limitations.

Bibliography

[1] G.G. Whiteneck, S.W. Charlifue, H.L. Frankel, M.H. Fraser, B.P. Gardner, K.A. Gerhart, K.R. Krishnan, R.R. Menter, I. Nuseibeh, D.J. Short, and J.R. Silver. Mortality, morbidity and psychosocial outcomes of persons spinal cord injured more than 20 years ago. *Spinal Cord*, 30(9):617–630, sep 1992.

[2] C.O. Tan, R.A. Battaglino, and L.R. Morse. Physical Medicine & Rehabilitation Spinal Cord Injury and Osteoporosis : Causes , Mechanisms , and Rehabilitation Strategies. *International Journal of Physical Medicine & Rehabilitation Review*, 1(4):1–5, 2013.

[3] C. Alexandre and L. Vico. Pathophysiology of bone loss in disuse osteoporosis. *Joint Bone Spine*, 78(6):572–576, 2011.

[4] A. Kozlowski, T. Bryce, and M. Dijkers. Time and Effort Required by Persons with Spinal Cord Injury to Learn to Use a Powered Exoskeleton for Assisted Walking. *Topics in Spinal Cord Injury Rehabilitation*, 21(2):110–121, 2015.

[5] H. White, S. Forbes, S. Hayes, and M. White. The Effect of Using a Powered Exoskeleton Training Programme on Joint Range of Motion on Spinal Injured Individuals : A Pilot Study. *International Journal of Physical Therapy & Rehabilitation*, 1:1–5, 2014.

[6] L.L. Saunders, J. S. Krause, N.D. DiPiro, S. Kraft, and S. Brotherton. Ambulation and complications related to assistive devices after spinal cord injury. *The journal of spinal cord medicine*, 36(6):652–9, 2013.

[7] J. Cuadrado, U. Lugris, F. Mouzo, and F. Michaud. Musculo-skeletal Modeling and Analysis for Low-Cost Active Orthosis Customization and SCI Patient Adaptation. In E. Zahariev and J. Cuadrado, editors, *IUTAM Symposium on Intelligent Multibody Systems – Dynamics, Control, Simulation*, pages 41–54. 2019.

[8] R. Huston. *Principles of Biomechanics*. CRC Press, 2008.

[9] B.M. Carlson. The Nervous System. In *The Human Body*, chapter Chapter 6, pages 137–175. Elsevier, 2019.

[10] M.R. Pierrynowski and J.B. Morrison. A physiological model for the evaluation of muscular forces in human locomotion: theoretical aspects. *Mathematical Biosciences*, 75:69–101, 1985.

[11] D.E. Hardt. Determining muscle forces in the leg during normal human walking - An application and evaluation of optimization methods, 1978.

[12] A. Nagano, T. Komura, S. Fukashiro, and R. Himeno. Force, work and power output of lower limb muscles during human maximal-effort countermovement jumping. *Journal of Electromyography and Kinesiology*, 15(4):367–376, 2005.

[13] C.L. Vaughan. Theories of bipedal walking: an odyssey. *Journal of Biomechanics*, 36(4):513–523, apr 2003.

[14] J. Perry and J.M. Burnfield. Gait Analysis: Normal and Pathological Function. *Journal of Sports Science & Medicine*, 9(2):353, jun 2010.

[15] D.J. Magee. *Orthopedic physical assessment*. Elsevier Health Sciences, Philadelphia : Saunders, fourth edi edition, 2002.

[16] D. Levine, J. Richards, and M.W. Whittle. *Whittle's Gait Analysis*. Churchill edition, 2012.

[17] U. Lugris, J. Carlin, A. Luaces, and J. Cuadrado. Gait analysis system for spinal cord injured subjects assited by active orthoses and crutches. *Journal of Multi-body Dynamics*, 227, No. 4:363–374, 2013.

[18] G.E. Loeb and R. Davoodi. Musculoskeletal Mechanics and Modeling. *Scholarpedia*, 11(11):12389, 2016. revision #169693.

[19] F.E. Zajac. Muscle and tendon: properties, models, scaling, and application to biomechanics and motor control. *Critical Reviews in Biomedical Engineering*, 17:359–411, 1989.

[20] P. Favre, C. Gerber, and J.G. Snedeker. Automated muscle wrapping using finite element contact detection. *Journal of Biomechanics*, 43(10):1931–1940, 2010.

[21] F. Gao, M. Damsgaard, J. Rasmussen, and S. Tørholm Christensen. Computational method for muscle-path representation in musculoskeletal models. *Biological Cybernetics*, 87(3):199–210, 2002.

[22] B.A. Garner and M.G. Pandy. The obstacle-set method for representing muscle paths in musculoskeletal models. *Computer Methods in Biomechanics and Biomedical Engineering*, 3(1):1–30, 2000.

[23] M.T. Silva. *Human Motion Analysis Using Multibody Dynamics And Optimization Tools*. PhD thesis, Universidade Técnica de Lisboa, 2003.

[24] J. Rasmussen, M. Damsgaard, E. Surma, S. Tørholm, M. de Zee, and V. Vondrak. *AnyBody - a software system for ergonomic optimization*. 01 2003.

[25] Simm (software for interactive musculoskeletal modeling).

[26] S.L. Delp, F.C. Anderson, A.S. Arnold, P. Loan, A. Habib, C.T. John, E. Guendelman, and D.G. Thelen. Opensim: Open-source software to create and analyze dynamic simulations of movement. *IEEE Trans. Biomed. Engineering*, 54(11):1940–1950, 2007.

[27] A.J. Meyer, I. Eskinazi, J.N. Jackson, A. V. Rao, C. Patten, and B.J. Fregly. Muscle Synergies Facilitate Computational Prediction of Subject-Specific Walking Motions. *Frontiers in Bioengineering and Biotechnology*, 4(October), 2016.

[28] S. Heintz and E.M. Gutierrez-Farewik. Static optimization of muscle forces during gait in comparison to EMG-to-force processing approach. *Gait and Posture*, 26(2):279–288, 2007.

[29] M. Damsgaard, J. Rasmussen, S.T. Christensen, E. Surma, and M. de Zee. Analysis of musculoskeletal systems in the AnyBody Modeling System. *Simulation Modelling Practice and Theory*, 14(8):1100–1111, 2006.

[30] J. Dul, M.A. Townsend, R. Shiavi, and G.E. Johnson. Muscular synergism—I. On criteria for load sharing between synergistic muscles. *Journal of Biomechanics*, 17(9):663–673, jan 1984.

[31] W. Herzog and P. Binding. Cocontraction of pairs of antagonistic muscles: analytical solution for planar static nonlinear optimization approaches. *Mathematical Biosciences*, 118:83–95, 1993.

[32] C.A.M. Doorenbosch and G.J. Schenau van Ingen. The role of mono- and biarticular muscles during contact control leg tasks in man. *Human Movement Science*, 14:279–300, 1995.

[33] J.A.C. Ambrosio and A. Kecskemethy. Multibody dynamics of biomechanical models for human motion via optimization. *In J.C. Garcia Orden, J.M. Goicolea, J. Cuadrado (Eds.) Multibody Dynamics – Computational Methods and Applications*, pages 245–270, 2007.

[34] R.D. Crowninshield, R.C. Johnston, J.G. Andrews, and R.A. Brand. A biomechanical investigation of the human hip. *Journal of Biomechanics*, 11:75–85, 1978.

[35] A.E. Patla. Some Characteristics of EMG Patterns During Locomotion. *Journal of Motor Behavior*, 17(4):443–461, dec 1985.

[36] B.L. Davis and C.L. Vaughan. Phasic behavior of EMG signals during gait: Use of multivariate statistics. *Journal of Electromyography and Kinesiology*, 3(1):51–60, jan 1993.

[37] K.S. Olree and C.L. Vaughan. Fundamental patterns of bilateral muscle activity in human locomotion. *Biological Cybernetics*, 73(5):409–414, oct 1995.

[38] Y.P. Ivanenko, R.E. Poppele, and F. Lacquaniti. Five basic muscle activation patterns account for muscle activity during human locomotion. *The Journal of Physiology*, 556(1):267–282, 2004.

[39] M.S. Shourijeh, T.E. Flaxman, and D.L. Benoit. An approach for improving repeatability and reliability of non-negative matrix factorization for muscle synergy analysis. *Journal of Electromyography and Kinesiology*, 26:36–43, 2016.

[40] R.L. Waters and S. Mulroy. The energy expenditure of normal and pathologic gait. *Gait and Posture*, 9(3):207–231, 1999.

[41] P.G. Montgomery, D.J. Green, N. Etxebarria, D.B. Pyne, P.U. Saunders, and C.L. Minahan. Validation of Heart Rate Monitor-Based Predictions of Oxygen Uptake and Energy Expenditure. *Journal of Strength and Conditioning Research*, 23(5):1489–1495, aug 2009.

[42] G. Merati, P. Sarchi, M. Ferrarin, A. Pedotti, and A. Veicsteinas. Paraplegic adaptation to assisted-walking: energy expenditure during wheelchair versus orthosis use. *Spinal Cord*, 38(1):37–44, jan 2000.

[43] M.J. Ijzerman, G. Baardman, M.A. Van 't Hof, H.B.K. Boom, H.J. Hermens, and P.H. Veltink. Validity and reproducibility of crutch force and heart rate

measurements to assess energy expenditure of paraplegic gait. *Archives of Physical Medicine and Rehabilitation*, 80(9):1017–1023, 1999.

[44] A.P. Hills, N. Mokhtar, and N.M. Byrne. Assessment of Physical Activity and Energy Expenditure: An Overview of Objective Measures. *Frontiers in Nutrition*, 1, jun 2014.

[45] L.J. Bhargava, M.G. Pandy, and F.C. Anderson. A phenomenological model for estimating metabolic energy consumption in muscle contraction. *Journal of Biomechanics*, 37(1):81–88, 2004.

[46] B.R. Uumberger, K.G.M. Gerritsen, and P.E. Martin. A Model of Human Muscle Energy Expenditure. *Computer Methods in Biomechanics and Biomedical Engineering*, 6(2):99–111, 2003.

[47] H. Houdijk, M.F. Bobbert, and A. De Haan. Evaluation of a Hill based muscle model for the energy cost and efficiency of muscular contraction. *Journal of Biomechanics*, 39(3):536–543, 2006.

[48] R.H. Miller. A comparison of muscle energy models for simulating human walking in three dimensions. *Journal of Biomechanics*, 47(6):1373–1381, 2014.

[49] E.P. Ravera, M.J. Crespo, and P.A. Catalfamo Formento. Assessment of the energy-related cost function over a range of walking speeds. *Biomechanics and Modeling in Mechanobiology*, jun 2019.

[50] S.C. Kirshblum, S.P. Burns, F. Biering-Sorensen, W. Donovan, D.E. Graves, A. Jha, M. Johansen, L. Jones, A. Krassioukov, M.J. Mulcahey, M. Schmidt-Read, and W. Waring. International standards for neurological classification of spinal cord injury (Revised 2011). *The Journal of Spinal Cord Medicine*, 34(6):535–546, nov 2011.

[51] J.R. Fox and W. Lovegreen. 22 - lower limb orthoses. In Joseph B. Webster and Douglas P. Murphy, editors, *Atlas of Orthoses and Assistive Devices (Fifth Edition)*, pages 239 – 246.e1. Philadelphia, fifth edition edition, 2019.

[52] T.Q. Lee and P.J. McMahon. Shoulder biomechanics and muscle plasticity: implications in spinal cord injury. *Clinical orthopaedics and related research*, (403 Suppl):S26–36, oct 2002.

[53] C.L. Vaughan, B.L. Davis, and J.C. O'Connor. *Dynamics of Human Gait (2nd ed.)*. Kiboho Publishers, 1999.

[54] F. Romero, F.J. Alonso, J. Cubero, and G. Galán-Marín. An automatic SSA-based de-noising and smoothing technique for surface electromyography signals. *Biomedical Signal Processing and Control*, 18:317–324, apr 2015.

[55] K.R.S. Holzbaur, W.M. Murray, and S.L. Delp. A model of the upper extremity for simulating musculoskeletal surgery and analyzing neuromuscular control. *Annals of Biomedical Engineering*, 33(6):829–840, 2005.

[56] M.G. Hoy, F. E. Zajac, and M.E. Gordon. A musculoskeletal model of the human lower extremity: The effect of muscle, tendon, and moment arm on the moment-angle relationship of musculotendon actuators at the hip, knee, and ankle. *Journal of Biomechanics*, 23(2):157–169, jan 1990.

[57] Y. Ou. *An analysis of optimization methods for identifying muscle forces in human gait*. PhD thesis, 2011.

[58] M.G. Pandy, F.C. Anderson, and D.G. Hull. A Parameter Optimization Approach for the Optimal Control of Large-Scale Musculoskeletal Systems. *Journal of Biomechanical Engineering*, 114(4):450–460, nov 1992.

[59] D.G. Thelen, F.C. Anderson, and S.L. Delp. Generating dynamic simulations of movement using computed muscle control. *Journal of Biomechanics*, 36(3):321–328, mar 2003.

[60] J.M. Winters. An improved muscle-reflex actuator for use in large-scale neuromusculoskeletal models. *Annals of Biomedical Engineering*, 23(4):359–374, 1995.

[61] J.W. Lee and K. Rim. Maximum Finger Force Prediction Using a Planar Simulation of the Middle Finger. *Proceedings of the Institution of Mechanical Engineers, Part H: Journal of Engineering in Medicine*, 204(3):169–178, sep 1990.

[62] S. Mukherjee, A. Chawla, B. Karthikeyan, and A. Soni. Finite element crash simulations of the human body: Passive and active muscle modelling. *Sadhana*, 32:409–426, 08 2007.

[63] B. Katz. The relation between force and speed in muscular contraction. *The Journal of Physiology*, 96(1):45–64, jun 1939.

[64] C.F. Martin and L. Schovanec. The Control and Mechanics of Human Movement Systems. *Progress in Systems and Control Theory*, pages 25:173–202, 1999.

[65] Edward J. Haug. *Computer aided kinematics and dynamics of mechanical systems*. Allyn & Bacon, Inc., Needham Heights, MA, USA, 1989.

[66] Javier García de Jalón and Eduardo Bayo. *Kinematic and dynamic simulation of multibody systems: the real time challenge*. Springer-Verlag, 1994.

[67] B. Paul and D. Krajcinovic. Computer analysis of machines with planar motion: Part 1—Kinematics. *Journal of Applied Mechanics*, 37(3):697–702, 1970.

[68] P. N. Sheth and J. J. Uicker. IMP (Integrated Mechanisms Program), a computer-aided design analysis system for mechanisms and linkage. *Journal of Engineering for Industry*, 94(2):454–464, 1972.

[69] D.A. Smith, M.A. Chace, and A.C. Rubens. The automatic generation of a mathematical model for machinery systems. *Journal of Engineering for Industry*, 95(2):629–635, 1973.

[70] D. Dopico. MBSLIM: Multibody Systems en Laboratorio de Ingeniería Mecánica, http://lim.ii.udc.es/MBSLIM, 2016.

[71] K.C. Gupta. *Solution Manual for Mechanics and Control of Robots*. Mechanical Engineering Series. Springer New York, New York, NY, 1997.

[72] H. Mokhtarzadeh, L. Perraton, L. Fok, M.A. Muñoz, R. Clark, P. Pivonka, and A.L. Bryant. A comparison of optimisation methods and knee joint degrees of freedom on muscle force predictions during single-leg hop landings. *Journal of Biomechanics*, 47(12):2863–2868, sep 2014.

[73] U. Lugris, J. Carlin, A. Luaces, and J. Cuadrado. Gait analysis system for spinal cord injured subjects assited by active orthoses and crutches. *Journal of Multi-body Dynamics*, 227, No. 4:363–374, 2013.

[74] M. Raison, C. Detrembleur, P. Fisette, and J.C. Samin. Assessment of antagonistic muscle forces during forearm flexion/extension. *Computational Methods in Applied Sciences*, 23(July):215–238, 2011.

[75] R.D. Crowninshield and R.A. Brand. A physiologically based criterion of muscle force prediction in locomotion. *Journal of Biomechanics*, 14(11):793–801, 1981.

[76] J. Rasmussen, M. Damsgaard, and M. Voigt. Muscle recruitment by the min/max criterion — a comparative numerical study. *Journal of Biomechanics*, 34(3):409–415, 2001.

[77] K.N. An, B.M. Kwak, E.Y. Chao, and B.F. Morrey. Determination of Muscle and Joint Forces: A New Technique to Solve the Indeterminate Problem. *Journal of Biomechanical Engineering*, 106(4):364–367, nov 1984.

[78] G. Pipeleers, B. Demeulenaere, I. Jonkers, P. Spaepen, G. Van der Perre, A. Spaepen, J. Swevers, and J. De Schutter. Dynamic simulation of human motion: Numerically efficient inclusion of muscle physiology by convex optimization. *Optimization and Engineering*, 9(3):213–238, 2008.

[79] A. Rajagopal, C.L. Dembia, M.S. DeMers, D.D. Delp, J.L. Hicks, and S.L. Delp. Full body musculoskeletal model for muscle-driven simulation of human gait. *IEEE transactions on bio-medical engineering*, 63(10):2068–2079, oct 2016.

[80] A.L. Hof. The relationship between electromyogram and muscle force. *Sportverletzung · Sportschaden*, 11(03):79–86, sep 1997.

[81] C.L. Banks, M.M. Pai, T.E. McGuirk, B.J. Fregly, and C. Patten. Methodological Choices in Muscle Synergy Analysis Impact Differentiation of Physiological Characteristics Following Stroke. *Frontiers in Computational Neuroscience*, 11(August):1–12, 2017.

[82] C. M. Niu, Y. Bao, C. Zhuang, S. Li, T. Wang, L. Cui, Q. Xie, and N. Lan. Synergy-based fes for post-stroke rehabilitation of upper-limb motor functions. *IEEE Transactions on Neural Systems and Rehabilitation Engineering*, 27(2):256–264, Feb 2019.

[83] S. Ferrante, N. Chia Bejarano, E. Ambrosini, A. Nardone, A. M. Turcato, M. Monticone, G. Ferrigno, and A. Pedrocchi. A Personalized Multi-Channel FES Controller Based on Muscle Synergies to Support Gait Rehabilitation after Stroke. *Frontiers in neuroscience*, 10:425, sep 2016.

[84] A. Gopalakrishnan, L. Modenese, and A.T.M. Phillips. A novel computational framework for deducing muscle synergies from experimental joint moments, 2014.

[85] M. Shourijeh and B.J. Fregly. Muscle synergies modify static optimization estimates of joint stiffness during walking. *Journal of Biomechanical Engineering*, 07 2019.

[86] D.G. Thelen and F.C. Anderson. Using computed muscle control to generate forward dynamic simulations of human walking from experimental data. *Journal of Biomechanics*, 39(6):1107–1115, jan 2006.

[87] A.E. Minetti and R.McN. Alexander. A Theory of Metabolic Costs for Bipedal Gaits. *Journal of Theoretical Biology*, 186(4):467–476, 1997.

[88] M.A. Johnson, J. Polgar, D. Weightman, and D. Appleton. Data on the distribution of fibre types in thirty-six human muscles. *Journal of the Neurological Sciences*, 18(1):111–129, jan 1973.

[89] J. Mendez and A. Keys. Density and composition of mammalian muscle. *Metabolism*, Clinical and Experimental(9):184–188, 1960.

[90] U. Lugris, J. Carlin, A. Luaces, and J. Cuadrado. Solution methods for the double-support indeterminacy in human gait. *Multibody System Dynamics*, 30(3):247–263, 2013.

[91] P. Westerhoff, F. Graichen, A. Bender, A. Halder, A. Beier, A. Rohlmann, and G. Bergmann. In vivo measurement of shoulder joint loads during walking with crutches. *Clinical Biomechanics*, 27(7):711–718, 2012.

[92] J.M. Font-Llagunes, D Clos, U. Lugrís, F. Romero Sánchez, F.J. Alonso, and J. Cuadrado. Design , control and evaluation of a low-cost active orthosis for the gait of spinal cord injured subjects. In *XXI Congreso Nacional de Ingeniería Mecánica: libro de artículos, 1-6*, pages 196–201, 2016.

[93] M.S. Orendurff, A.D. Segal, G.K. Klute, J.S. Berge, E.S. Rohr, and N.J. Kadel. The effect of walking speed on center of mass displacement. *The Journal of Rehabilitation Research and Development*, 41(6):829, 2004.

[94] R.A. Brand, D.R. Pedersen, and J.A. Friederich. The sensitivity of muscle force predictions to changes in physiologic cross-sectional area. *Journal of Biomechanics*, 19(8):589–596, jan 1986.

Appendices

Appendix A

Muscle parameters

a. data taken from Delp [26].
b. data taken from Brand [94].
c. data taken from Johnson [88].
d. data taken from Holzbaur [55].

Muscles	$F_0^{M\,a}$ [**N**]	$l_0^{M\,a}$ $[m]$	$l_S^{T\,a}$ $[m]$	${\alpha_0}^a$ [°]	A^b $[cm^2]$	ST^c [%]
Gluteus Medius Anterior	546	0,054	0,078	8	25	50
Gluteus Medius Middle	382	0,085	0,053	0	16,21	50
Gluteus Medius Posterior	435	0,065	0,053	19	21,21	50
Gluteus Minimus Anterior	180	0,068	0,016	10	6,76	50
Gluteus Minimus Middle	190	0,056	0,026	0	8,2	50
Gluteus Minimus Posterior	215	0,056	0,026	21	11,98	50
Gluteus Maximus Anterior	382	0,142	0,125	5	20,2	52,4
Gluteus Maximus Middle	546	0,147	0,127	0	19,59	52,4
Gluteus Maximus Posterior	368	0,144	0,145	5	20	52,4
Adductor Longus	418	0,138	0,110	6	22,73	50
Adductor Brevis	286	0,133	0,020	0	16,86	50
Adductor Magnus Superior	346	0,087	0,060	5	25,52	58,4
Adductor Magnus Middle	312	0,121	0,130	3	18,35	58,4
Adductor Magnus Inferior	444	0,131	0,260	5	16,95	58,4
Tensor Fasciae Latae	155	0,095	0,425	3	8	50
Pectineus	177	0,133	0,001	0	9,03	50
Iliacus	429	0,100	0,090	7	23,33	50
Psoas	371	0,104	0,130	8	25,7	50
Quadratus femoris	254	0,054	0,024	0	21	50
Gemellus	109	0,024	0,039	0	6,46	50
Piriformis	296	0,026	0,115	10	20,54	50
Semitendinosus	328	0,201	0,262	5	13,05	50
Semimembranosus	1030	0,080	0,359	15	46,33	50
Biceps Femoris Long Head	717	0,109	0,341	0	27,34	66,9
Biceps Femoris Short Head	402	0,173	0,100	23	8,14	66,9
Sartorius	104	0,579	0,040	0	2,9	49,6
Gracilis	108	0,352	0,140	3	3,74	50
Rectus Femoris	779	0,084	0,346	5	42,96	38,1
Vastus Medialis	1294	0,089	0,126	5	66,87	47
Vastus Intermedius	1365	0,087	0,136	3	82	50
Vastus Lateralis	1871	0,084	0,157	5	64,41	48
Gastrocnemius Medial	1113	0,045	0,408	17	50,6	48,2
Gastrocnemius Lateral	1113	0,064	0,385	8	14,3	48,2
Soleus	4234	0,030	0,268	25	186,69	75
Tibialis Posterior	1516	0,031	0,310	12	26,27	73
Tibialis Anterior	603	0,098	0,223	5	16,88	50
Flexor Digitorum Longus	310	0,034	0,400	7	6,4	50
Flexor Hallucis Longus	322	0,043	0,380	10	18,52	50
Extensor Digitorum Longus	341	0,102	0,345	8	7,46	47,3
Extensor Hallucis Longus	108	0,111	0,305	6	6,49	50
Peroneus Brevis	348	0,050	0,161	5	19,61	62,5
Peroneus Longus	754	0,049	0,345	7	24,65	62,5
Peroneus Tertius	90	0,079	0,100	13	4,14	35
External Obliques	864	0,125	0,211	13	4,14	50
Internal Obliques	712	0,125	0,165	13	4,14	0
Erector Spinae	2974	0,120	0,030	13	4,14	58,4

Table A.1 – Muscles parameters of lower extremity used in the models of this work.

Muscles	$F_0^{M\,d}$ [**N**]	$l_0^{M\,d}$ $[m]$	$l_S^{T\,d}$ $[m]$	$\alpha_0{}^{d}$ [º]	A^{b} $[cm^2]$	ST^{c} [%]
Coracobrachialis	242,46	0,093	0,097	0	4,14	50
Deltoďd Ant.	1142,6	0,098	0,093	22	8,2	35
Deltoďd Mid.	1142,6	0,108	0,11	15	8,2	35
Deltoďd Post.	259,9	0,137	0,038	18	1,9	35
Infraspinatus	1210,8	0,076	0,031	19	8,6	35
Lat. Thoracic	389,1	0,254	0,12	25	2,8	35
Lat. Lumbar	389,1	0,254	0,12	19	2,8	35
Lat. Iliac	281,7	0,279	0,14	21	2	35
Pec. Maj. Clav.	364,4	0,144	0,003	17	2,6	35
Pec. Maj. Ster.	515,4	0,138	0,089	25	3,7	35
Pec. Maj. Ribs.	390,5	0,138	0,132	25	2,8	35
Subscapularis	1377,8	0,087	0,033	20	9,8	35
Supraspinatus	487,8	0,068	0,04	20	7	35
Teres Maj.	425,4	0,162	0,02	16	3	35
Teres Min.	354,3	0,074	0,071	24	2,5	35
Anconeus	350	0,027	0,018	1	2,5	35
Biceps long	624,3	0,116	0,272	2	4,5	35
Biceps short	435,6	0,132	0,192	3	3,1	35
Brachialis	987,3	0,086	0,054	4	7,1	35
Brachioradialis	261,3	0,173	0,133	5	1,9	35
Ext. Carpi. Rad. Long.	304,9	0,081	0,224	6	2,2	35
Pronator Teres	566,2	0,049	0,098	10	4	35
Triceps Lat.	624,3	0,114	0,098	9	4,5	35
Triceps Med.	624,3	0,114	0,091	9	4,5	35
Triceps long	798,5	0,134	0,143	9	5,7	35
Supinator	476	0,033	0,028	11	3,4	35

Table A.2 – Muscles parameters of upper extremity used in the models of this work.

Appendix B

Works derived from this thesis

This work was funded by the Spanish MINECO under project DPI2015-65959-C3-1-R, co-financed by the EU through the EFRD program, and by the Galician Government under grant ED431B2016/031. Moreover, Florian Michaud enjoyed the doctoral research contract BES-2016-076901, co-financed by the EU through the ESF program. Several works have arisen from this thesis, including journal paper and conference papers. Moreover, some other journal papers have been submitted, but they are still under review. The list is exposed hereafter.

Published book paper

J. Cuadrado, U. Lugris, F. Mouzo, F. Michaud. Musculo-skeletal Modeling and Analysis for Low-cost Active Orthosis Customization and SCI Patient Adaptation. IUTAM Symposium on Intelligent Multibody Systems - Dynamics, Control, Simulation, ed. by E. Zahariev and J. Cuadrado, Springer, 2019.

Published journal paper

F. Michaud, F. Mouzo, U. Lugrís, J. Cuadrado. Energy expenditure estimation during crutch-orthosis-assisted gait of a spinal-cord-injured subject. Frontiers in Neurorobotics, vol. 13, article 55, 11 pages, 2019.

Submitted journal papers (under review)

F. Michaud, U. Lugris, J. Cuadrado and A. Kecskemethy. A procedure to define customized musculoskeletal models for the analysis of the crutch-orthosis-assisted gait of SCI subjects. J. of Biomechanical Engineering.

F. Michaud, M. S. Shourijeh, B.J. Fregly, and J. Cuadrado. Do muscle synergies improve optimization prediction of muscle activations during gait?. Frontiers In Computational Neuroscience.

F. Mouzo, F. Michaud, U. Lugris and J. Cuadrado. Leg-orthosis contact force estimation from gait analysis. Mechanism and Machine Theory.

Journal papers in preparation

F. Michaud, F. Mouzo, U. Lugris, J. Cuadrado, Estimating physiologically feasible muscle forces in human motion through co-simulation of muscular and skeletal dynamics, J. of Biomechanical Engineering.

Conference communications

U. Lugris, J. Carlin, F. Michaud, J. Cuadrado Joint Efforts Calculation in the Gait of Incomplete Spinal Cord Injured Subjects. 2nd Joint Int. Conference on Multibody System Dynamics (IMSD). Stuttgart, Germany, 2012-05.

D. Dopico, A. Luaces, F. Michaud, J. Cuadrado. Simulation of the Anchor Lifting Maneuver of a Ship Using Contact Detection Techniques and Continuous Force Models. The Sixth Asian Conference on Multibody Dynamics ACMD2012. Shanghai, China, 2012-08.

J. Cuadrado, U. Lugris, F. Michaud, F. Mouzo. Role of Multibody Dynamics Based Simulation in Human, Robotic and Hybrid Locomotion Benchmarking. Workshop on Benchmarking Bipedal Locomotion, 2014 IEEE-RAS Int. Conference on Humanoid Robots. Madrid, Spain, 2014-11.

F. Michaud, U. Lugris, Y. Ou, J. Cuadrado, A. Kecskemethy. Influence of Muscle Recruitment Criteria on Joint Reaction Forces During Human Gait. ECCOMAS Thematic Conference on Multibody Dynamics 2015. Barcelona, Spain, 2015-06.

F. Michaud, U. Lugris, Y. Ou, J. Cuadrado, A. Kecskemethy. Comparison of Forward-dynamics Approaches to Estimate Muscular Forces in Human Gait. 4th Joint Int. Conference on Multibody System Dynamics (IMSD 2016). Montreal, Canada, 2016-05.

F. Michaud, U. Lugris, J. Cuadrado. A Co-integration Approach for the Forward-dynamics Based Solution of the Muscle Recruitment Problem (Premio al mejor trabajo teórico). 7º Congresso Nacional de Biomecânica. Guimaraes, Portugal, 2017-02.

F. Michaud, U. Lugris, Y. Ou, J. Cuadrado, A. Kecskemethy. Optimization Methods for Identifying Muscle Forces in a Spinal-cord-injured Subject during Crutch-assisted Gait. 8th ECCOMAS Thematic Conference on Multibody Dynamics. Prague, Czech Republic, 2017-06.

J. Cuadrado, U. Lugris, F. Mouzo, F. Michaud. Strain Measurements in Active Orthoses for Multibody Model Validation and Control Robustness Improvement. IUTAM Symposium on Intelligent Multibody Systems: Dynamics, Control, Simulation. Sozopol, Bulgaria, 2017-09.

U. Lugris, R. Vilela, E. Sanjurjo, F. Mouzo, F. Michaud. Implementation of an Extended Kalman Filter for Robust Real-time Motion Capture Using IR Cameras and Optical Markers. IUTAM Symposium on Intelligent Multibody Systems: Dynamics, Control, Simulation. Sozopol, Bulgaria, 2017-09.

F. Michaud, U. Lugris, J. Castro, J. Cuadrado. Estimation of Muscle Energy Expenditure in a Spinal-cord-injured Subject during Crutch-assisted Gait. 5th Joint Int. Conference on Multibody System Dynamics (IMSD 2018). Lisbon, Portugal, 2018-06.

U. Lugris, R. Vilela, E. Sanjurjo, F. Mouzo and F. Michaud. Implementation of an Extended Kalman Filter for Optical Motion Capture with Real-time 3D Visualization. 5th Joint Int. Conference on Multibody System Dynamics (IMSD 2018). Lisbon, Portugal, 2018-06.

J. Cuadrado, U. Lugris, F. Mouzo and F. Michaud. Skeletal Multibody Model for Leg-Orthosis Contact Force Estimation in SCI Subjects. 12th Int. Congress on Mechanics, HSTAM 2019. Thessaloniki, Greece, 2019-09.

Appendix C

Resumen extendido

Introducción

Los avances en el cuidado de los lesionados medulares han resultado en una mayor esperanza de vida entre esta población [1]. Levantarse y caminar regularmente tiene enormes beneficios para el estado general de salud de estas personas, ya que reduce las consecuencias negativas del sedentarismo. Un ejemplo es la osteoporosis [2], es decir, la pérdida ósea debida a la descarga mecánica esquelética. Mientras que la plasticidad muscular o la estimulación eléctrica muscular atenúan la atrofia muscular, ninguno de ellos conserva la masa ósea [3]. Por lo tanto, la adherencia a la marcha asistida es importante, pero existe un riesgo de abandono debido a varios problemas, como dolor, fatiga o muy baja velocidad, lo que puede hacer que el sujeto vuelva a usar únicamente la silla de ruedas. Los lesionados medulares con alguna capacidad de actuación en cadera pero con poca o nula capacidad de actuación en rodilla y tobillo, pueden en muchos casos caminar con la ayuda de órtesis de rodilla-tobillo-pie y muletas [4] [5]. Sin embargo, dado que las rodillas se mantienen extendidas en todo momento, incluso durante la fase de balanceo, la marcha resulta muy incómoda, pues la cadera debe levantarse para permitir el balanceo de la pierna, lo que conlleva un alto coste energético que hace aparecer la fatiga rápidamente. Además, el uso de muletas produce cargas elevadas en algunas articulaciones, especialmente en los hombros, lo que puede generar lesiones a largo plazo. El resultado es que muchos pacientes prefieren usar la silla de ruedas [6], perdiendo así los beneficios de caminar para su rehabilitación y para su estado de salud general. Para paliar estos problemas, se han propuesto órtesis activas que detectan la intención de dar el paso y lanzan un ciclo de flexión-extensión de rodilla [7], aproximando así la marcha normal, lo que puede hacer la marcha más cómoda y aumentar las posibilidades reales de caminar para los usuarios. Algunas magnitudes, como las reacciones en las articulaciones o el coste energético, pueden servir como indicadores para evaluar el efecto de los dispositivos de asistencia en un usuario específico y, por lo tanto, la probabilidad de su uso real a largo plazo. El uso combinado de la captura de movimiento-fuerza-EMG y los modelos neuromusculoesqueléticos personalizados permite estimar las magnitudes mencionadas, sin la necesidad de largas y agotadoras pruebas experimentales que difícilmente podrían afrontar estos pacientes. Por lo tanto, el presente trabajo está dedicado, por un lado, a revisar, seleccionar, adaptar,

mejorar y/o desarrollar, y validar, todos los métodos y herramientas necesarios que se requieren para este propósito: (i) modelos músculoesqueléticos personalizados; (ii) métodos de análisis a nivel esquelético y musculoesquelético; (iii) métodos de estimación de coste energético. Y, por otro lado, a aplicarlos a dos lesionados medulares, bilateral y unilateral, respectivamente, y a comparar una nueva órtesis activa con una pasiva convencional.

Objetivos

El objetivo de este trabajo es evaluar el efecto de los dispositivos ortésicos en lesionados medulares y la probabilidad de su uso a largo plazo, mediante la estimación de algunos indicadores como fuerzas de reacción y coste energético, que a su vez requieren la estimación de las activaciones y fuerzas musculares. Para ello, se establecen algunos objetivos parciales:

- Selección de un modelo neuromusculoesquelético para sujetos sanos y adaptación a lesionados medulares.
- Comparación, en términos de precisión y eficiencia, de varios métodos para la solución del problema de reclutamiento muscular, y propuesta de criterios de uso según la aplicación.
- Validación de dos métodos para estimar el coste energético en la marcha normal.
- Aplicación de los modelos y métodos previamente seleccionados a la marcha asistida por órtesis y muletas de lesionados medulares y comparación entre un dispositivo ortésico pasivo y otro activo.

Estructura de la tesis

El cuerpo principal de esta tesis se organiza de la siguiente manera:

Capítulo 2 presenta el modelo musculoesquelético, el modelo muscular y la formulación de la dinámica de sistemas multicuerpo utilizados en esta tesis.

Capítulo 3 compara varios métodos de optimización para estimar las fuerzas musculares en la marcha humana utilizando enfoques de dinámica inversa y directa.

Capítulo 4 presenta dos métodos de la literatura para estimar el gasto energético muscular: los métodos de Umberger y Bhargava.

Capítulo 5 muestra la aplicación de los métodos propuestos en capítulos anteriores a dos lesionados medulares que caminan con dos tipos de dispositivos ortésicos y compara su efecto en la marcha de los sujetos.

Capítulo 6 extrae las conclusiones de la tesis e indica futuras líneas de investigación.

Metodología

El objetivo de esta tesis era evaluar el efecto de distintos dispositivos ortésicos en lesionados medulares, junto con la probabilidad de su uso a largo plazo, a través de la estimación de algunos indicadores como fuerzas de reacción y coste energético, que a su vez requieren la estimación de las activaciones y fuerzas musculares. Por lo tanto, desde el punto de vista académico, la tesis se centró en el análisis de la marcha humana mediante métodos computacionales a nivel musculoesquelético. El trabajo se puede dividir en dos partes principales. En la primera parte, se aplicaron, validaron y compararon métodos para sujetos sanos. En la segunda parte, los métodos seleccionados en la primera parte se aplicaron a dos lesionados medulares, claramente diferentes, que caminaban con muletas y utilizaban dos tipos de dispositivos ortésicos, que fueron objeto de comparación.

Experimentos y resultados

En la primera parte, se aplicaron varios métodos de optimización para estimar las fuerzas musculares y se compararon para cinco sujetos sanos. Primero se compararon distintos enfoques de optimización basados en dinámica inversa, cuatro estáticos y tres fisiológicos, y mostraron resultados similares. Se comprobó que una mayor complejidad del método no garantiza mejores resultados, ya que las mejores correlaciones con los valores experimentales se obtuvieron con el criterio más simple y común. El enfoque fisiológico fue difícil de implementar, y presentó el tiempo de cálculo más largo entre todos los enfoques comparados basados en dinámica inversa, mientras que su forma simplificada se ejecutó más de 100 veces más rápido y mostró casi los mismos resultados.

Se pueden sacar las mismas conclusiones para el enfoque de optimización con sinergias estudiado en esta tesis. La consideración de los efectos de las sinergias para resolver el problema de reparto de las fuerzas musculares complicó la programación y condujo a algoritmos más lentos. Sin embargo, las correlaciones obtenidas no mostraron ninguna mejora con respecto a los enfoques que no consideran las sinergias. El aspecto positivo fue que el enfoque SynO puede extraer las sinergias musculares y, a su vez, ofrecer una predicción razonable de las activaciones musculares reproduciendo bien los pares articulares de la pierna entera. Sin embargo, la combinación propuesta de SO con NMF mostró resultados pobres con respecto a los pares articulares. Por lo tanto, el enfoque SynO podría resultar útil para la aplicación a la estimulación eléctrica funcional, el control de movimiento y la predicción, ya que reduce el espacio dimesional de control.

Otro enfoque práctico para el control de movimiento o la predicción se basa en la dinámica directa. En este trabajo, se utilizaron métodos basados en dinámica directa para movimientos registrados con el fin de compararlos con los métodos anteriores, basados en dinámica inversa. Se propuso un nuevo método, basado en el *Computed Torque Control* (CTC). Consiste en un algoritmo de co-simulación donde las ecuaciones multicuerpo y de dinámica muscular se simulan por separado, lo que permite utilizar los códigos multicuerpo existentes. Se sugirieron dos versiones del algoritmo: (i) el enfoque estándar (CSS), que requiere la solución del reparto de

fuerzas musculares en cada iteración; (ii) el enfoque aproximado (CSA), que limita la solución del reparto de fuerzas musculares a la primera iteración. Estos algoritmos se compararon con un método de referencia, el popular *Computed Muscle Control* (CMC), para el caso de un péndulo simple accionado por dos músculos. El CSS fue el enfoque más lento debido a sus numerosas optimizaciones e integraciones. Sin embargo, el CSA mostró un mejor rendimiento computacional que el CMC aunque a costa de una menor precisión. Se podría encontrar un compromiso, optimizando el tiempo de CPU y la precisión. Luego, se aplicó el algoritmo estándar de co-simulación al análisis de la marcha de los cinco sujetos sanos y se compararon varios criterios de optimización. Los resultados obtenidos presentaron las mismas conclusiones que el análisis basado en dinámica inversa: el criterio más simple fue el más eficiente, y el fisiológico fue mucho más lento y no mejoró las correlaciones con medidas de electromiografía (EMG).

Sin embargo, a pesar de sus desventajas, el enfoque fisiológico basado en dinámica inversa resultó útil para implementar los dos métodos de gasto de energía basados en el modelo de músculo de Hill, ya que es el único enfoque que proporciona las variables musculares requeridas como entradas. Si se usa la forma simplificada con tendón rígido, la tasa de trabajo mecánico resulta casi nula, debido a las pequeñas variaciones de longitud de la parte contráctil del músculo. Los resultados obtenidos con los dos métodos de gasto energético se validaron experimentalmente para un sujeto sano durante varios ciclos de marcha a diferentes velocidades. Se obtuvieron buenas correlaciones con ambos enfoques, pero los resultados mostraron que es necesaria una calibración por sujeto de la tasa metabólica basal de todo el cuerpo. Sin embargo, las pendientes (coste energético frente a velocidad de la marcha) obtenidas con ambos métodos fueron coincidentes, y fueron coincidentes con las de la literatura, siendo la pendiente el punto esencial para comparar dos actividades realizadas por el mismo sujeto y utilizando el mismo método.

Posteriormente, se aplicó la misma metodología utilizada para el sujeto sano para estudiar la marcha de dos lesionados medulares y evaluar la eficacia de una órtesis activa con respecto a la clásica pasiva. Para cada sujeto, se utilizó un modelo musculoesquelético personalizado debido a la singularidad de las lesiones.

El primer sujeto, bilateral, mostró mejoras significativas gracias a la actuación motora en ambas rodillas: pudo caminar más rápido usando un paso más largo y una cadencia más alta. Su patrón de marcha cambió significativamente, con reducción del movimiento de la pelvis que produjo un menor desplazamiento lateral del centro de masas. Se obtuvo una estimación razonable de las activaciones musculares para este caso, lo que respalda la metodología utilizada.

Con el segundo sujeto, unilateral, se llevaron a cabo capturas de movimiento-fuerza-EMG utilizando tanto la órtesis pasiva como la activa, lo que permitió una comparación más completa de los dispositivos. La aceptable correlación entre las mediciones de EMG y las activaciones musculares estimadas, sirvió para validar las entradas proporcionadas para los cálculos de coste energéticos. Un mejor patrón de marcha y un menor consumo de energía fueron los resultados del uso del dispositivo activo de asistencia mientras que no se encontró una reducción significativa en las fuerzas de reacción en los hombros.

Conclusiones y trabajo futuro

Se demostró que los modelos y análisis computacionales pueden proporcionar indicadores valiosos, como reacciones articulares y consumo enegético, para evaluar el efecto de los dispositivos asistivos en pacientes, sin necesidad de acudir a pruebas experimentales largas y agotadoras.

La investigación realizada en esta tesis deja algunos temas sin explorar que pueden convertirse en futuras líneas de investigación.

El primero es hacer una comparación entre los resultados obtenidos de la captura de movimiento-fuerza-EMG de los cinco sujetos sanos por los métodos desarrollados internamente y el software de referencia OpenSim. Aunque, en esta tesis, se utilizó la geometría muscular de OpenSim, los modelos y métodos son diferentes. Se debe realizar una comparación para la cinemática, pares articulares y activaciones musculares estimadas.

Luego, se observó que el gasto energético podía estimarse utilizando el modelo de tendón rígido. Sería interesante validar esta observación y probar otros métodos de optimización para estimar el consumo de todo el cuerpo, como por ejemplo enfoque de sinergias (SynO).

En cuanto a los estudios con lesionados medulares, padecieron algunas limitaciones en este trabajo. La primera limitación fue que sólo se estudiaron dos lesionados medulares debido a las dificultades experimentadas para encontrar candidatos válidos, y al costoso y lento proceso requerido para construir los dispositivos personalizados. La segunda limitación fue que los lesionados medulares realizaron pocas sesiones de entrenamiento con el dispositivo ortésico activo. Hubiera sido deseable continuar el estudio durante un período más largo y ver la evolución de las reacciones articulares y el coste energético a medida que los usuarios se familiarizaban más con los nuevos dispositivos. Los trabajos futuros podrían ir en la dirección de superar estas limitaciones. Repetir el estudio para más lesionados medulares y abarcar períodos más largos.

Finalmente, el conocimiento adquirido y el software desarrollado podrían aplicarse a diferentes actividades y/o a sujetos que sufran de otras limitaciones.

Trabajos derivados de la realización de esta tesis

Se agradece la ayuda del MINECO a través del proyecto DPI2015-65959-C3-1-R, co-financiado con la UE vía el programa EFRD, y del gobierno gallego a través de la beca ED431B2016/031. Además, Florian Michaud disfrutó del contrato predoctoral de investigación BES-2016-076901, financiado por el MINECO y co-financiado por la UE vía el programa ESF. Varios trabajos se han derivado de esta tesis, incluyendo artículos de revistas y conferencias. Adicionalmente, otros artículos han sido enviados a revistas, pero siguen en revisión.

Artículo de libro

J. Cuadrado, U. Lugris, F. Mouzo, F. Michaud. Musculo-skeletal Modeling and Analysis for Low-cost Active Orthosis Customization and SCI Patient Adaptation.

IUTAM Symposium on Intelligent Multibody Systems - Dynamics, Control, Simulation, ed. by E. Zahariev and J. Cuadrado, Springer, 2019.

Artículo de revista publicado

F. Michaud, F. Mouzo, U. Lugrís, J. Cuadrado. Energy expenditure estimation during crutch-orthosis-assisted gait of a spinal-cord-injured subject. Frontiers in Neurorobotics, vol. 13, article 55, 11 pages, 2019.

Artículos de revista enviado (bajo revisión)

F. Michaud, U. Lugris, J. Cuadrado and A. Kecskemethy. A procedure to define customized musculoskeletal models for the analysis of the crutch-orthosis-assisted gait of SCI subjects. J. of Biomechanical Engineering.

F. Michaud, M. S. Shourijeh, B.J. Fregly, and J. Cuadrado. Do muscle synergies improve optimization prediction of muscle activations during gait?. Frontiers In Computational Neuroscience.

F. Mouzo, F. Michaud, U. Lugris and J. Cuadrado. Leg-orthosis contact force estimation from gait analysis. Mechanism and Machine Theory.

Artículos de revista en preparación

F. Michaud, F. Mouzo, U. Lugris, J. Cuadrado, Estimating physiologically feasible muscle forces in human motion through co-simulation of muscular and skeletal dynamics, J. of Biomechanical Engineering

Comunicaciones en congresos

U. Lugris, J. Carlin, F. Michaud, J. Cuadrado Joint Efforts Calculation in the Gait of Incomplete Spinal Cord Injured Subjects. 2nd Joint Int. Conference on Multibody System Dynamics (IMSD). Stuttgart, Germany, 2012-05.

D. Dopico, A. Luaces, F. Michaud, J. Cuadrado. Simulation of the Anchor Lifting Maneuver of a Ship Using Contact Detection Techniques and Continuous Force Models. The Sixth Asian Conference on Multibody Dynamics ACMD2012. Shanghai, China, 2012-08.

J. Cuadrado, U. Lugris, F. Michaud, F. Mouzo. Role of Multibody Dynamics Based Simulation in Human, Robotic and Hybrid Locomotion Benchmarking. Workshop on Benchmarking Bipedal Locomotion, 2014 IEEE-RAS Int. Conference on Humanoid Robots. Madrid, Spain, 2014-11.

F. Michaud, U. Lugris, Y. Ou, J. Cuadrado, A. Kecskemethy. Influence of Muscle Recruitment Criteria on Joint Reaction Forces During Human Gait. ECCOMAS Thematic Conference on Multibody Dynamics 2015. Barcelona, Spain, 2015-06.

F. Michaud, U. Lugris, Y. Ou, J. Cuadrado, A. Kecskemethy. Comparison of Forward-dynamics Approaches to Estimate Muscular Forces in Human Gait. 4th Joint Int. Conference on Multibody System Dynamics (IMSD 2016). Montreal, Canada, 2016-05.

F. Michaud, U. Lugris, J. Cuadrado. A Co-integration Approach for the Forward-dynamics Based Solution of the Muscle Recruitment Problem (Premio al mejor trabajo teórico). 7º Congresso Nacional de Biomecânica. Guimaraes, Portugal, 2017-02.

F. Michaud, U. Lugris, Y. Ou, J. Cuadrado, A. Kecskemethy. Optimization Methods for Identifying Muscle Forces in a Spinal-cord-injured Subject during Crutch-assisted Gait. 8th ECCOMAS Thematic Conference on Multibody Dynamics. Prague, Czech Republic, 2017-06.

J. Cuadrado, U. Lugris, F. Mouzo, F. Michaud. Strain Measurements in Active Orthoses for Multibody Model Validation and Control Robustness Improvement. IUTAM Symposium on Intelligent Multibody Systems: Dynamics, Control, Simulation. Sozopol, Bulgaria, 2017-09.

U. Lugris, R. Vilela, E. Sanjurjo, F. Mouzo, F. Michaud. Implementation of an Extended Kalman Filter for Robust Real-time Motion Capture Using IR Cameras and Optical Markers. IUTAM Symposium on Intelligent Multibody Systems: Dynamics, Control, Simulation. Sozopol, Bulgaria, 2017-09.

F. Michaud, U. Lugris, J. Castro, J. Cuadrado. Estimation of Muscle Energy Expenditure in a Spinal-cord-injured Subject during Crutch-assisted Gait. 5th Joint Int. Conference on Multibody System Dynamics (IMSD 2018). Lisbon, Portugal, 2018-06.

U. Lugris, R. Vilela, E. Sanjurjo, F. Mouzo and F. Michaud. Implementation of an Extended Kalman Filter for Optical Motion Capture with Real-time 3D Visualization. 5th Joint Int. Conference on Multibody System Dynamics (IMSD 2018). Lisbon, Portugal, 2018-06.

J. Cuadrado, U. Lugris, F. Mouzo and F. Michaud. Skeletal Multibody Model for Leg-Orthosis Contact Force Estimation in SCI Subjects. 12th Int. Congress on Mechanics, HSTAM 2019. Thessaloniki, Greece, 2019-09.